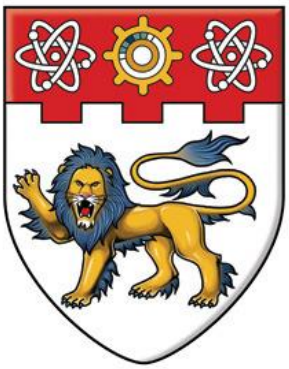

NANYANG TECHNOLOGICAL UNIVERSITY

IN-SITU INFRARED SPECTROSCOPY STUDIES OF SURFACE REACTIONS OVER IRRADIATED PHOTOCATALYSTS

GONG DANGGUO

SCHOOL OF MATERIALS SCIENCE AND ENGINEERING

2013

IN-SITU INFRARED SPECTROSCOPY STUDIES OF SURFACE REACTIONS OVER IRRADIATED PHOTOCATALYSTS

GONG DANGGUO

2013

IN-SITU INFRARED SPECTROSCOPY STUDIES OF SURFACE REACTIONS OVER IRRADIATED PHOTOCATALYSTS

GONG DANGGUO

SCHOOL OF MATERIALS SCIENCE AND ENGINEERING

A thesis submitted to the Nanyang Technological University

in fulfillment of the requirement for the degree of

Doctor of Philosophy

2013

Acknowledgement

First and foremost, I am deeply indebted to my supervisors Assoc. Prof. Chen Zhong and Dr. James Highfield (ICES) for the continuous encouragement and munificent support. Thank Prof. Chen for the freedom given to explore, continuous advisement to let me focus and valuable suggestions guiding my research along the way. Thank James for the involvement in every tiny part of my research, from idea discussion, experimental set up, data analysis to final thesis writing. I leant a lot how to be a good scientist from both of you, although I might not be one at this moment.

I would also like to express gratitude to Dr. Pierre Pichat (CNRS, France), Prof. Simon Pehkonen (Masdar Institute, Abu Dhabi, UAE) and Prof. Alex Orlov (Stony Brook, NY, USA) for frequent consultation, and to Dr. Zhong Ziyi and Ms. Jaclyn Teo (ICES) for giving the convenience to use their facilities.

It is almost impossible to finish this work without the help for various materials characterization from FACTS technicians Ms. Guo Jun, Ms. Heng Joon Hua Irene and ICES central lab technicians Ms. Wang Zhan April, Ms. Chia Sze Chen, Ms. Ong Li Li, Ms. Chen Qianhan and Mr. Wong Hon Yue Kenneth.

Countless discussions with my group members, Mr. Tang Yuxin, Dr. Lai Yuekun, Dr. Vishnu Priya Subramaniam, Dr. Cheng Yu Hua, Dr. Kanhere Pushkar Dilip, Dr. Wang Danping, Miss. Tay Qiuling and Miss. Lim Ying Wen Linda, have been fruitful to refresh and reshape my idea. FYP students Mr. Ho Weng Chye Jeffrey, Ms. Pearlie Low and Mr. Ng See Zhong Edison have done

quite a lot of work that contributes significantly to the thesis. Thank you all, I hope you also enjoyed the research.

Thank my friend Mr. Shen Youde, Mr. Wang Lei for witnessing me going through every hard time, comforting and backing up me all the time, and pushing me to take the ambitious adventure. Thank my friend Ms. Chen Ye, Ms. Lai Linfei and Mr. Ran Maofei for the happiness brought into the life in ICES.

Thank my parents, my sister and my wife, for the unconditional love and support all the time. Although you might not understand any tiny portion of my research, I hope I have made you proud.

Last but not least, thank the Environment and Water Industry Program Office (EWI) under the National Research Foundation of Singapore (grant MEWR 651/06/160) for funding the research and my scholarship.

Table of Contents

List of Figures

List of Tables

Synopsis

Interest in photocatalysis driven by solar energy has risen greatly over the past four decades due to the fact that it is one of the most promising approaches to help solve the energy crisis and effectively combat environmental contamination. TiO_2-based nanomaterials remain attractive candidates as photocatalysts due to their high photo-efficiency, strong oxidizing power, good stability, and non-toxicity. Great attention has been given to improving its conventional (UV-driven) performance by exploiting, *inter alia*, the synergy of mixed (anatase/rutile) phase junctions, or making more perfect crystals (defects act as charge recombination centers) without sacrificing texture (surface area) etc. In the last two decades, intensive studies have been devoted to overcoming arguably the greatest limitation of TiO_2, viz., its insensitivity to visible light. Early attention was given to bulk doping with transition metal ions but many act as recombination centers. This led to a related strategy with anions, where some success has been achieved with nitrogen as dopant. However, no major breakthrough is forthcoming as yet and other approaches are attracting serious interest, e.g., *sensitization* by narrow-band gap semiconductors, decoration with nanoparticulate metals having plasmon resonance absorption, or organic polymers less susceptible to photo-bleaching than conventional dyes. Furthermore, while major efforts have been expended in materials synthesis, characterization and testing, spectroscopic investigations at the reactant/catalyst interfaces are sparse. In particular, *in situ* studies at the photocatalyst surface are vital to unravel the mechanistic detail, yielding key information integral to the design and development of new materials with superior performance.

In the present work, two complementary techniques, Diffuse Reflectance Infrared Fourier Transform Spectroscopy (DRIFTS) and Attenuated Total Reflection (ATR) Fourier Transform Infrared (FTIR) Spectroscopy have been used for *in situ* investigations of some typical photocatalytic reactions at the gas/solid and liquid/solid interfaces, respectively. Commercial material, Degussa P25 TiO_2, was used mainly for system verification and fundamental studies on the state of material under band-gap excitation, especially ATR-FTIR, and as a benchmark (in pristine and metalized form) for novel visible-sensitized photocatalysts prepared in this thesis.

DRIFTS studies were made initially on P25 TiO_2 and its platinized form to establish any changes in state under illumination and its relation with the ambient gas environment, water vapour and O_2 in particular. Earlier reports of long-lived and reversible photochromism due to free carriers (electrons) were confirmed, and a detailed study made of the conditions that optimize the effect. The photo-generated charge carriers recombine quickly in dry inert atmosphere (N_2), but are stabilized in the presence of H_2O vapor, which is believed to act principally on the surface-trapped holes. The electron spectrum shows a featureless continuum absorption of increasing intensity towards lower frequency characteristic of free carriers in the bulk. However, deviations from the power law are attributed to partial trapping at surface Ti^{4+} sites. Under inert gas, and depending on the humidity level, photo-adsorption of water is promoted by surface-trapped holes and repelled (or substantially weakened) by surface-trapped electrons. Oxygen acts as a charge-recombination center and rapidly quenches the electron spectrum in a reversible manner. Addition of a more powerful hole-scavenger, e.g., ethanol, results in the accumulation of excess electrons due to irreversible oxidative photo-abstraction of H. These electrons migrate to the surface and effect photo-metallization, viz., reduction of adsorbed metal ions, such as Pt^{4+}, to

deposit metallic Pt nanoparticles. In an O_2-rich atmosphere, ethanol itself is seen to be mineralized over P25 TiO_2, i.e., photo-oxidized to CO_2 and H_2O via acetaldehyde and acetic acid (acetate) intermediates.

Due to the strong absorption of IR radiation by solvent (H_2O in this case), the investigation of photo-reactions at the liquid/solid interface has been severely hampered until recently. ATR-FTIR is applied to liquid-phase photo-oxidation of ethanol over TiO_2, both in the pristine and metalized form. Intermediates in both the adsorbed and bulk forms were identified and tracked to elucidate the reaction pathway and assess the rate-limiting step(s). Just as in DRIFTS (*vide ultra*), development of charge carrier absorption in the pristine photocatalyst was also seen in ATR-FTIR and served as a marker of O_2 depletion during photo-degradation experiments. Pt deposits act as efficient electron sinks (as judged by quenching of the continuum absorption) and activate the reductive component of the photocatalytic cycle (through ionosorption of dioxygen and/or reduction of protons), further enhancing the overall efficiency.

Knowledge learnt from Degussa P25, a *de facto* standard, was then applied to investigate two groups of in-house prepared visible light active photocatalysts. These comprised (1) melon-modified titanate/TiO_2 prepared from urea and (2) Ag modified titanate/TiO_2. The abundance of surface OH groups on titanate promotes the efficient formation of melon, as compared to pre-formed anatase TiO_2. *In-situ* DRIFTS confirmed the presence of melon, an organic polymeric semi-conductor, and further showed that it is a photo-stable visible light sensitizer. Melon-modified titanate/TiO_2 nanomaterials were active for degradation of organic dye Methyl Orange (MO), and oxidation of ethanol under visible light irradiation. Decoration of TiO_2 with Ag nanoparticles extends the absorption range into the visible due to the surface plasmon

resonance (SPR) effect. These materials were also active in degradation of MO dye and ethanol photo-oxidation under visible light irradiation. The best performance for the Ag-decorated material in visible light and the pristine TiO_2 under UV excitation were obtained after identical thermal treatment (450 °C) thus showing the importance of the semi-conductor. A model is proposed for visible photo-activity via SPR-promoted electron transfer from Ag metal to TiO_2.

It is hoped that the *in-situ* spectroscopic investigations at the reactant/catalyst interface expounded in this Thesis give major impetus to subsequent research in the field. More specifically, the real-time inter-relationship between changes in the optical state of the catalyst, adsorbed intermediates, and their correlation with performance, provides valuable clues towards the rational design of better photocatalysts.

Chapter 1. Introduction

1.1 Background and current challenges

Energy and environment are two key problems facing the world in the 3rd millennium.[1] As many Third World nations struggle towards technical modernization, the consumption of hydrocarbon fuels (petroleum, natural gas and coal) is slated to increase dramatically. Unfortunately, the sustained use of conventional fuels poses an ever increasing threat to the natural environment. Since most of the energy on the Earth is directly or indirectly obtained from the sunlight, solar-energy-driven processes look particularly attractive in the long term. In principle, solar energy can be harnessed both to provide renewable hydrogen and to combat environmental pollution by the process of photocatalysis.

Since the discovery of photocatalytic water splitting on a TiO_2 anode under ultraviolet (UV) light by Fujishima and Honda in 1972,[2] enormous efforts have been devoted to its development during the past four decades. Unfortunately, progress has been hindered by its mechanistic complexity, together with the fact that it is a thermodynamically uphill (endergonic) process. On the other hand, applications of photocatalysis to environmental remediation (photo-oxidation & mineralization of organic pollutants) are already close to commercialization, mainly because these are downhill (exothermic) processes and the concentrations of pollutants are generally low already.

Development of highly efficient, especially visible light active, photocatalysts is an increasingly intense field of study. However, although various materials, including well-established semiconductor oxides like TiO_2 and non-oxides, e.g., chalcogenides,

have been developed for hydrogen generation and environmental remediation, mechanistic investigations under working conditions are limited to date. Conventional surface science techniques are valuable but can strictly be classified as *ex-situ* due to the almost invariable requirement of high vacuum. *In situ* mechanistic investigations are crucial to elucidate the photocatalytic process and serve as the key scientific basis for the rational design of better photocatalysts. These bridge the gap between intrinsic properties of materials and their extrinsic catalytic performance under working conditions.

1.2 Objective & novelty

In the present work, we investigate photocatalytic reactions under various conditions by *in situ* spectroscopies: the gas/solid interface by Diffuse-Reflectance Infrared Fourier-Transform (DRIFT), and the liquid/solid interface by Attenuated-Total Reflectance Fourier-Transform Infrared (ATR-FTIR). The real time information related to changes in state of the photocatalyst under working condition, and mechanism elucidation, i.e., the sequential formation of intermediates and products, and identification of the rate-determining step(s) provides a fundamental correlation between material properties and performance.

A scheme of the overall experimental methodology is shown in Figure 1-1. To verify the instrumental set-up and for fundamental studies on the state of material under band-gap excitation, a "benchmark" photocatalyst, viz., Degussa P25 TiO_2 was employed, initially at the gas/solid interface, and then at the technically more arduous liquid/solid interface. With this as reference point, further spectroscopic investigations were made on some newly developed visible light active photocatalysts.

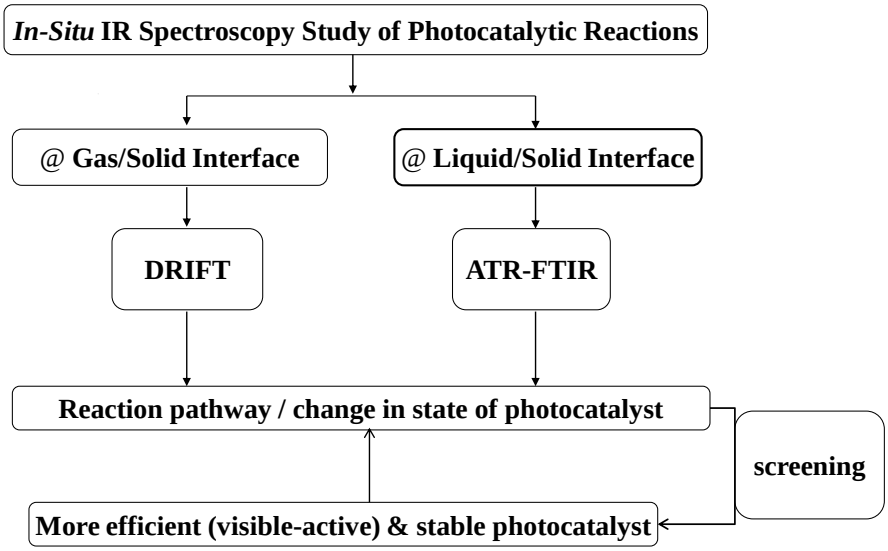

Figure 1-1 Experimental methodology

The three distinct experimental topics in order of increasing complexity were:

(1)Investigate photocatalytic reactions at the gas/solid interfaces: trace the changes in state of commercial photocatalyst P25 as indicated by the development/removal of quasi-continuum infrared band due to trapped electrons, and the effect thereon of simple molecules such as water and dioxygen; photo-deposition of metal nanoparticles and their effect on infrared absorption, including mechanism elucidation in several typical photocatalytic reactions, such as ethanol photo-oxidation.

(2)Develop and optimize the ATR-FTIR (thin layer) methodology; investigate ethanol photo-oxidation as model reaction at the liquid/solid interface and observe changes in state of photocatalysts and reaction pathways.

(3) Investigate the efficiencies and stabilities of two in-house prepared visible light active photocatalysts in model reactions, and explore the photocatalytic mechanisms.

The novelty of this work lies on the observation of changes in state of photocatalysts under working conditions, such as the accumulation and quenching of trapped electrons, and its correlation with the reaction efficiency. This feature is found to be a valuable marker of kinetic balance (or imbalance) between redox half-reactions proceeding at the reactant/catalyst interface. In addition, this work also extends the scope to explore some new visible light active photocatalysts.

Chapter 2. Literature Review

In this chapter, the principle of photocatalysis and the historical development of photocatalysts, featuring doping and surface modification of TiO_2, are introduced. This is followed by a review of mechanistic investigations of photocatalytic reactions at the reactant/catalyst interface, with particular emphasis on *in situ* infrared spectroscopic techniques.

2.1 Photocatalysis and titanium dioxide (TiO_2)

In fundamental terms, photocatalysis has a long history, but its recognition as a potential renewable energy alternative was essentially triggered as a response to the so-called "oil embargo" of the early 70s. This was given added impetus by the discovery of photocatalytic water splitting (H_2 generation) on a TiO_2 coated electrode by Fujishima and co-workers in 1972.[2] Even after 4 decades, TiO_2-based materials still remain attractive due to their inherent advantages (*vide infra*), although many alternative candidates, e.g., metal oxides like ZnO, Fe_2O_3, WO_3, MnO_2, chalcogenides like CdS, and non-oxides like AgX (X = halide) and graphitic C_3N_4, are receiving increasing attention. Nevertheless, TiO_2 is by far the most popular and well-studied semiconductor photocatalyst due to its high photo-efficiency, high oxidizing power, good stability, insolubility in water, and its non-toxic properties.[3] It has a wide range of potential application, as shown schematically in Figure 2-1.

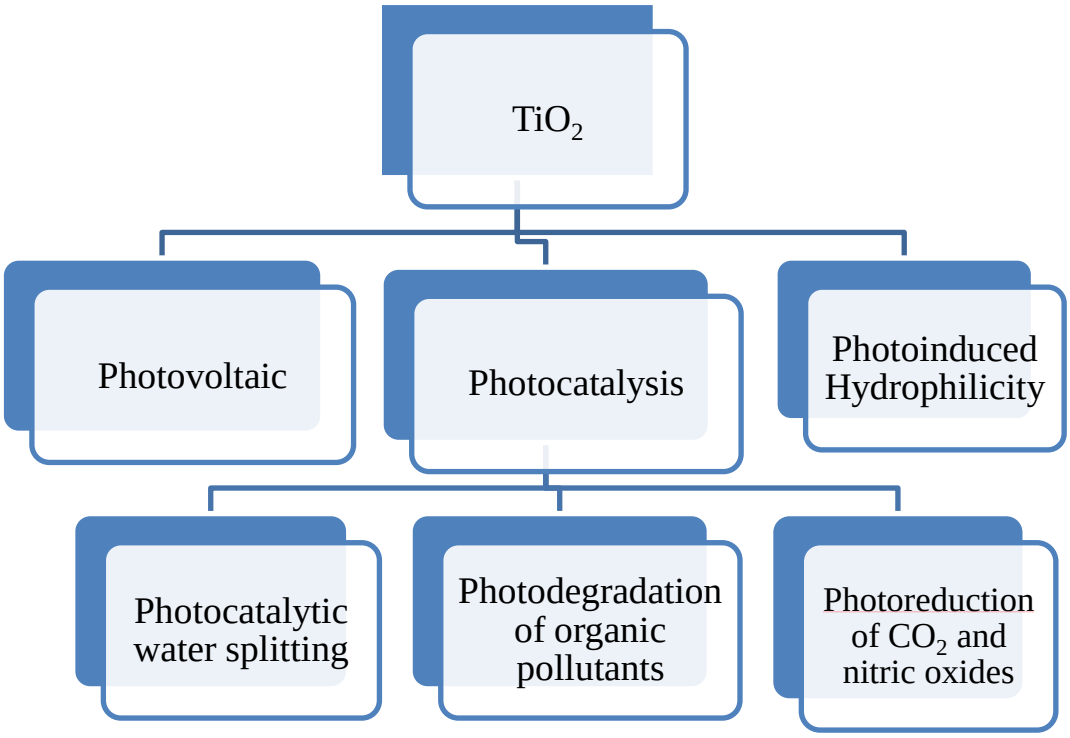

Figure 2-1 Photo-induced application of TiO_2

When a semiconductor oxide like anatase TiO_2 is illuminated with photons of energy exceeding, or equal to, the band-gap energy electrons in the valence band are excited to the conduction band, leaving behind "holes" (positive charges) in the valence band (Eqn. 2.1). Depending on their lifetimes, and in the absence of charge recombination, these photo-generated electrons and holes (free carriers) eventually migrate to the surface where they may drive redox processes that effect desirable chemical change in a variety of adsorbed species. The key reactions are summarized below:

$$TiO_2 \xrightarrow{hv} e^- + h^+ \quad (2.1)$$

$$e^- + h^+ \rightarrow heat \quad (2.2)$$

$$h^+ + R-H \rightarrow R_{ad}\bullet + H^+ \quad (2.3)$$

$$h^+ + OH^- \rightarrow OH\cdot \quad (2.4)$$

$$e^- + M^{n+} \rightarrow M^{(n-1)+} \quad (2.5)$$

$$2e^- + 2H^+ \rightarrow H_2 \quad (2.6)$$

$$e^- + O_2 \rightarrow O_2 \cdot^- \quad (2.7)$$

Typically, most of the photo-generated electrons and holes recombine quickly and release heat if there are no reactants in the environment (Eqn. 2.2). Free charge carriers (holes/electrons) that migrate to the nanoparticle surface will become available to drive redox chemistry in the surrounding environment, e.g., by reacting with adsorbed H_2O or O_2 to produce highly oxidative radicals (as shown in Figure 2-2):[4] The redox potential for photogenerated holes in TiO_2 is +2.53 eV. These holes can directly react with surface adsorbed organic compounds or H_2O (Eqns. 2.3, 2.4). When reacting with water, they will produce hydroxyl (OH) radicals, which still have very high oxidizing power of +2.27 eV. These can further react with adsorbed organic molecules; e.g., abstracting H-atoms (as protons) from hydrocarbons, alcohols, etc. The redox potential for conduction band electrons is –0.52 eV. These electrons can be involved in direct reduction, e.g., generating H_2 from protons, or reducing metal ions (Eqns. 2.5, 2.6). More commonly, they are trapped at Ti(IV)O-H surface sites leading to Ti(III)O-H^- species with some loss of reducing power. Excited electrons can also react with oxygen (from the gas phase) to produce (photo-) adsorbed superoxide ion (Eqn. 2.7). These radicals can further react with a wide variety of organic ad-species (from the air or water) leading to complete mineralization, viz., total oxidation to CO_2 and H_2O. This is the basis of applications in environmental remediation.

To ensure the photo-stability of TiO_2, the reduction process and oxidation process should proceed simultaneously and at compatible rates in order to sustain charge

balance. Generally, the build-up of excess charge in the photocatalyst is deleterious to performance in TiO_2 and often leads to photo-corrosion in less stable materials.

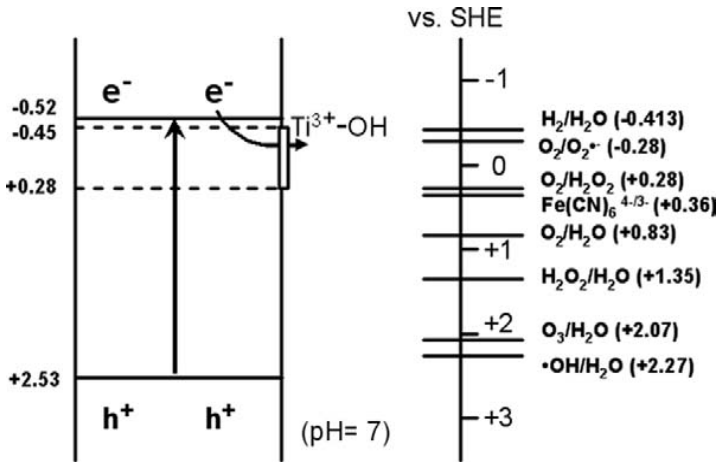

Figure 2-2 Schematic diagram showing the potentials for various redox processes occurring on the TiO_2 surface[4]

2.2 Development of highly efficient photocatalysts

Many attempts to improve the performance of TiO_2-based materials have been made, but the task is complex and it's fair to say that only modest gains have been achieved. The main approaches can be sub-classified into three groups:

(1) To improve the efficiency of pristine TiO_2 by fabricating it in higher surface area form while maintaining a high degree of crystallization on the nano-scale,[5,6] preferably with a high percentage of active facets; [7-15] This is generally difficult because the above attributes are mutually antagonistic and often self-cancelling.

(2) To enhance the separation of photo-generated charges; e.g., by synthesizing mixed-phase TiO_2, akin to the commercial benchmark Degussa P25 (typically 80% anatase TiO_2, 20% rutile TiO_2), or anatase-TiO_2 (B) core-shell structured nanofibers;[16,17] or by depositing noble metals to act as "electron sinks";[18]

(3) To extend the optical response into the visible light range; e.g., by doping with anions or cations, [19-21] and/or creating composites with other narrower band gap semiconductors like CdS, [22-24] or by utilizing the surface plasmon effect of noble metal nanoparticles.[25-27]

2.2.1 Optimizing the crystallinity, surface area and exposed facets

As a special type of heterogeneous catalyst, photocatalysts also benefit, in principle, from similar textural effects, e.g., dispersion into smaller particles increases the specific surface area, thereby promoting faster and stronger adsorption of reactants at the interface, ultimately leading to higher rates. Problems of charge recombination already mentioned can be mitigated by enhancing the crystallinity of the photocatalyst. Unfortunately, a process that most readily increases the crystallinity, viz., annealing or thermal treatment leads inexorably to surface area loss by sintering, thus dictating a practical compromise between these two factors.

Titania exists naturally in four phases, namely anatase, rutile, brookite and TiO_2(B). Their crystal structure, band gap and density parameters are summarized in Table 2-1.[3,28] Rutile is the most stable phase at high temperatures, usually existing in large particle size and low surface area form, while the other three phases are typically obtained at lower temperatures in relatively smaller particle size and larger surface area. As a new phase, TiO_2(B) was first synthesized in 1980 by Marchand et al.,[29] and although it has lower photoactivity than anatase TiO_2, it has since attracted lots of attention as an alternative photocatalyst due to its relative open structure.

Anatase and rutile TiO_2 have been well studied in photocatalysis, in part due to their ease of preparation. Of the two common forms, anatase has the higher band-gap and a conduction band minimum sufficiently negative to reduce protons. Its

photoactivity is also generally superior to that of rutile. However, the latter is the most completely characterized by surface science techniques because large single crystals of anatase have been difficult to prepare. For anatase TiO_2, both the theoretical prediction and experimental results show that its {001} facets are more active than {101}facets, however, the latter normally dominates the surfaces in the equilibrium state. By fluorine-termination of anatase TiO_2, the desired {001}facets can comprise up to 50% of the surface.[7] However, a greener chemical process to efficient photocatalysts (by control of exposed facets) would be preferred to the current method of etching in HF.

Table 2-1 Bulk properties of TiO_2 in its different phases

Crystal Structure	**Crystal System**	**Band Gap (eV)**	**Density (g/cm^3)**
Rutile	Tetragonal	3.00	4.13
Brookite	Orthorombic	3.13	3.99
Anatase	Tetragonal	3.20	3.79
TiO_2(B)	Monoclinic	3.20	3.64

2.2.2 Development of mixed-phase photocatalysts

Although the relative photocatalytic efficiency of anatase and rutile TiO_2 is still under debate, it is now well-established that mixed-phase photocatalysts show enhanced performance as compared to either single phase. The success of Degussa P25 TiO_2, the benchmark widely used for comparison of other photocatalysts, is a prime example. Commercial P25 is made by the "aerosil process", yielding individual particles consisting of roughly 20 % rutile and 80 % anatase. [30]The high performance

is attributed to the abundance of "rectifying" phase junctions that facilitate uni-directional (and opposite) flow of free carriers, thereby facilitating charge separation.[31] However, the nature of the atomic level contact between anatase and rutile is still not well understood,[32] and recent work [33] has demonstrated that the distribution of phases can be further improved for photocatalytic action by controlled annealing.

Based on the above principle, anatase and TiO_2(B) mixed-phase samples have been synthesized by hydrothermal treating of titanate nanobelts, and their efficiencies were found to be comparable to that of commercial Degussa P25.[16,17]

2.2.3 Development of visible light active photocatalysts

While titania (TiO_2) is an excellent photocatalyst, it has one key limitation. Due to its wide band-gap (see Table 2.1), it only responds to ultraviolet (UV) light, which constitutes less than 5% of the solar power spectrum. For better use of sunlight, various ways of "sensitizing" TiO_2 to the visible range (~40% of the solar spectrum) have been under intensive investigation in the last decade. Historically, the most popular approach has been by doping with colour centers, such as transition metal cations, but with mixed results. This has been superseded by attempts to "narrow" the band-gap of TiO_2 using anion dopants like N, S, and C, or most recently, by various means of surface modification, e.g., by mixing with narrow band-gap semiconductors, noble metal particles (Ag, Au, etc.) having plasmon resonance absorption, or colored organic polymers like g-C_3N_4. Significant attention is also being paid to non-TiO_2 based materials.

2.2.3.1 Bulk doping of TiO_2

The optical response of any material is determined by its intrinsic electronic structure, which is a strong function of chemical composition, crystal structure, and, to some extent, physical dimension (quantum size effects). The chemical composition of TiO_2 can be altered either by replacing the cation (titanium) or the anion (oxygen), referred to here as metal and non-metal doping, respectively.

When TiO_2 is doped with altervalent transition metal ions, such as Co^{II}, Ni^{II}, Cu^{II}, $Fe^{II/III}$, Cr^{III}, V^{III}, Mn^{IV}, Nb^{V}, $Mo^{V/VI}$, an electron occupied level will be formed and the electrons are localized around each dopant.[3] As the dopant concentration increases, the localized level shifts to lower energy and can even reach the top of valence band for Co^{II}.[20] Electrons can be excited from this defect state to the conduction band by photons with lower energy, i.e., in the visible range.

Band gap narrowing of TiO_2 can also be achieved by non-metal doping, using anions such as N, C, B, F, P, S and I.[3,21,34-37] N and C doping are the two most investigated cases. In Asahi et al.'s pioneering work,[21] substitutional doping of N (for O) was proposed as the most effective band gap narrowing due to mixing of p states between N and O. However, accumulating evidence suggests that N-doping introduces mid-gap levels slightly above the O 2p valence band.[3] For C-TiO_2, the dopant introduces deep states in the gap.[36,37] The intrinsic defects of TiO_2, such as reduced Ti species and oxygen vacancies, also lead to the formation of localized states which may merge to form sub-band gap level, thus creating a lower energy excitation pathway.[3,38]

The actual photocatalytic efficiency of doped TiO_2 is largely dependent on dopant concentration and homogeneity, which is highly-dependent on the preparational method. Although doping with either metal or nonmetal elements definitely confers

visible light absorption and associated photo-activity, the overall performance under UV-Vis irradiation may even fall below that of pristine TiO_2 due to deterioration of crystallinity and/or creation of particular defect sites that tend to promote charge recombination.

2.2.3.2 Metal and narrow band gap semiconductor sensitization

An alternative approach has been to create TiO_2-based composites with colored (narrow band gap) semiconductors such as CdS, CdSe, etc. [22-24], where a synergy is evident due to directional inter-phase charge transfer analogous to mixed-phase TiO_2. However, resort to narrow band-gap materials introduces its own key drawback, i.e., instability via photocorrosion.

Noble metal nanoparticles have been widely used as surface modifiers for TiO_2-based photocatalysts. These enhance charge separation by acting as "electron sinks", thereby promoting efficient photo-reduction. The pioneering work by Sclafani et al[39] studied the effect of silver deposits on the photocatalytic activity of TiO_2. Noble metal nanoparticles have the unique property of being optically excited even in the visible region due to the so-called surface plasmon resonance (SPR) effect. These are now under intensive investigation as potential visible sensitizers. Although gold or silver nanoparticles supported on insulating oxides already show photocatalytic activity under visible light,[40,41] this has hitherto been attributed to artifacts, e.g., enhanced thermal catalysis caused by equilibrated local-heating effects [40] and/or instantaneous heat-assisted photo-excitation of Ag electrons to higher energy states. [41] However, a series of papers have now reported that when Au nanoparticles are supported on a photo-reducible oxide like titania, the visible photo-effect is more pronounced and, more importantly, the *action spectrum* for photo-activity resembles the SPR absorption spectrum implying that, by analogy with the better known phenomenon of

dye sensitization,[42] charge injection from the metal to the semiconductor is indeed possible.[27,43,44] The intriguing possibility of visible sensitization of wide band gap semiconductors by noble metal nanoparticles has just been reviewed.[45] Compared to Au, Ag is a cheaper and more practical alternative, thus of great interest.

2.2.3.3 Surface modification with melon and graphitic carbon nitride

Although N-doped TiO_2 has been extensively studied, the origin of the visible light response is still under debate. Most of the preparation methods use an organic compound as N-source in a "wet" chemical process, usually followed by calcination at mild temperature. The choice of nitrogen source, as well as the preparational conditions, have a large influence on photocatalytic activity in the resulting product, possibly due to the presence of diverse nitrogen species, such as oxidic (NO_x), nitridic or amidic (NH_s). The most commonly used nitrogen source is urea and its derivatives. A careful recent study by Mitoraj and Kisch [46-48] based on urea has clearly proved that a condensed polymeric layer of melon is formed on the TiO_2 surface, and that this is the chromophore responsible for visible light activity. As this surface-overlayer-based system is quite distinct from the (bulk) doped type, they state that it is best classified as "melon-modified" TiO_2.

The formation of melon from urea is a condensation process involving the surface hydroxyl groups of the substrate. It can be conveniently divided into three stages:[47,48] (1) thermal decomposition of urea into isocyanic acid and ammonia at 320~400 °C （Eqn. 2.8); (2) cyanamide, and eventually melamine, formation by the reaction of iscocyanic acid with surface OH groups of TiO_2 (Eqns. 2.9, 2.10). The balance of these reactions is melamine formation from urea in the presence of TiO_2 at 400 °C （Eqn. 2.11); (3) melamine then undergoes polycondensation to form melem, melam

and finally melon (as shown in Figure 2-3). The (yellow) melon is believed to be the principal structure conferring visible light sensitization.

$$(NH_2)_2CO \xrightarrow{320\sim400^oC} HNCO + NH_3 \quad (2.8)$$

$$\equiv Ti\text{-}OH + O=C=N\text{-}H \longrightarrow \equiv Ti\text{-}NH_2 + CO_2 \quad (2.9)$$

$$\equiv Ti\text{-}NH_2 + H-O-C\equiv N \longrightarrow \equiv Ti\text{-}OH + H_2N-C\equiv N \quad (2.10)$$

$$6(NH_2)_2CO \xrightarrow{400^oC/TiO_2} C_3H_6N_6 + 6NH_3 + 3CO_2 \quad (2.11)$$

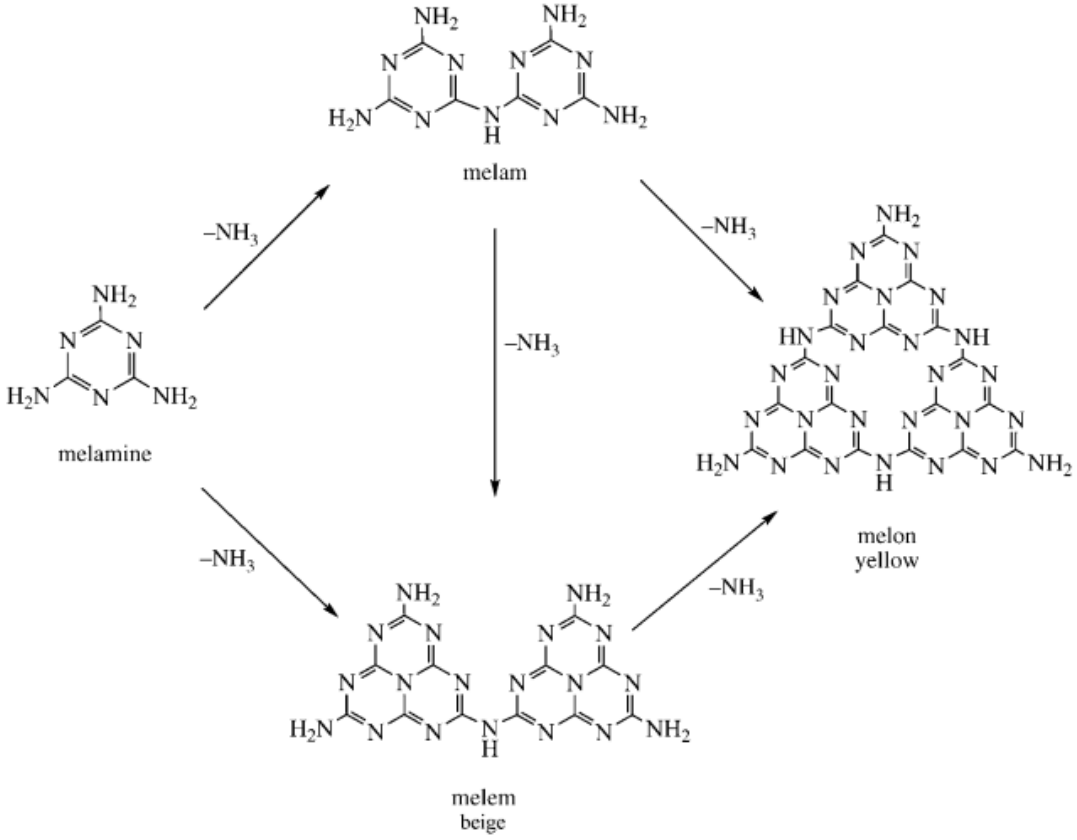

Figure 2-3. Scheme illustrating polycondensation of melamine to melam, melem and melon[47]

It is interesting to note that a more condensed graphitic carbon nitride (g-C_3N_4)-based sample, sharing the same heptazine unites with melon but with a higher degree

of polymerization, has been extensively studied for photocatalytic water splitting under visible light recently.[49-51]

2.3 *In situ* surface characterization methods

Elucidation of the reaction mechanism is vital to gain insight into the current limitations of photocatalysts and to improve their efficiency and stability by rational design. Despite extensive exploration of a wide range of (modified) materials in multitudinous photocatalytic applications, not much molecular level information is available on the processes occurring at the respective reactant/catalyst interfaces. Most of the current studies are based on analysis of stable (isolable) reaction intermediates. Thus, more *in situ* studies at the photocatalyst surface under working conditions are essential to unravel the mechanistic detail.

To investigate the properties of surfaces and interfaces, a well-established set of spectroscopies are already available, e.g., electron energy loss spectroscopy (EELS), X-ray photoelectron spectroscopy (XPS) and ultra violet photoelectron spectroscopy (UPS).[52] Unfortunately, many of these require vacuum conditions such that studies of interfacial processes in real time are "*de facto*" ruled out, as are mechanistic studies unless stable (long-lived) intermediates are involved. These techniques are still powerful but are generally now termed *ex-situ* methods. As evidence has grown that the physico-chemical properties, and even the topology, of surfaces can be influenced substantially by their environment, the major trend in surface and catalytic science in the last 20 years has been towards *in-situ* measurements. [53]

Techniques that are more amenable, or have been developed, for *in-situ* studies include, e.g., Infrared spectroscopy (IR), X-ray absorption spectroscopy (XAS), sum frequency generation (SFG) and surface enhanced Raman spectroscopy (SERS).

Among these, infrared spectroscopy is one of the most versatile. Furthermore, an FTIR spectrometer is a relatively common laboratory item because it is inexpensive and quite easy to learn and operate. FTIR provides information on vibrations at surfaces (and the underlying sub-surface), as well as characteristic vibrations of adsorbed species at these surfaces.

The most widely used and straightforward type of IR spectroscopy is the transmission method, which measures the absorption of infrared irradiation at specific wavelengths as it passes through the sample. However, heterogeneous photocatalysts are almost invariably solid powders, which scatter light strongly. These sample types are generally not amenable to transmission measurements. Although the so-called "pressed-wafer technique" continues to be used, its popularity is on the wane due to the exacting problems of creating self-supporting (microns-thick) wafers that are extremely fragile and difficult to mount. In pressed form, the sample also may not allow proper access of reactant gas to the surface. Alternative techniques are now available that take advantage of the remarkable sensitivity of FT-based signal processing. Among these *in-situ* options, diffuse reflectance infrared Fourier transform (DRIFT) spectroscopy is specifically designed to facilitate studies on loose powders, thereby simulating a packed-bed catalytic reactor. The emerging technique of choice for corresponding studies at the optically more demanding liquid/solid interface is attenuated total reflection Fourier transform infrared (ATR-FTIR) spectroscopy.

2.3.1 DRIFT spectroscopy

In DRIFTS, the infrared irradiation that penetrates several particle layers is remitted or reflected isotropically (as shown in Figure 2-4), hence the term *diffuse reflectance*.

The DRIFT accessory collects reflected photons over a large angle range and provides information simultaneously on intermediates (species in the adsorbed state), reactants and products (species in the gas phase), as well as the condition of the underlying catalyst in real time.

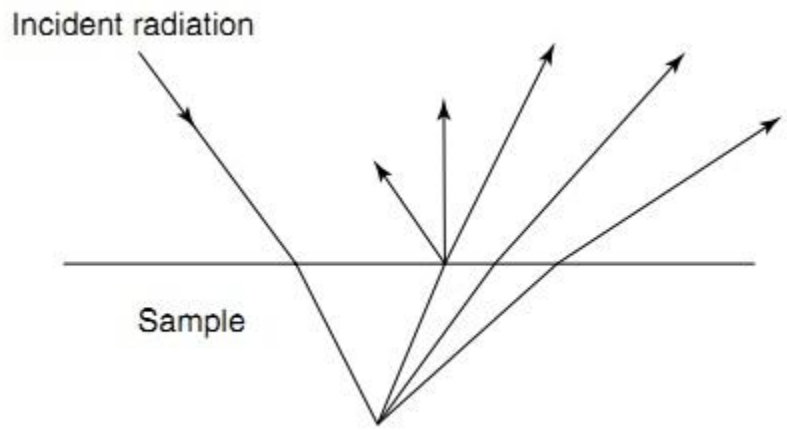

Figure 2-4 Illustration of diffuse reflectance

This method was pioneered by Griffiths et al.,[54] mainly for studies at the gas/solid interface. All modern DRIFTS accessories are designed to reject the specular component, which has undergone no penetration and, thus, contains no information on absorption features. However, DRIFTS has some limitations, especially in terms of temperature definition.[55]

2.3.2 ATR-FTIR

While traditional (pressed-disk) transmission and Diffuse Reflectance (DRIFT) techniques for *in-situ* studies of powdered samples at the gas/solid interface have continued to dominate research over the last two decades, there is a growing need to extend investigations to catalysts immersed in liquids as reactants and/or solvents.

Generally, IR spectroscopy is difficult to apply to liquid/solid interfaces by conventional transmission because of the strong absorption of the solvent and scattering phenomena at the substrate/sample/solution interface.

The optical sampling variant known as Attenuated Total Reflectance (ATR), which greatly reduces interference from solvent absorption due to shallow penetration by the evanescent IR probe wave, is now emerging as the tool of choice to derive qualitative and semi-quantitive information at the liquid/solid interface.[56,57] Unusual mediating effects of liquid water on the reactivity of adsorbed species have also been claimed in a recent review of this technique.[58] However, the ATR signal has a complex origin and is not amenable to theoretical treatment. Thus, no simple relation exists between absorption (or extinction) coefficient and sample concentration, at least across a wide spectral energy range.

ATR-FTIR is one kind of internal reflection infrared spectroscopy in which the sample is placed in contact with an internal reflection element (IRE) with high refractive index. Although the phenomenon of internal reflection was discovered as early as the 17th century, the concept and feasibility of applying this phenomenon to measure samples in close contact with an IRE was only established by Harrick in the 1960s.[59,60]

Total internal reflection occurs only when the angle of incidence is larger than a certain angle, called *the critical angle*. Considering a light radiation passing from an IRE (with high refractive index n_1) into the sample (with low refractive index n_2), the light emanating from the interface is partially reflected backwards to the IRE and partially transmitted into the sample (as shown in Figure 2-5). The geometry of incidence, reflectance and transmittance of the light is determined by Snell's law (Eqn.

2.12). When the incident angle is increased sufficiently, the transmitted angle reaches 90°. At this point no light is transmitted into the sample and total reflection occurs. The critical angle θ_c is determined by the ratio of n_2/n_1 ($n_2 < n_1$; the refractive index of the sample must be smaller than that of the IRE), because $\sin\theta_t = 1$ in this situation.

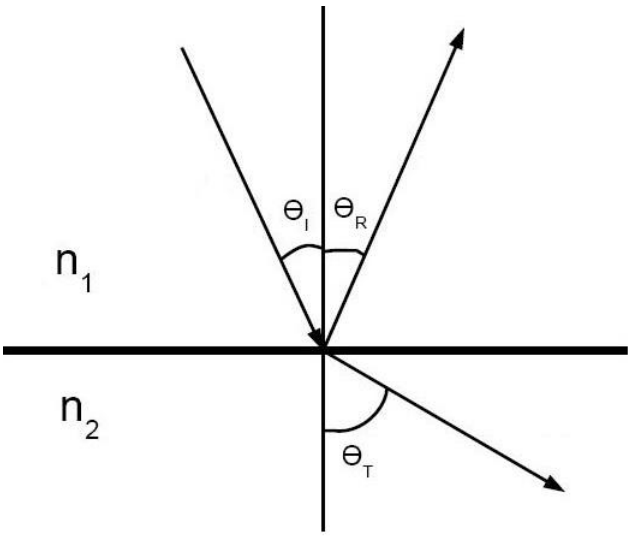

Figure 2-5 Schematic representation of Snell's law

$$n_1 \sin\theta_i = n_2 \sin\theta_t \tag{2.12}$$

$$\sin\theta_c = \frac{n_2}{n_1} \tag{2.13}$$

From Maxwell's theory, an evanescent wave perpendicular to the total reflection surface is formed under this condition. If a fraction of the energy of this wave is absorbed by the sample, the propagating wave is attenuated. The penetration depth is positively related to the wavelength (Eqn. 2.14), so a higher absorption from the sample is expected in the long wavelength range.

$$d_p = \frac{\lambda}{2\pi\sqrt{(n_1^2 \sin^2\theta - n_2^2)}} \tag{2.14}$$

For ATR-FTIR, infrared beam is focused onto the edge of the IRE, then reflected or "bounced" several times along the IRE, and finally directed to a suitable detector (see Figure 2-6). Although total reflection occurs at the sample/IRE interface, infrared radiation (the evanescent wave) penetrates a short distance into the sample, where it can be absorbed.[56] Each bounce results in incremental absorption by the sample, such that the integrated result of multiple bounces is a higher absorption (better sensitivity). Something akin to an absorption spectrum of the sample, with the aforementioned provisos, can thus be obtained.

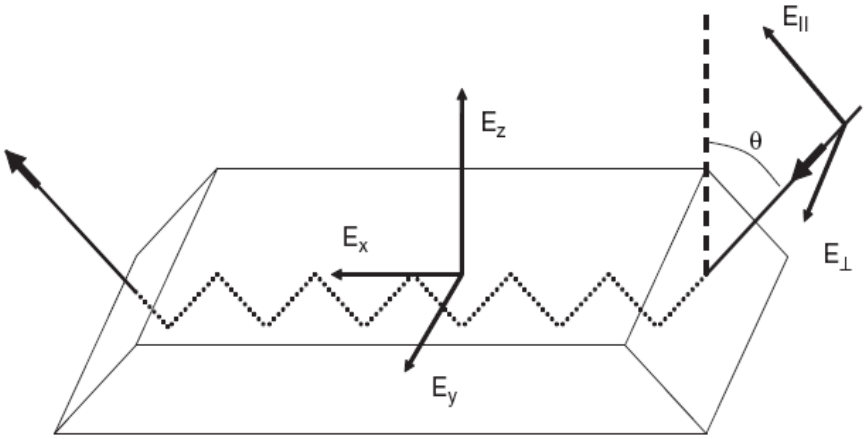

Figure 2-6 ATR principle[56] where θ is the angle of incidence; $E_{//}$ and $E_{\perp}$ denote the direction of the electric field components of the incident light with respect to the plane of incidence (x, z). E_x, E_y, and E_z are the electric field components with respect to a coordinate system fixed on the IRE.

The great advantage of ATR-FTIR is that it simultaneously provides vibrational information on dissolved or adsorbed reactants, intermediates, products, and even the catalyst itself (shown in Figure 2-7).[56] But by the same token, such a holistic measurement can be difficult to unravel in terms of assignment of IR peaks and analysis of the catalytic process.

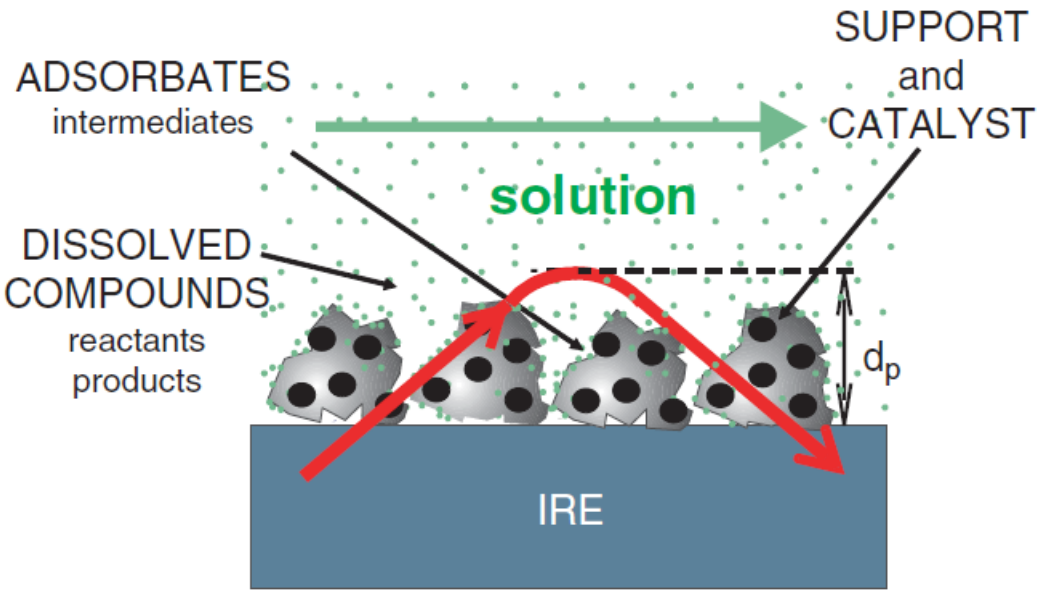

Figure 2-7 *In situ* ATR-FTIR spectroscopy of heterogeneous solid/liquid catalytic reactions gives simultaneous information on both dissolved and adsorbed species[56]

2.4 Investigation of photocatalytic processes by *in-situ* infrared spectroscopy

2.4.1 The gas/solid interface

Using DRIFTS, Hoffmann's group have discovered an infrared continuum (free-electron-like) absorption in irradiated TiO_2 that decays only slowly over several minutes.[55] This corroborates earlier studies of long-lived photochromism in TiO_2 observed using UV-visible photoacoustic spectroscopy.[61] The Hoffmann group also reported a pronounced Stark effect, viz., shifts in the vibrational frequencies of surface hydroxyl groups in the vicinity of deep and shallow electron traps.[62] Elsewhere, DRIFTS has been employed for, *inter alia*, studies of photo-oxidation of hydrogen sulfide,[63] nitrogen monoxide,[64] gaseous formaldehyde,[65] ethanol,[66] acetone,[66,67] benzene vapor[68] and for photo-reforming of methanol over platinized TiO_2.[69]

Chuang and Yu[66] reported that the photo-oxidation of ethanol over TiO_2 depends on the coverage of $CH_3CH_2OH_{ad}$/$CH_3CH_2O_{ad}$ and H_2O_{ad}. When ethanol is present at low coverage, mainly CO_2 is produced via a parallel/series reaction pathway, with formate ($HCOO_{ad}^-$) as a major intermediate. In contrast, at high ethanol coverage acetate ($CH_3COO^-_{ad}$) was the primary intermediate species, which further oxidized to CO_2.

As many chemical reactions involve several elementary steps in sequence, there is often a slow step which controls the overall rate. This is known as the *rate-determining step (RDS)*, and it is the most important to activate catalytically. In principle, it can be recognized from the build-up of an identifiable intermediate, although there can also be so-called "spectator species" that form in a side reaction that proceeds no further, instead equilibrating by back-reaction. Taking ethanol again as probe molecule, it has been confirmed that $CH_3COO^-_{ad}$ is the major intermediate of the photo-oxidation, and the rate typically drops (often inversely) as the acetate accumulates to a steady-state. Furthermore, the required chemical oxidant (molecular oxygen) must also be activated, such that oxidant supply eventually becomes rate-limiting in the total mineralization of ethanol.[70] Some important findings by DRIFTS are summarized in Table 2-2.

Table 2-2 Summary of notable DRIFTS observations relating to photocatalysis over TiO_2 based photocatalysts

Sample/Condition	Observation	Reference
Degussa P25 & in-house prepared anatase/ vacuum	•Continuous IR absorption extending to high frequency due to trapped electrons; surface trapping at Ti(IV)OH centers leads to Ti(III)O-H. •Intensities and positions of surface hydroxyl groups absorption sensitive to trapped electrons; reversible abstraction of trapped electrons by O_2.	Hoffmann et al. [55,62,71]

Degussa P25 /ethanol	•Intermediates CH_3CHO, CH_3COOH, HCOOH, CO_2 and H_2O identified; •Ethanol photo-oxidation pathway highly dependent on relation $CH_3CH_2OH_{ad}$ /$CH_3CH_2O_{ad}$ and H_2O_{ad}; •Oxygen supply is the rate-limiting step; •Rate inhibition by adsorbed carboxylate species	Anderson et al.[72]; Chuang et al.[66,70]
Degussa P25 /water	• H_2O desorption from TiO_2 surface during UV irradiation attributed to heating; • Reduced TiO_2 surface hardly adsorbs H_2O.	Anpo et al.[73]
Pt/TiO_2 (in-house prep.) /methanol:water	• Photo-metallization $\rightarrow$ high frequency continuum absorption • Photo/thermal synergy drives methanol reforming	Highfield et al.[69]

2.4.2 The liquid/solid interface

In-situ ATR-FTIR at the liquid/solid interface has been extensively reviewed,[56-58,74] so applications mainly related to photocatalysis are considered here. Compared with gas/solid work, only a few studies have been reported that give direct spectroscopic information on the composition of the adsorbate layer during photoreaction. The first ATR-FTIR study of photocatalysis at the liquid/solid interface was done by McQuillan et al.[75] The relationship between shallow-trapped electrons and adsorbed species, especially H_2O, was noteworthy.[76-78]

ATR-FTIR has been applied to identify the primary intermediates when TiO_2 particle films in contact with water are illuminated with band-gap irradiation. Nakato et al.[79,80] identified the surface peroxo species as the primary intermediate of O_2 photo-reduction and O_2 photo-evolution. The influence of adsorbed water on TiO_2

was also investigated.[76] After removal of bulk water, several bands below 1000 cm^{-1}, attributed to surface peroxo species, appeared under near-UV irradiation. In environmental applications where low levels of pollutants are typical, instrumental sensitivity issues have confined many early studies to reactants with strong IR chromophores, e.g., oxalic acid,[81-83] malonic acid,[84] and other dicarboxylic acids.[85] Bahnemann et al.[81-83] found that oxalate adopts two bidentate conformations: A (carbon-carbon σ bond parallel to the surface) and B (carbon-carbon σ bond perpendicular to the surface) on anatase TiO_2 surface under dark conditions. Typically, species A predominates during and after UV illumination, suggesting that species B is more easily attacked and degraded by photo-generated radicals. However, the absence of identifiable intermediates made further mechanistic insight difficult. In addition, Bürgi et al.[84,85] found that oxalate is a major intermediate in the photo-mineralization of malonate. Succinate is degraded to malonate initially, which is then further degraded to oxalate[85] in what appears to be a stepwise shortening of the hydrocarbon chain by the photo-Kolbe reaction.

ATR-FTIR has also been employed to investigate the adsorption and reaction over TiO_2 of oxalic acid,[86] salicylic acid, adipic acid, oleic acid,[87] poly-(sodium 4-styrene sulfonate), phenolic wastewater treatment by the photo-Fenton reaction.[88,89] Elsewhere, selective photo-oxidation of cyclohexane to cyclohexanone has been studied by Mul and co-workers, both over anatase TiO_2[90] and vanadia catalyst,[91] while Bürgi and co-workers have used ATR-FTIR [in combination with UV-Visible spectroscopy and transmission electron microscopy(TEM)] to study the fate of monolayer protected gold nanoparticles on TiO_2 upon illumination.[92] A brief summary of the key findings is shown in Table 2-3.

Table 2-3 Summary of key findings in photocatalysis over TiO_2 by ATR-FTIR at the liquid/solid interfaces

Sample	Observation	Reference
TiO_2 layer ex $TiCl_4$ hydrolysis;	The 1st *in situ* spectroscopic study of TiO_2/aqueous solution interface;	McQuillan et al.[75]
Degussa P25;	The molecular origin of TiO_2 surface charge;	
JRC-TiO-7 (anatase),	TiO_2 phonon modes are sensitive to the nature of adsorbed molecules;	McQuillan et al.[76]
JRC-TiO-7 (anatase),	Wet anatase TiO_2 (≤30 nm) exhibits p-type behavior and removal of H_2O results its reversion to n-type;	McQuillan et al.[77]
JRC-TiO-7 (anatase),	Existence of shallow electron traps is controlled by the water content of the thin film;	McQuillan et al.[78]
JRC-TiO-3 (rutile);	Oxalate leads to increase of trapped electrons.	
JRC-TiO-2 (100% anatase, size: 80 nm) JRC-TiO-5 (90% rutile, size: 640 nm)	Surface peroxo as the primary intermediates of oxygen photo-reduction and oxygen photo-evolution.	Nakato et al.[79,80]
Degussa P25 & in-house prepared TiO_2	Adsorption of oxalate, malonate and succinate on TiO_2 and change of adsorption geometry of oxalate during UV irradiation.	Bahnemann et al. [82,83,93,94]
Degussa P25 TiO_2 and home-made TiO_2	Photodegradation of malonic, dicarboxylic, amino acids and adsorption of thiol-protected gold nanoparticles on TiO_2 and their behavior under UV light irradiation.	Bürgi et al.[84,85,92,95]

2.5 Summary & outlook

In this chapter, the principle of photocatalysis and development of photocatalysts, including doping and modification of TiO_2, are firstly introduced. Then, mechanistic investigation of photocatalytic reactions at the reactant/catalyst interface, especially by *in situ* infrared spectroscopy, is reviewed.

TiO_2-based nanomaterials have been well studied as photocatalysts for various applications, including water-splitting, air/water purification, self-cleaning surface development, etc., and much effort has been devoted to their improvement during the last four decades. Unfortunately, the paucity of information on the chemical state existing at the interface and temporal changes during photocatalytic reaction impedes a fundamental understanding of the reaction mechanism. Without this input, the development of catalysts with greater efficiency and durability remains nothing more than "inspired guesswork". IR spectroscopy is an important and powerful tool to bridge this gap, allowing us to investigate the gas/solid interface (by DRIFTS) and the liquid/solid interface (by ATR-FTIR). To date, most studies of this kind have focused on model reactions using a standard photocatalyst like Degussa P25 TiO_2. While this benchmarking approach remains important, and constitutes a significant part of the thesis work (Chapters 4-5), related studies on some promising visible light photocatalysts, prepared in-house, are also reported (see Chapter 6).

Chapter 3. Experimental

The first section (3.1) deals with the principal techniques employed, viz., Diffuse Reflectance Infrared Fourier Transform (DRIFT) spectroscopy and Attenuated Total Reflection Fourier Transform Infrared (ATR-FTIR) spectroscopy. Section 3.2 introduces the various conventional materials characterization methods used in this work along with a description of the liquid-phase photocatalytic testing set-up and off-line analysis. For materials, Degussa P25 TiO_2 is used throughout this work. Finally, section 3.3 describes the preparation and characterization of some visible light active photocatalysts.

3.1 *In situ* infrared spectroscopies

3.1.1 DRIFTS

This DRIFTS system has been established by Dr. James Highfield in Institute of Chemical and Engineering Sciences (ICES), Singapore, and its digital photo and scheme are shown in Figure 3-1.[69] It consisted of a heatable reaction cell (HVC-DRP, Harrick Scientific) mounted into a Praying Mantis (Harrick Scientific) optical accessory, located in the front sample compartment of a Digilab Excalibur FTS-3000 FTIR spectrometer (Varian Inc.). The reaction cell was fitted with a pair of CaF_2 windows for incident and remitted IR radiation, and a quartz window for optical pumping from an Oriel 150W Xe DC short arc lamp. The UV-Vis pump beam was directed onto the sample via a suitably clamped 1 meter length high-grade fused quartz light pipe with focusing adapter. For visible light experiments, a filter cutting off wavelengths below 400 nm was inserted into the holder at the exit from the lamp housing. Gas flow was conveniently tapped off the mass-flow controlled supply from

a Setaram Setsys Evolution 12 thermogravimetric (TG) analyzer. With a custom-built (heat-traced) gas-switching bank configured in "bypass" mode, flow is through the standard TG-FTIR interface, consisting of a heated transfer line and 10 cm pathlength gas cell. This arrangement enabled pre-equilibration and calibration of reactant gas mixtures before introduction to the DRIFT cell. Alternatively, operating in the "series" mode, the vent stream from the DRIFT cell passes through the gas cell, thereby offering higher sensitivity detection of gaseous products. N_2 gas is used directly in most experiments. When the humidity control is needed, the auxiliary gas passed through a Setaram Wetsys. By adjusting the H_2O temperature inside the Wetsys and the ratio of dry and wet gas flow, we can get the desired humidity. For photo-oxidation work, "synthetic air" was used. This was, actually purified air diluted by an equal flow of N_2 (10% O_2/N_2), as dictated by the dual-flow configuration of the Setaram TG.

Time-resolved IR spectra were collected and averaged every two minutes using the kinetics mode of the Resolutions Pro 4a software over the range 6500-1000 cm^{-1} at 4 cm^{-1} resolution.

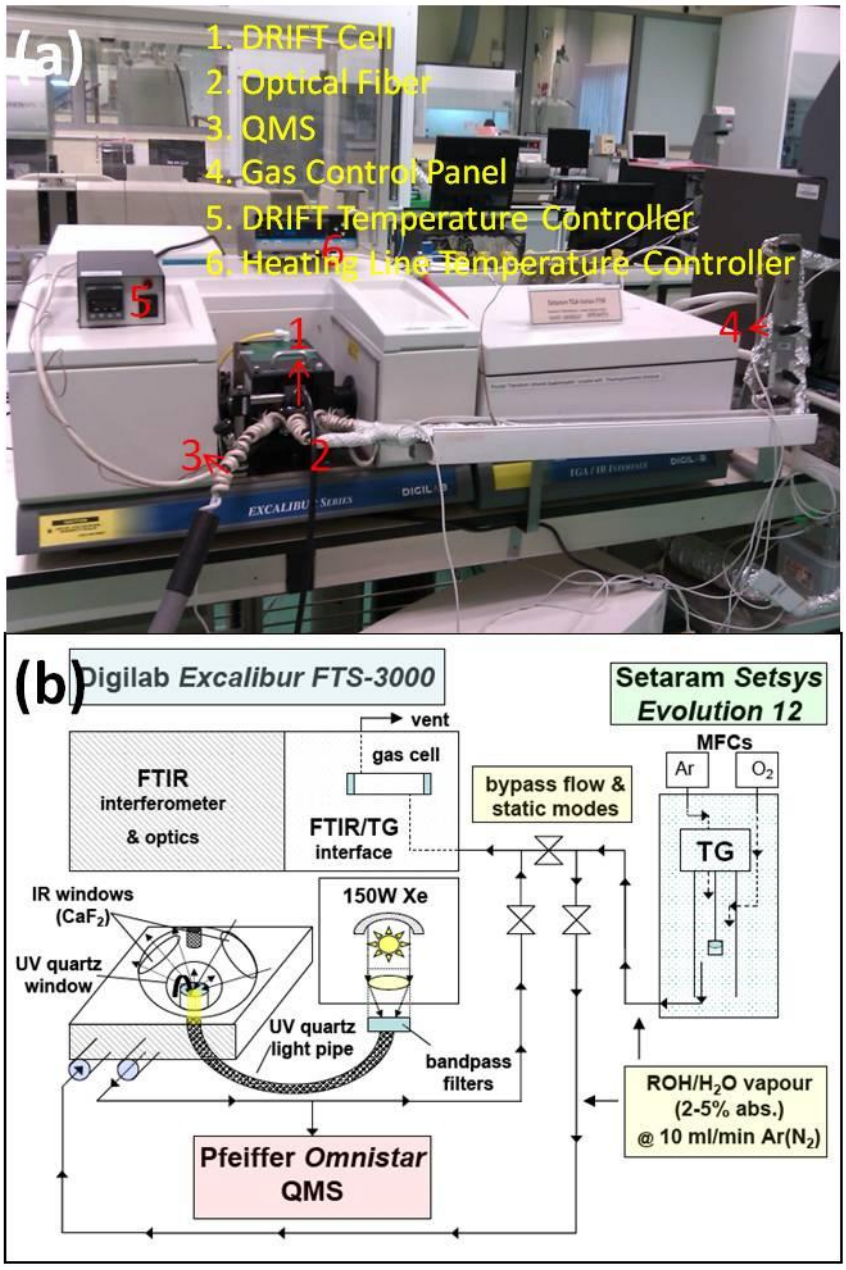

Figure 3-1 Lab snapshot (a) and scheme (b) of DRIFT system

3.1.2 ATR-FTIR

3.1.2.1 Introduction to the set-up

The ATR accessory as-supplied (Pike, model: 21372) was not suitable for interfacing to the pump directly and had to be re-machined for purposes of photocatalysis and flow recirculation. It was supplied with liquid reactants from a

liquid circulating pump at a typical flow rate of 1-5 ml $\cdot$min^{-1}. A photo and scheme of the ATR-FTIR set-up are shown in Figure 3-2.

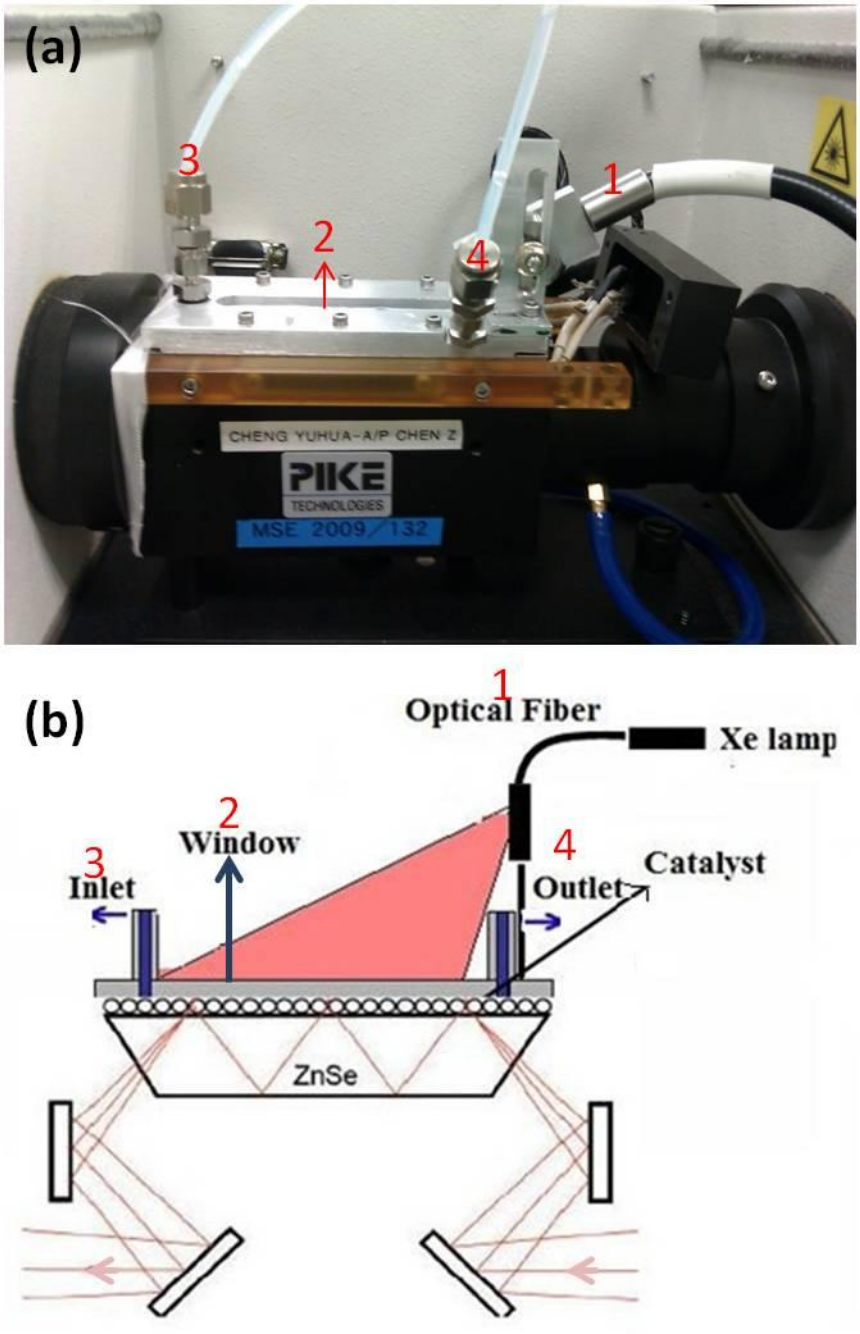

Figure 3-2 Snapshot (a) and scheme (b) of the ATR-FTIR set-up

A new top plate was machined with a narrow rectangular aperture cut to accept a fused silica window (size: 78 ×12 ×1.5 mm), thereby allowing for UV-Vis illumination via an optical fiber bundle (1m high-quality quartz - Oriel 77539), actually designed for coupling to a monochromator slit, but here used in reverse. This provided a slightly diverging rectangular output from an Oriel 150W Xe DC short arc lamp, permitting illumination of roughly 80% of the sample area by careful adjustment of the fiber mounting clamp. One disadvantage of this set up is that the ATR collects some information from the small un-illuminated sample area at each end of the crystal, potentially lowering the reactive 'contrast' between light and dark experiments. The flow cell (internal volume ~ 2 ml) contained an optically dense crystal (ZnSe unless otherwise indicated) as the internal reflection element (IRE). A crystal (dimensions = 80 ×10 × 4 mm) with a 45° entrance angle was chosen as it allows 10 infrared beam reflections for progressive absorption and good sensitivity. The ATR/flow cell was mounted kinematically in the front sample compartment of the Digilab FTIR spectrometer as previously described (see Section 3.1.1). The ethanol and acetaldehyde aqueous solutions used in the present work, respectively 0.86M and 0.89M (5% in volume percentage), were close to neutral pH. The acetic acid solution (1mM) was rendered less acidic (pH raised to ~5 with NaOH) to protect the IRE from corrosion. DI water was firstly circulated through the cell and a background spectrum was taken under dark (reference) conditions. The aqueous solution of reactant, pre-sparged in air, was then supplied into the cell and its IR bands were tracked. Once these reached steady-state, the pump was stopped and then the lamp was turned on. In other words, the reaction was studied in *static* conditions, without additional O_2 supply, to develop spectral changes in response to optical (UV-vis) pumping. Time-

resolved IR spectra were collected every two minutes (120 co-added scans per spectrum to improve signal-to-noise) over the range 4000–1000 cm^{-1} at 4 cm^{-1} resolution using the *kinetics* mode of the Resolutions Pro 4a software supplied with the spectrometer.

3.1.2.2 Thin film TiO_2 deposition

ATR-FTIR is a type of internal reflection spectroscopy in which the sample is placed in close contact with an IRE of high refractive index. As shown in Figure 3-2, powdered catalysts must be immobilized as a thin film onto the IRE (ZnSe crystal in our experiments) in as homogeneous a manner as possible. Powdered photocatalyst (Degussa P25) was firstly suspended in deionized water at a concentration of 10 $mg\ ml^{-1}$. The suspension was then treated in an ultrasonic bath for 30 minutes and 400 µl of this suspension was gently and evenly spread onto the ZnSe crystal and left to dry overnight at room temperature. The coverage of the final dry layer of TiO_2 particles thus obtained was ca. 5 $mg\ cm^{-2}$ and the layer appeared homogenous under visual inspection. The thickness of this layer was estimated as typically around 4 µm based on the bulk density of TiO_2.

Because the refractive index of the ZnSe IRE is 2.4 and the incidence angle of IR irradiation is fixed at 45° by the ATR accessory, total reflection occurs only when the refractive index (n) of the thin film is less than 1.7 (calculated from Equation 2-13). Although the refractive index of bulk TiO_2 (n = 2.6 for anatase) is slightly larger than that of ZnSe (n = 2.4), the effective refractive index of the porous particle film of TiO_2 in contact with water (n = 1.33) could be effectively reduced to below 1.7.[57] The penetration depth of the evanescent wave into the TiO_2 layer was estimated to be less than 1.4 µm at 1640 cm^{-1} ($ZnSe/H_2O$ system),[56] so most of the spectral information was assumed to derive from the fraction closest to the IRE.

3.2 Materials characterization and photocatalytic testing

3.2.1 Materials characterization

To identify the crystalline structure and phase transformation of samples, X-ray diffraction (XRD) measurements were performed on a Shimadzu 6000 powder diffractometer equipped with a Cu Kα source. The morphology and particle size of the samples were investigated by JEOL 2010 transmission electron microscopy (TEM), operating at an accelerating voltage of 200 KV. Brunauer–Emmett-Teller (BET) surface areas and pore diameters were determined by N_2 physisorption (77 K) on a Micromeritics ASAP 2420 Surface Area and Porosity Analyzer. All solid state MAS ^{13}C NMR spectra were recorded with a Bruker Ultrashield AVANCE 400WB (400 MHz) spectrometer with the spin rate of 5000 s^{-1}. The weight percentages of C, N and H of the surface species were analyzed by a Euro Vector EA 3000 series elemental analyzer.

The thermal stability of the samples was investigated by a Setaram Setsys 12 thermo-balance coupled to the FTIR gas cell. The optical absorption spectra of samples were measured on a Shimadzu 3600 UV-Vis-NIR spectrometer in diffuse reflectance (DR) mode over the range 200-800 nm against a $BaSO_4$ standard.

3.2.2 Photocatalytic Testing

Methyl orange (MO) was chosen as the target molecule to assess the photocatalytic performance of photocatalysts in liquid suspension. For each experiment, 50 mg photocatalyst was dispersed into 50 ml of MO solution at a concentration of 10 ppm and stirred for 2 hours in the dark before illumination to establish the adsorption/desorption equilibrium. An Asahi spectra HAL 320 high power xenon lamp was used as light source and the intensity was set to 200 mW cm^{-2}. A “super

cold" filter was interposed to remove infrared radiation and minimize evaporative losses for the full spectrum UV-Vis test, abbreviated as UV for convenience. For visible light (VIS) experiments, an additional optical filter was used to remove radiation below 420 nm. The concentration change in MO was determined periodically on extracted aliquots based on its absorption peak at 464.5 nm using a Shimadzu UV-VIS 2501 spectrometer.

3.3 Photocatalysts

3.3.1 Pristine and platinized P25 TiO_2

Pristine titanium dioxide used throughout this study was Degussa (Now Evonik) P25 TiO_2, which is composed of ca. 80% anatase phase and 20% rutile phase. Its primary particle size is ca. 30 nm and its BET surface areas is ca.56 m^2 g^{-1} (as shown in Figure 3-3).

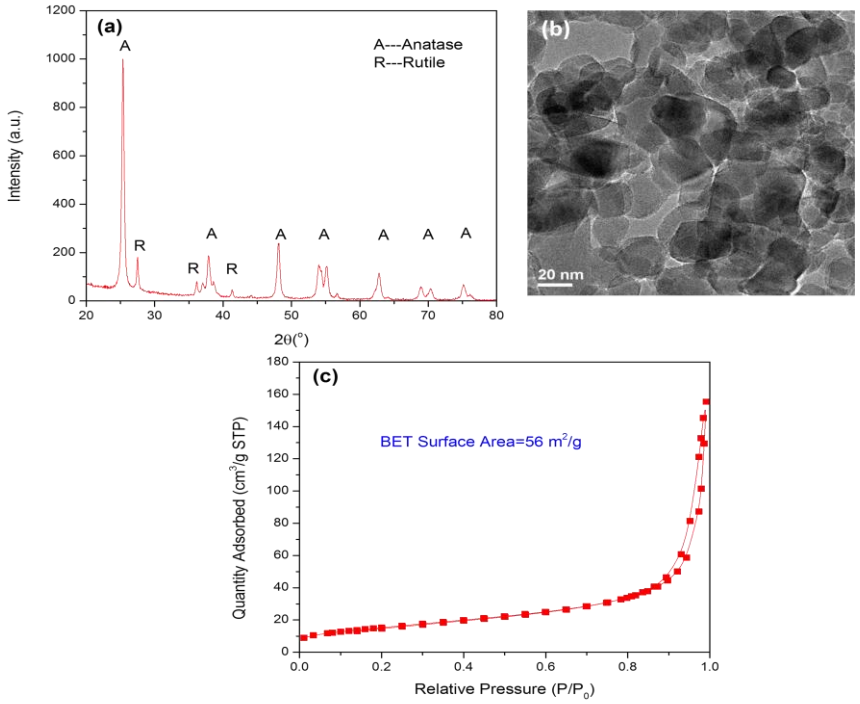

Figure 3-3 Characterization of Degussa P25 TiO_2 (a) XRD pattern; (b) TEM image; (c) N_2 sorption isotherm

Platinized P25 TiO_2 was prepared through a photo-reductive deposition process. Suitable amounts of TiO_2 and H_2PtCl_6, to arrive at a nominal loading of 0.5 wt% Pt, were added to a mixture of deionized water and methanol in a volume ratio of 5:1 and illuminated by a 450W Xe lamp (total flux ≈200 mW cm^{-2}) for 2 hours. The suspension was isolated by centrifugation, washed 3x in deionized water and dried in an oven at 70 °C overnight. TEM confirmed that the Pt was homogeneously dispersed on the TiO_2 in a fairly narrow particle diameter range of 2-3 nm (as shown in Figure 3-4). All other chemicals were bought from Sigma-Aldrich and used directly without any further purification.

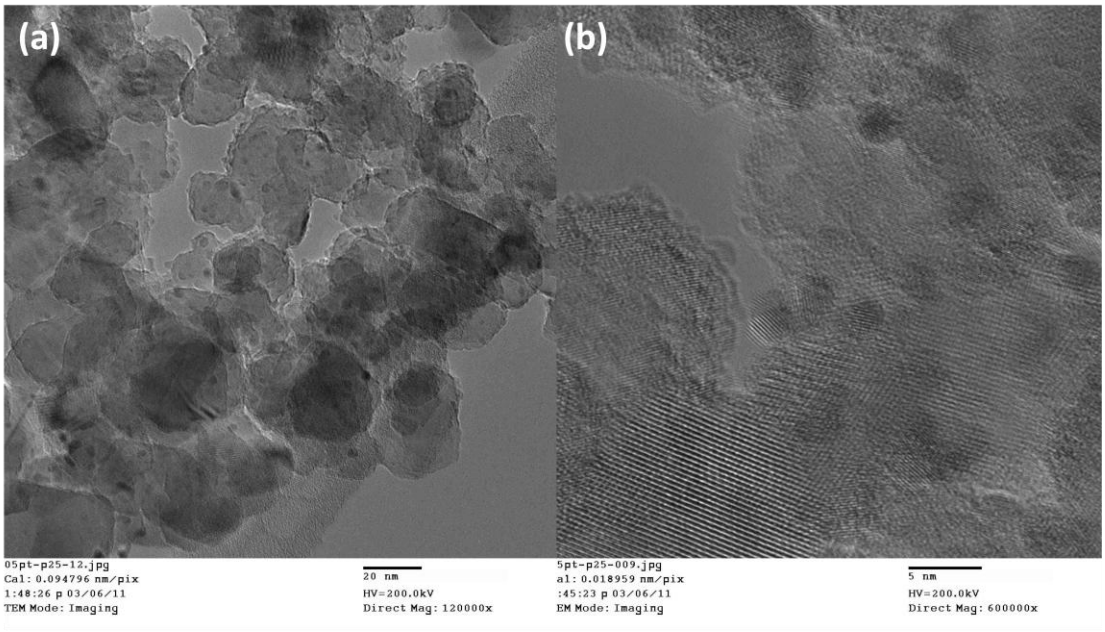

Figure 3-4. TEM (a) and HRTEM (b) images of 0.5wt% Pt/P25 TiO_2

3.3.2 Visible light active photocatalysts

In addition to the standard Degussa (Now Evonik) P25 TiO_2, two groups of visible light active photocatalysts, including melon-modified titanate/TiO_2, and silver nanoparticle decorated titanate/TiO_2, have also been investigated. Their preparation methods are described below.

3.3.2.1 Titanate

Titanate nanotubes (TNTs) and nanobelts (TNBs) were synthesized through a conventional hydrothermal method.[96] The detailed procedure is as follows: 2g anatase TiO_2 powder (Aldrich, 99.8%) was suspended in 50 ml of 10 M NaOH (Schedelco, Grade A.R.), sonicated for 30 minutes and then transferred to a teflon-lined autoclave. The slurry was then heated to 150 °C or 200 °C, respectively and held at these temperatures for 48 hours. The recovered samples were washed several times in deionized water until the pH was lowered to 9, and then washed in 0.1 M HNO_3 to ion-exchange any residual Na^+ ions for H^+, before oven drying at 80 °C. The sample is denoted as HT 150 or HT 200, indicating that it was synthesized at 150 °C or 200 °C and proton-exchanged. It was then subject to post-annealing at different temperatures, and respectively denoted as HT XXX (where XXX is the post annealing temperature).

3.3.2.2 Melon-modified titanate/TiO_2 and carbon nitride-modified TiO_2

To obtain melon-modified titanate/TiO_2, 500 mg of HT 150, HT 200, along with P25 and commercial anatase TiO_2 controls, were dispersed in urea solution (1 g urea dissolved in 40 ml ethanol) respectively and the mixtures were dried with continuous stirring at 70 °C. After ethanol was evaporated, the white powders were recovered and

heat treated (ramp rate: 5 °C/min) in a muffle furnace up to 400 °C, and then held at 400 °C for 2 hours under ambient air or nitrogen.

Graphitic carbon nitride (g-C_3N_4) was prepared through thermal polymerization of dicyandiamide in air up to 550 °C for 4 h. Then, mixture of g-C_3N_4 and titanate nanotubes (HT 150) in different ratios were heated again to 400 °C to yield g-C_3N_4 modified TiO_2 samples.

3.3.2.3 Ag nanoparticle decorated titanate/TiO_2

For silver loading, HT 150 powder was dispersed in deionized (DI) water and a suitable amount of $AgNO_3$ solution was added during stirring to achieve a nominal loading of 10 wt% Ag. After stirring for 1 hour, the solution was exposed to UV illumination for 2 hours, during which the color of the suspension changed from white to gray. After illumination, the samples were centrifuged and washed several times to neutral pH (~7). The as-synthesized sample is denoted as AgT 150, and the post-annealed sample is abbreviated as AgT XXX as above.

Chapter 4. Investigation of Photocatalytic Reactions at the Gas/Solid Interface by DRIFTS

In this chapter, *in situ* infrared spectroscopy studies of various photocatalytic reactions at the gas/solid interface are presented. The experimental themes are *in-situ* DRIFTS studies of simple molecules (e.g. H_2O, O_2, ethanol, etc.) and metallization over Degussa P25 TiO_2 and change in state of photocatalysts under various conditions.

4.1 Photo-induced IR spectral changes of TiO_2 in different atmospheres

Typical DRIFT spectra of Degussa P25 TiO_2 are shown in Figure 4-1. For the pristine material, two strong IR bands in the range 3600–2700 cm^{-1}(ν_{OH}) and 1700–1500 cm^{-1} (δ_{HOH}) are from adsorbed H_2O molecules. The pronounced absorption below 1000 cm^{-1} is characteristic of the intense TiO_2 lattice phonon. Drying in nitrogen flow causes the continuous weakening of H_2O bands, while isolated surface OH groups with absorptions around 3700 cm^{-1} become more distinct.

UV-Vis irradiation of TiO_2 in inert gas (N_2) causes a slight background increase below 2500 cm^{-1}(shown in Figure 4-2). This quasi-continuum absorption, more pronounced towards longer wavelengths (small wavenumbers), is characteristic of shallow trapped electrons.[55,62,71] The background shift in Fig. 4-2 is not as intense as that observed by Hoffmann et al.[55,62,71] on the same material *in vacuo*, because the desorption of pre-adsorbed O_2 *in vacuo* prevents the consumption of photo-generated electrons.

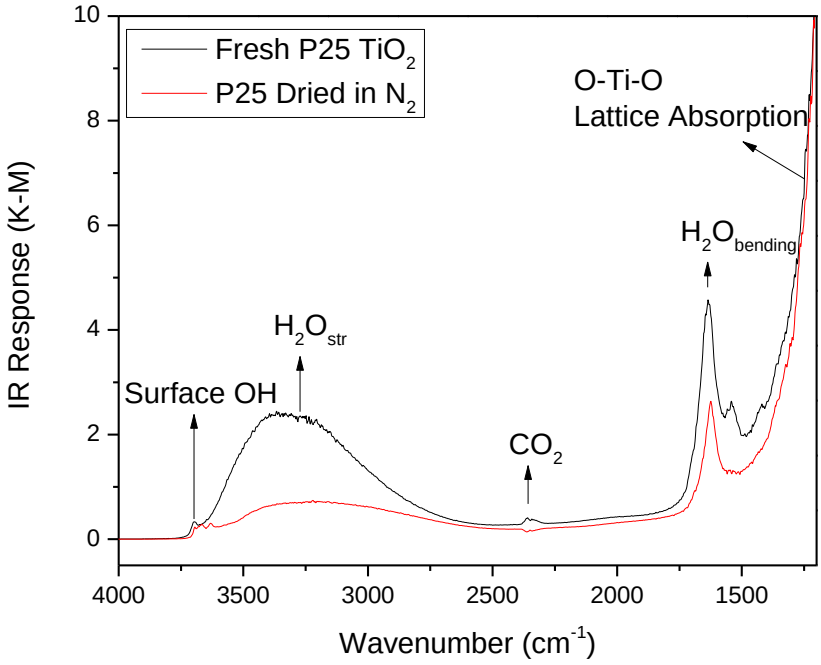

Figure 4-1 Typical DRIFT spectra of P25 TiO_2

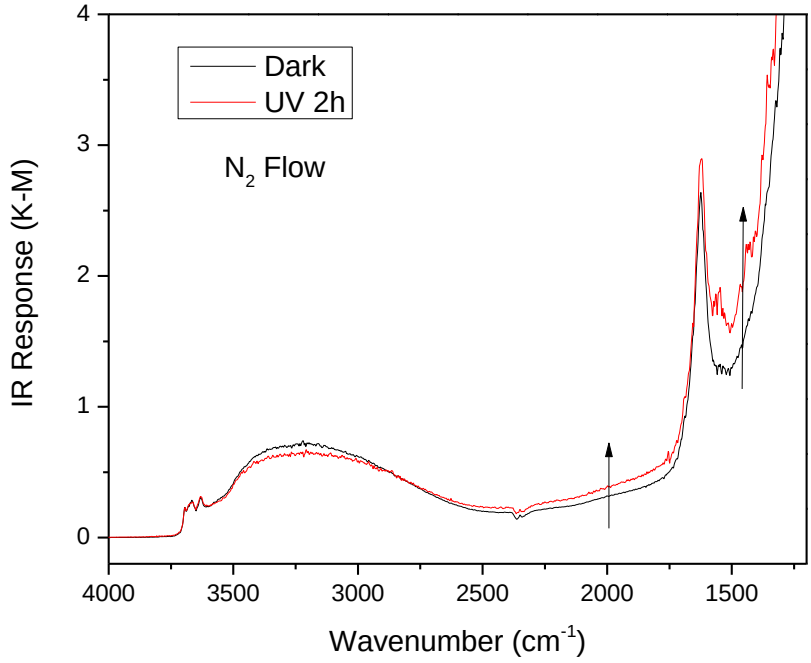

Figure 4-2 Photo-induced spectral changes in TiO_2 under N_2

Interactions of water molecules with the TiO_2 surface are important for the following reasons: (1) complete photo-dissociation of H_2O on TiO_2 surface is endergonic (uphill) and a potential route to renewable H_2;[2] (2) photo-induced hydrophilicity could be utilized to fabricate self-cleaning and anti-fogging surfaces;[38,97,98] (3) water provides OH^- ions that can be oxidized by surface trapped holes to yield OH radicals, strong oxidants involved in photo-mineralization of organic pollutants.[38,99]

Compared with the dry case, introducing 3.75%v H_2O (50% RH at 40 °C) vapor into the N_2 flow during band gap irradiation of TiO_2 ,which is maintained at 40 °C, causes a dramatic upward shift in the IR background absorption (Figure 4-3a). This indicates that more electrons are trapped on the surface, where they are remarkably stable and long-lived. The presence of H_2O is believed to stabilize the photo-generated holes rather than electrons, because it has electron donor properties. With a high dielectric constant (ε~80), this solvent effectively counters any Coulombic attraction forces tending to promote electron-hole recombination. The steady accumulation of trapped electrons over several hours suggests that reduction of protons into H_2 on the pristine TiO_2 surface is slow or non-existent.

The shape of the quasi-continuum feature (electron spectrum) is better seen by subtracting the dark spectrum (before irradiation). This reveals an exponential relation between absorption strength and wavelength, similar to that observed by Hoffmann et al.[55] At a particular wavelength, λ, the signal (S) can be expressed by Equation 4.1 and 4.2.[55]

$$S(\lambda) = A\lambda^{p} \tag{4.1}$$

$$Log(S(\lambda)) = Log(A) + pLog(\lambda) \tag{4.2}$$

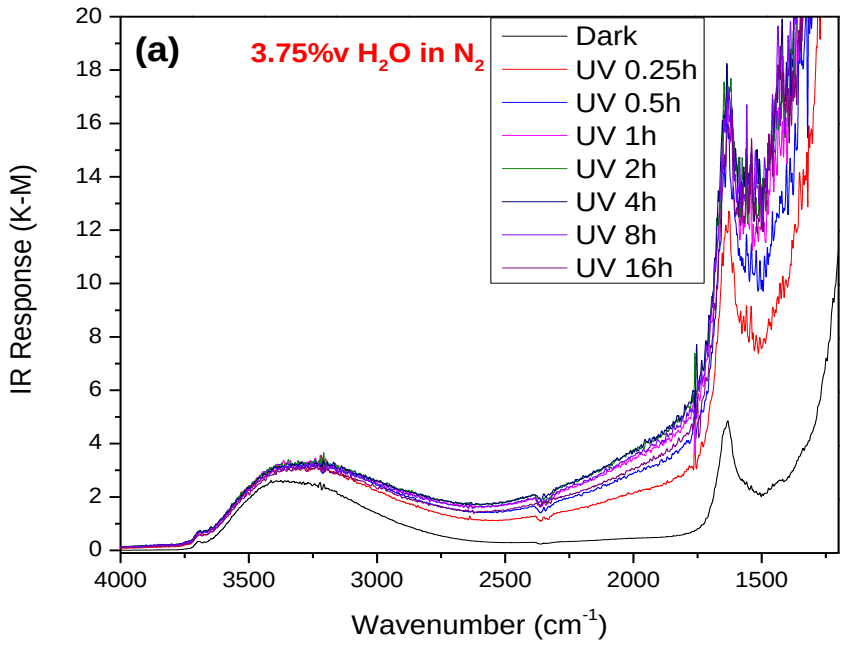
(a)
3.75%v H2O in N2
Dark
UV 0.25h
UV 0.5h
UV 1h
UV 2h
UV 4h
UV 8h
UV 16h
IR Response (K-M)
Wavenumber (cm-1)
20
18
16
14
12
10
8
6
4
2
0
4000
3500
3000
2500
2000
1500

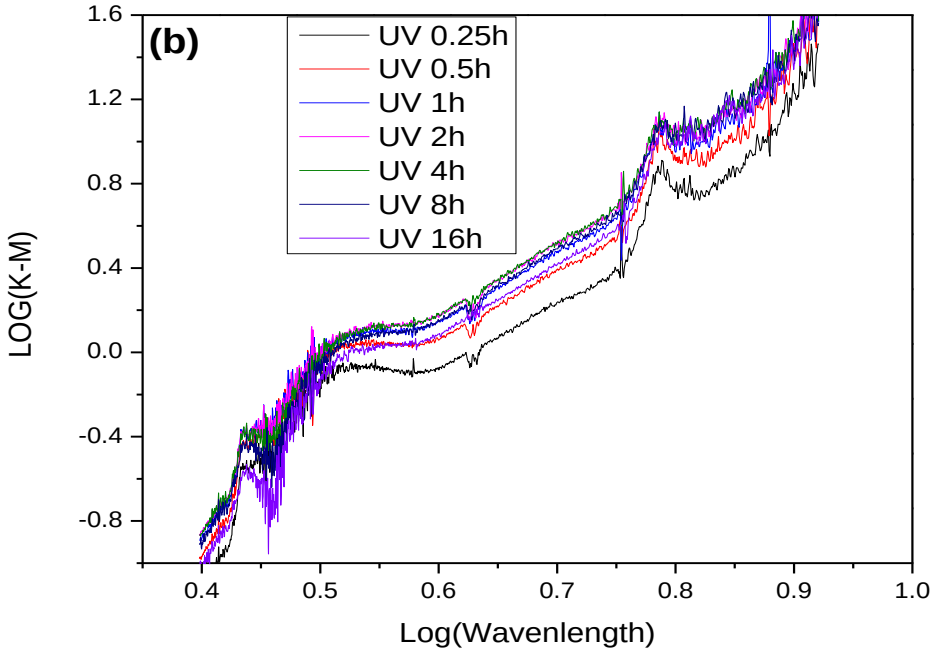
(b)
UV 0.25h
UV 0.5h
UV 1h
UV 2h
UV 4h
UV 8h
UV 16h
LOG(K-M)
Log(Wavenlength)
1.6
1.2
0.8
0.4
0.0
-0.4
-0.8
0.4
0.5
0.6
0.7
0.8
0.9
1.0

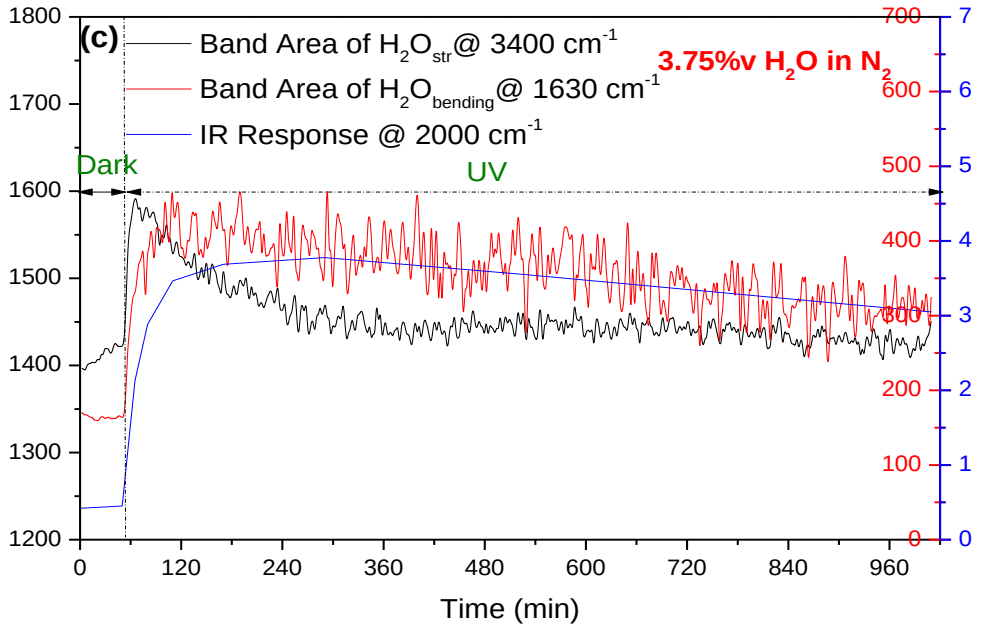

Figure 4-3 Photo-induced spectral changes in TiO_2 in the presence of 3.75%v H_2O in N_2 (a) K-M spectra over 16 hours; (b) log-log plot of the same graph; (c) respective band changes with the time

Thus, a log-log plot should be linear with slope = p (the exponent) and intercept = A (proportionality constant). Inspection of Fig. 4-3b shows that this is the case, at least in the region where features due to water and TiO_2 do not interfere (2500~1700 cm^{-1}). However, the p value is estimated to be ca. 3.3, i.e., almost double that reported by Hoffmann et al.,[55] possibly due to the presence of hole-scavenger H_2O.

Under continuous illumination, as shown in Fig. 4-3c, parallel changes were observed in the background and bands due to adsorbed H_2O, despite a fixed level of the latter being maintained in the vapour state. Both the background and the H_2O bands (stretching @ 3400 cm^{-1}, bending @ 1640 cm^{-1}) increased abruptly to a

maximum and then slowly weakened over the next 15 hours, although always remaining more intense than in the dark.

The rate of development of absorption due to trapped electrons was conveniently monitored by the IR response at 2000 cm^{-1} as representative. At this position, there are no interfering bands and it is also close to the maximum in the "instrument function", such that the signal-to-noise is high. As shown in Figure 4-4, the IR absorption increased almost immediately upon band gap irradiation, and approached a maximum within 2 hour. Switching back to the dark condition resulted in a slower decay compared with growth, and the signal level @ 2000 cm^{-1} decreased to c.a. 50% within 1.5 hours. The addition of O_2 can completely consume trapped electrons and restored the surface to initial states within 10 minutes.

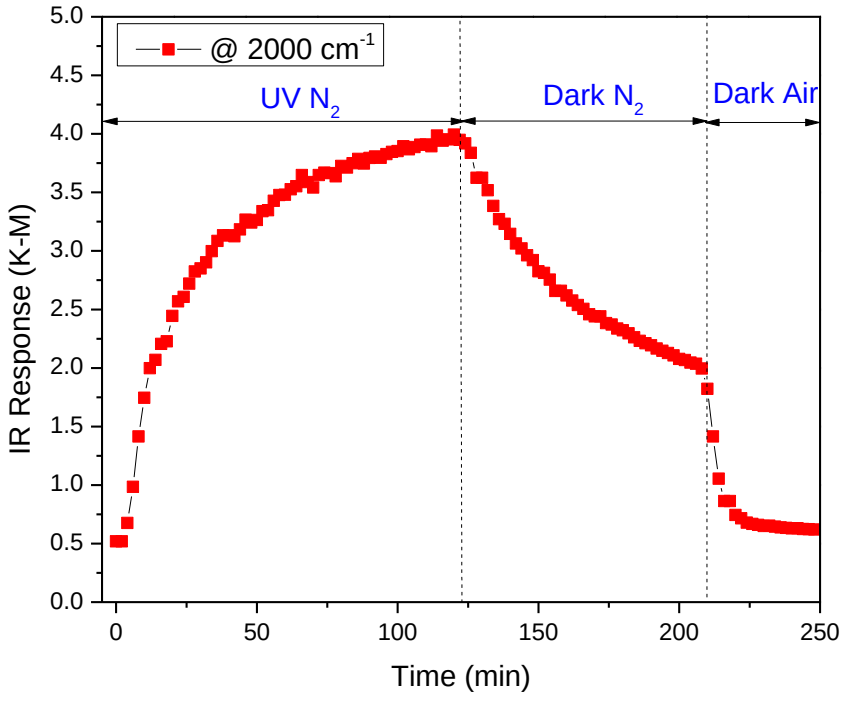

Figure 4-4 Growth and decay of electron spectrum Photo-induced spectral changes in TiO_2 in the atmosphere of 3.75%v H_2O

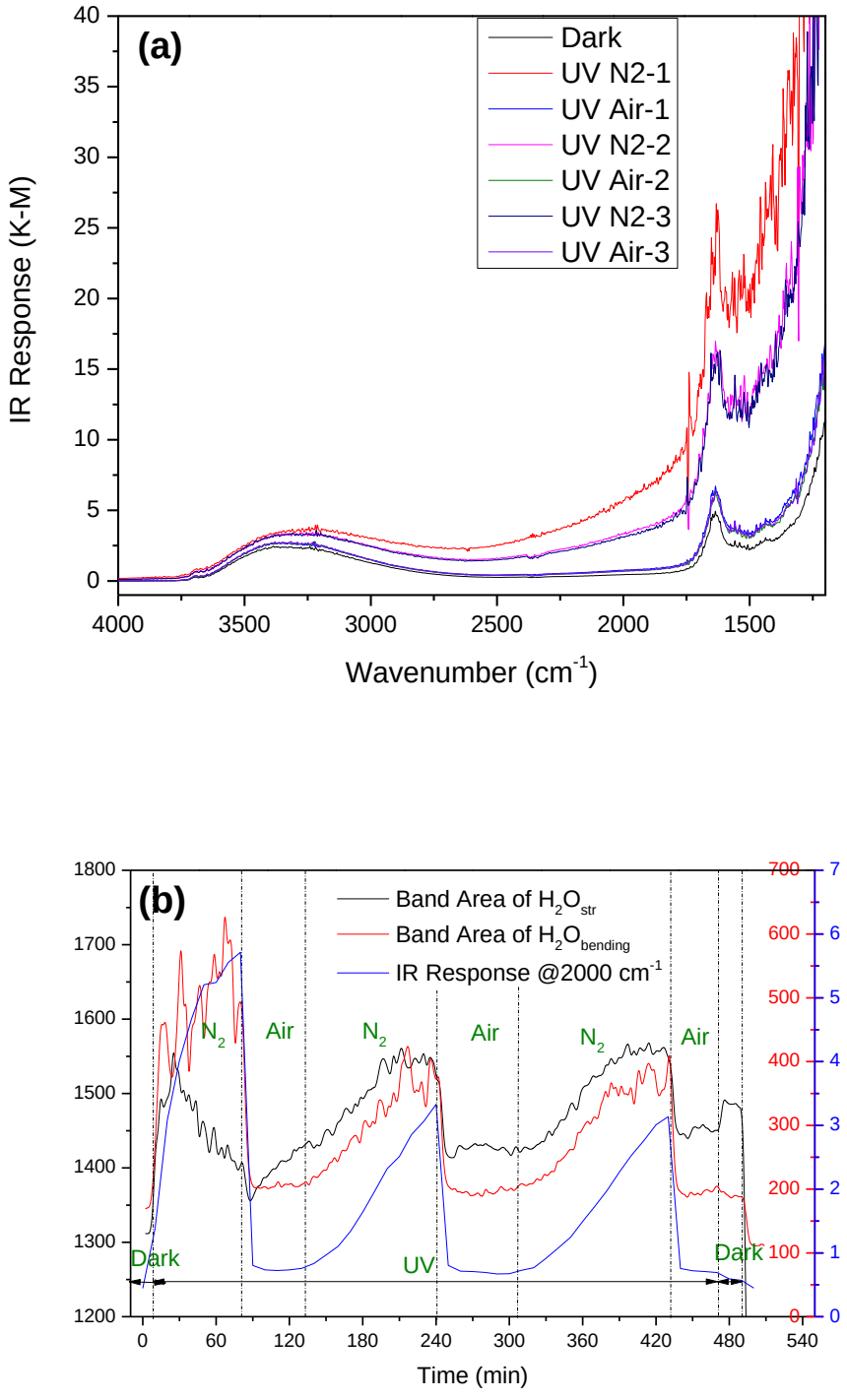

Figure 4-5 Band changes in P25 TiO_2 during UV-Vis irradiation under cycles of N_2 and air in the presence of 3.75%v H_2O: (a) corresponding DRIFT spectra; (b) marker responses for background and adsorbed water.

Figs. 4-5a and 4-5b shows the effect on DRIFT spectra and spectral markers, respectively, for P25 TiO_2 (under fixed humidity = 3.75 %v H_2O, 50% RH at 40 °C) due to cycling the carrier gas between N_2 and air under continuous illumination. After development of the previously observed features under humid N_2, the switching to humid air suddenly and dramatically suppressed (or quenched) the absorption due to trapped electrons almost back to the dark level within 10 minutes. O_2 quenches the absorption by reacting with trapped electrons to form superoxide O_2^-, as shown in eqn. 2.7.[4] A similar trend was observed in the $H_2O_{bending}$ marker. In contrast, after its initial rise under illumination in humid N_2, the H_2O_{str} marker was unstable, decreasing already before the switch to humid air, this last causing a recovery in intensity. It should be borne in mind that the stretching band envelope has contributions from both adsorbed water and H-bonded surface OH groups. Thus, its behavior is more difficult to unravel. During repetitive atmosphere switching, the band intensities in humid N_2 only become reproducible after the 2^{nd} cycle. The first cycle maxima were never attained in subsequent cycles, probably because previously adsorbed O_2 was not fully desorbed in the subsequent N_2 purge.

As a control test, the amount of physically-adsorbed H_2O on the TiO_2 surface under fixed humidity in the dark was evaluated by TGA. The result is shown in Figure 4-6. To obtain the dry reference position ($\Delta w = 0$), roughly 250 mg of TiO_2 (previously freed from organic contaminants by firing at 500 °C in air) was conditioned at 200 °C under dry N_2 flow. The weight stabilized in just over one hour, H_2O vapor was introduced at 3.75%v and the sample cooled in steps from 200 °C to 100 °C, then to 40 °C, the normal temperature for DRIFTS studies. The weight re-stabilized after 3

hours and corresponded to a gain of 2.8% relative. Taking the molecular cross-section of water to be 10 Å^2,[100] this was equivalent to 2 monolayers of H_2O.

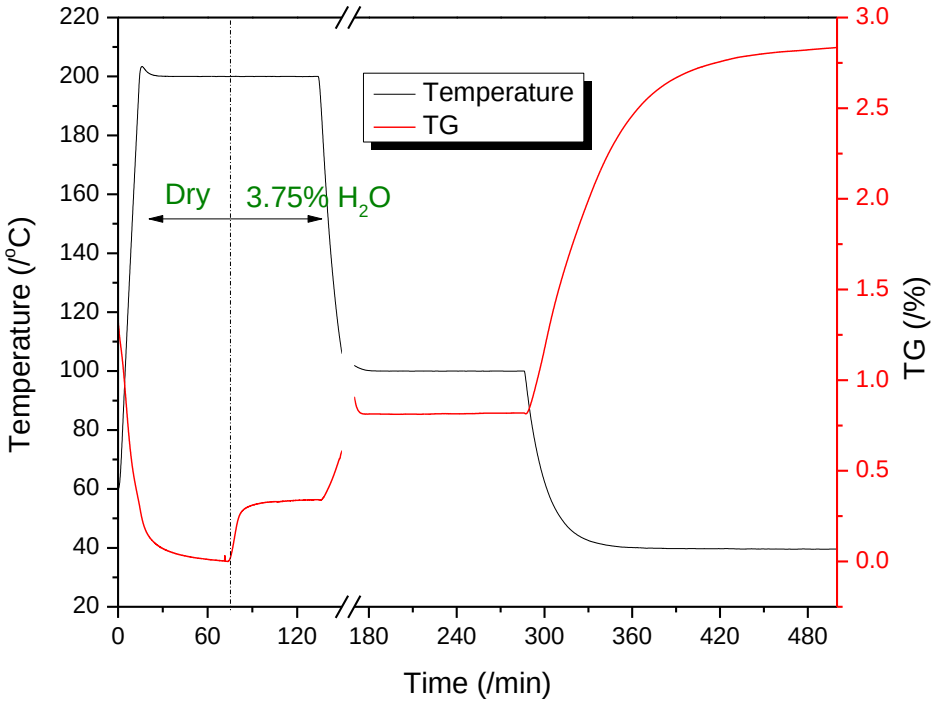

Figure 4-6 Equilibrium adsorption of water on P25 TiO_2 by TGA

When the H_2O vapour level was raised towards the saturation point (6.25%v, 85% RH at 40 °C), and conditioned in the dark, subsequent exposure to UV-Vis irradiation in N_2 rapidly developed the background absorption (as usual), but caused very little initial change in H_2O band intensities. The dominant trend was a slow and progressive weakening of the H_2O bands, as shown in Figure 4-7. The switch to humid air suppressed the background, but caused a recovery in the H_2O bands, almost to the dark level. This behavior was almost the opposite of that observed previously at lower relative humidity, and resembled the spectral trends seen by ATR-FTIR when TiO_2 is immersed in liquid water (see Chapter 5).

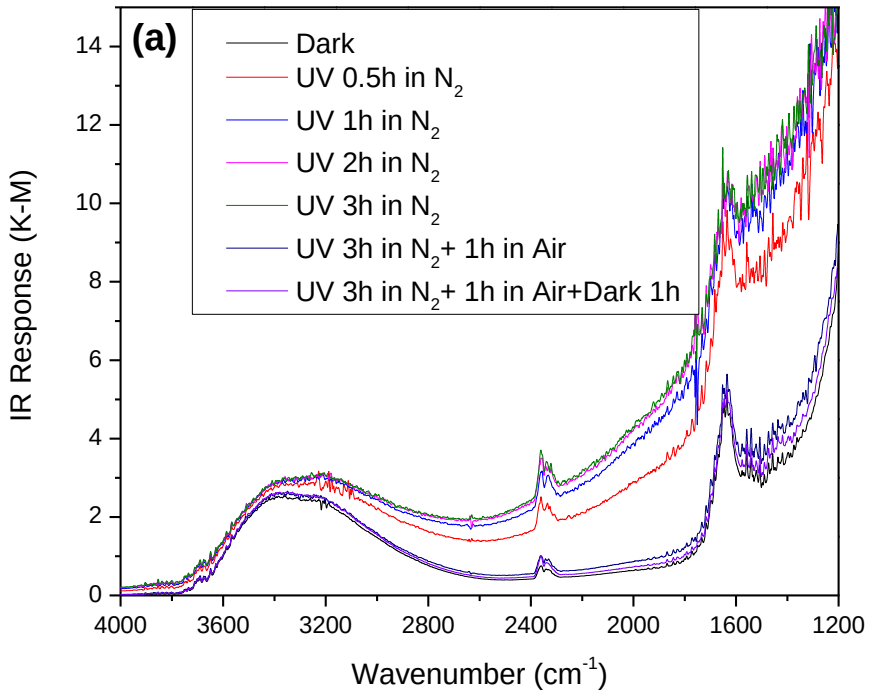

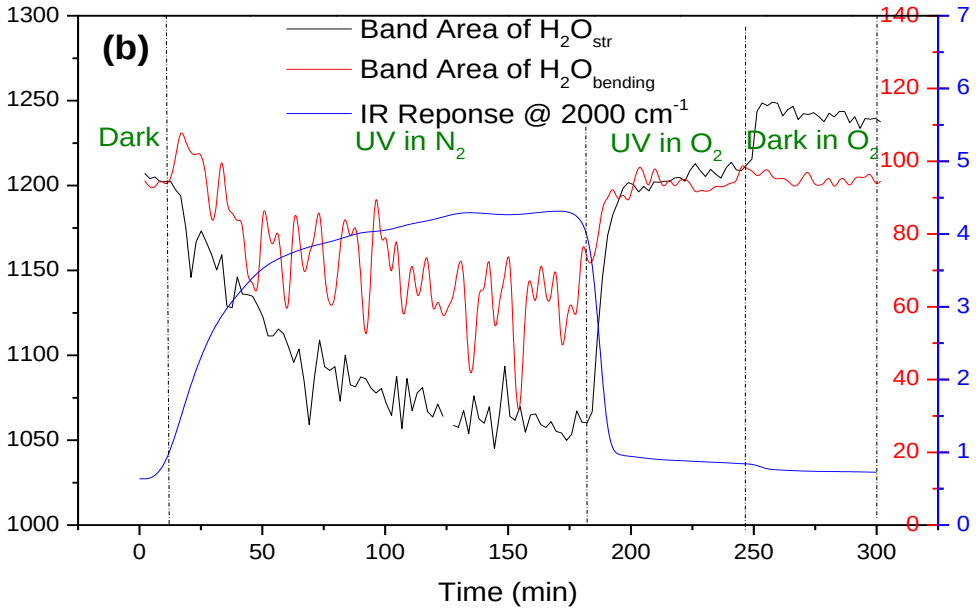

Figure 4-7 Photo-induced spectral changes in TiO_2 under 6.25%v H_2O (in N_2 or O_2)
(a) DRIFT spectra; (b) marker responses for background and adsorbed water

We believe the net observable is the sum of two effects: *repulsion* (or substantial weakening of the adsorbed state) of water at surface electron trap states, and its attraction (with multi-layer build-up) at surface hole traps. Thus, a net increase in adsorbed water level, anticipated by most researchers as a marker of the development of superhydrophilicity *per se*, is only seen at low humidity. Further clarification of this complex phenomenon is needed, e.g., by contact angle measurements on pressed pellets and AFM studies under direct UV-Vis irradiation *in situ*.

4.2 Photo-oxidation of ethanol

Compared with H_2O, ethanol is a more powerful hole-scavenger. It readily donates an electron to neutralize the hole, and releases a proton. This is expected to promote the build-up of excess trapped electrons on TiO_2 in an inert atmosphere. Figure 4-8 shows DRIFT spectra of TiO_2 exposed to band-gap illumination under dry ethanol vapor in N_2. This resulted in rapid growth in the background (electron spectrum), similar to that observed in the presence of H_2O/N_2. Switching to the dark caused the background to decay but only partially. Even subsequent exposure to air (O_2) did not quench the spectrum completely. Some trapped electrons remaining in excess in the ethanol case might be due to the irreversible hole annihilation.

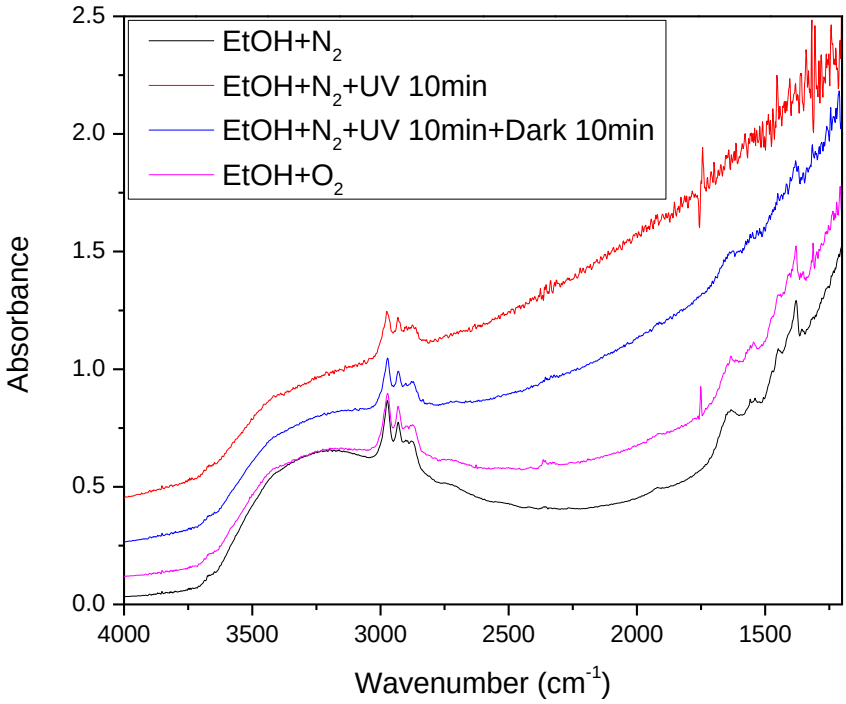

Figure 4-8 DRIFT spectral changes in P25 TiO_2 under dry ethanol vapor with light/dark and N_2/air switching.

Under band-gap illumination in the presence of air (O_2), the experiment effectively constitutes photo-oxidation of organic compounds, such as when applied for environmental purposes. Their complete breakdown to CO_2 and H_2O is known as "photo-mineralization". DRIFT spectra collected during photo-oxidation of ethanol (under static conditions) are shown in Figure 4-9a. The characteristic bands of ethanol, e.g., the CH_{str} envelope around 2900 cm^{-1}, decreased progressively and absorption bands of partial oxidation products acetaldehyde (carbonyl stretch, $\nu_{C=O}$, at 1715 cm^{-1}) and acetate (asymmetric and symmetric stretch of the carboxylate moiety (ν_{OCO}) at 1550 & 1415 cm^{-1}, respectively), developed within the first few hours of illumination. Build-up of gaseous CO_2 was also evident but only in the later stage of the experiment. These observations cohere with the previous reports by others.[66,70,72]

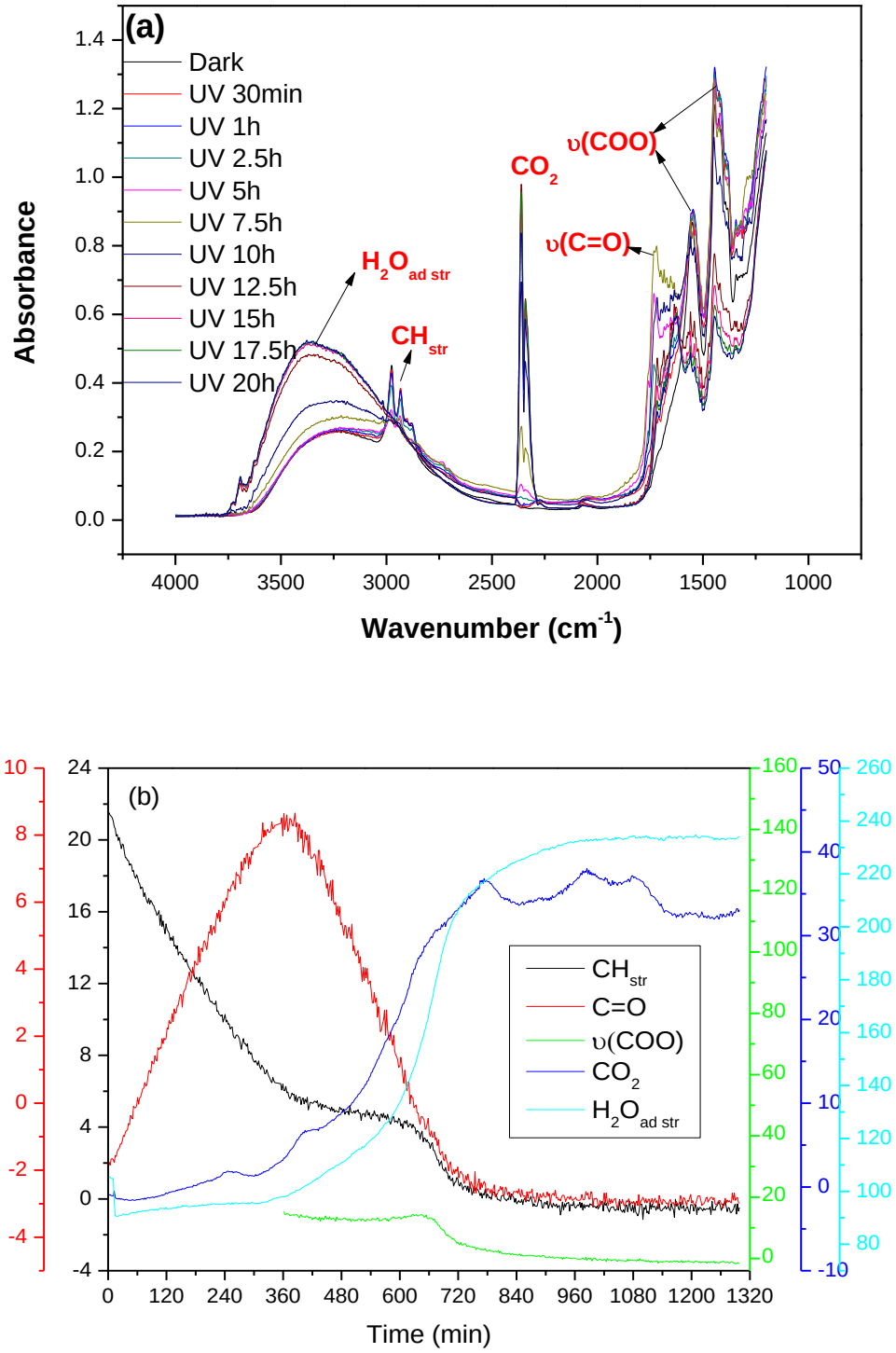

Figure 4-9 DRIFT spectral changes in TiO_2 during photo-oxidation in the presence of dry ethanol/air: (a). typical spectra; (b). marker response for adsorbed intermediates and end products.

From the respective marker response for intermediates and mineralization products, as shown in Fig.4-9b, photo-oxidation of ethanol is evidently sequential:

(1) 0~6 hours: the primary reaction is photo-dehydrogenation of ethanol to acetaldehyde, as indicated by the steady consumption of ethanol and accumulation of acetaldehyde (see Eqn. 4.3).

$$CH_3CH_2O^-_{ad} + h^+ \longrightarrow CH_3CHO + H\bullet \qquad (4.3)$$

[It was observed that the acetate bands (from previous experiment) also decreased, but only tiny CO_2 and H_2O were produced in this range];

(2) 6~10 hours: the acetaldehyde band passed through a maximum and then started to decrease, presumably due to exhaustion of ethanol and further oxidation of the aldehyde. Markers for mineralization products, viz., gas-phase CO_2 (2350 cm^{-1}) and adsorbed H_2O (3400 cm^{-1}), started to increase in parallel. The acetate bands were relatively stable in this range, suggesting a balanced *supply* (from acetaldehyde - see eqns. 4.4 & 4.5) and *consumption* (mineralization to CO_2 and H_2O - see eqn. 4.6). The formation of acetate can be either from direct O insertion to acetaldehyde (eqn. 4.4) or through derived from the *Cannizzaro* disproportionation (eqn. 4.5).

$$2CH_3CHO + O_2 \xrightarrow{TiO_2,UV} 2CH_3COOH \qquad (4.4)$$

$$2CH_3CHO + H_2O \longrightarrow CH_3CH_2OH + CH_3COOH \qquad (4.5)$$

$$CH_3COOH + 2O_2 \xrightarrow{TiO_2,UV} 2CO_2 + 2H_2O \qquad (4.6)$$

(3) 10~14 hours: acetaldehyde was consumed continuously, and photo-mineralization of acetate (Eqn. 4.6) became dominant, as indicated by the rapid decrease of acetate bands and formation of CO_2 and H_2O bands.

After 14 hours, the CH_{str}, acetaldehyde, and acetate bands were completely eliminated, while CO_2 and H_2O_{ad} bands reached their maximum values. The latter remained unchanged over the next 6 hours, signaling complete mineralization.

As a key intermediate of ethanol photo-oxidation, direct photo-mineralization of acetate was further investigated. Fig. 4-10 shows the spectral and respective band changes during UV irradiation. The two strong bands of acetate ν(COO) at 1560 cm^{-1} and 1440 cm^{-1} continues to decrease in intensity while the band areas of both CO_2 and H_2O increase with the time, indicating photo-mineralization of acetate to final products CO_2 and H_2O proceeds steadily in the presence of O_2.

The observations of intermediates, such as acetaldehyde and acetate, coherent with the previous by Anderson et al. [72,101] and Chuang et al.[66,70] Although formate was also found as an intermediate in their studies, we find that it is difficult to distinguish it with acetate here.

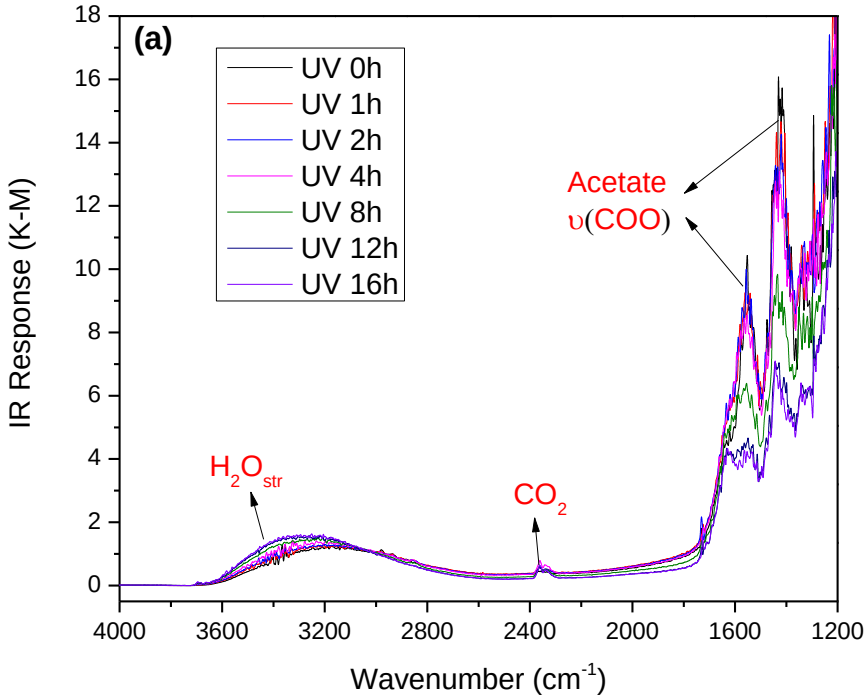

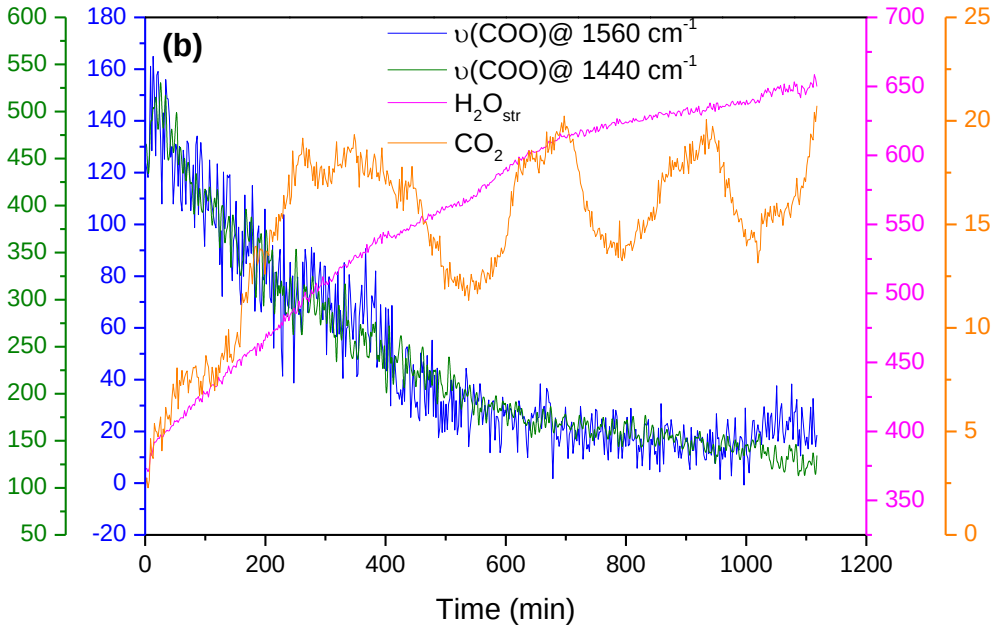

Figure 4-10 DRIFT spectral changes in TiO_2 during photo-mineralization of acetate in air: (a). typical spectra; (b). marker response for acetate, CO_2 and H_2O.

4.3 Photo-platinization of TiO_2

When TiO_2 is excited by band-gap illumination, electron-hole pairs are generated. Although most of them will recombine rapidly in the bulk, some will migrate to the surface, become trapped, and take part in subsequent reactions: holes for oxidation, electrons for reduction. The latter can be utilized to reduce metal ions in the vicinity and deposit zerovalent metallic nanoparticles to act as co-catalysts. As stated in Chapter 4.1, pristine TiO_2 is inactive for photocatalytic H_2 production from H_2O. Loading of co-catalysts like Pt (for H_2 evolution) and RuO_2 (for O_2 evolution) results in better performance. [3]

Photo-metallization is a popular and convenient method to deposit zerovalent metal crystallites on the surface of metal oxide semiconductors, typically by band-gap illumination in the presence of pre-sorbed complexes although direct photodeposition from contacting solution may also be viable.[69] Simple alcohols like methanol or ethanol are better hole-scavengers than water, so it is reasonable to use them as sacrificial agents for the oxidation half-cycle of the photo-redox process.

In this work, samples were prepared by prior impregnation of TiO_2 with H_2PtCl_6. UV illumination was conducted in the presence of ethanol as hole scavenger, entrained into a carrier flow of Ar from a liquid micro-pump/vaporizer.

DRIFTS monitoring of the photo-metallization process showed an interesting but complex sequence of spectral development, as shown in Figure 4-11a.

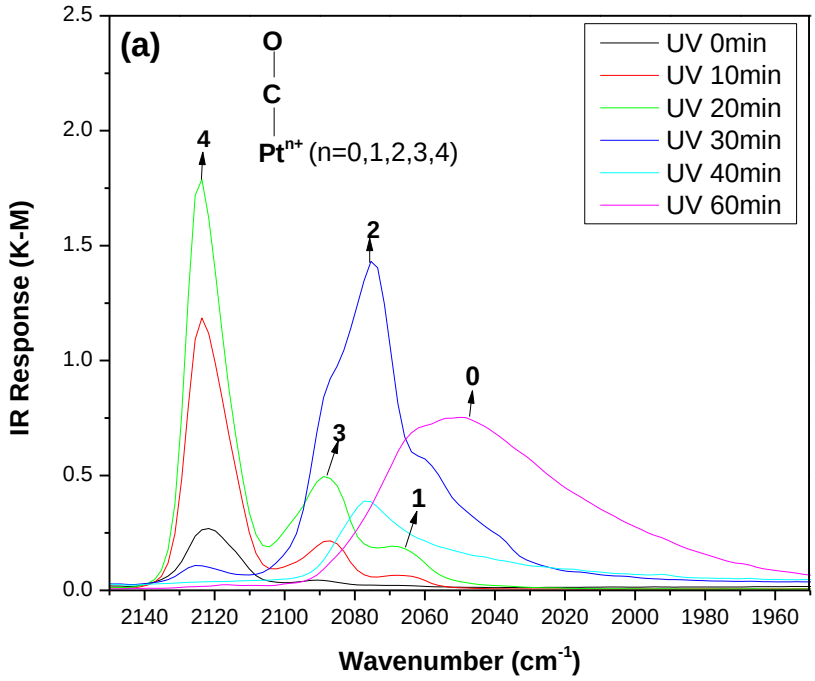

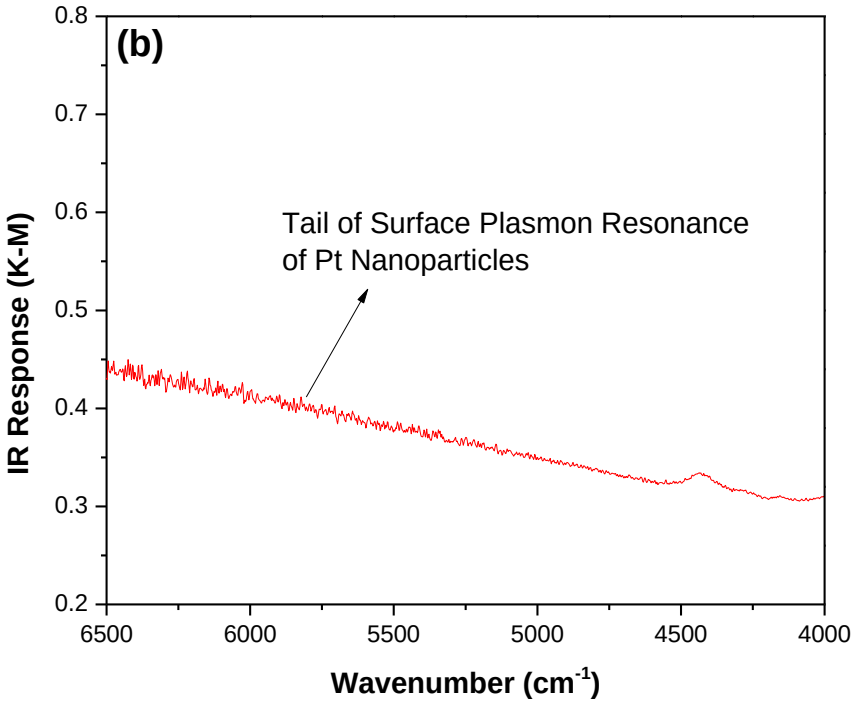

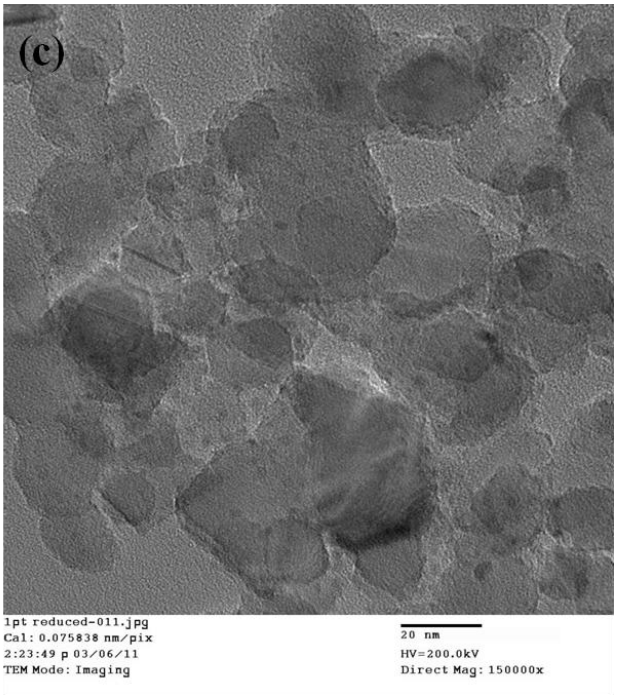

Figure 4-11 Photo-reduction of Pt^{n+} in the presence of ethanol (a) variation of Pt^{n+} - CO band with time during photo-metallization; (b) tail of surface plasmon resonance of Pt nanoparticles; (c) TEM images of Pt nanoparticles on TiO_2

The general position of the bands (2100 cm^{-1}) is typical of CO adsorbed on Pt clusters in a range of oxidation state(s).[69] However, the overall trend was, in effect, a shift of band position to lower wavenumber in a series of distinct stages, viz., 2120 cm^{-1}→ 2090 cm^{-1}→ 2075 cm^{-1}→ 2060 cm^{-1}→ 2050 cm^{-1}.

The five distinct peak positions and their temporal sequence enables tentative assignment to CO adsorbed on Pt clusters in average oxidation states IV (2120 cm^{-1}), III (2090 cm^{-1}), II (2075 cm^{-1}), I (2065 cm^{-1}) and zero (2050 cm^{-1}). The last peak, which reached a stable intensity after 1-2 hours, is diagnostic of CO on metallic Pt clusters in the nanometer range. This also implies the occurrence of significant aggregation over the same time-scale.[102]

The emergence of zerovalent Pt nanoparticles was also verified by the developing baseline, as shown in Fig. 4.11b. Its characteristic slope, with absorption increasing across the near IR towards the visible range, is suggestive of the low frequency tail of the surface plasmon resonance of deposited Pt nanoparticles.[103] This was supported by TEM micrographs, as shown in Figure 4-11c, indicating a mean Pt particle size around 2~3 nm.

4.5 Summary

In this chapter, Diffuse Reflectance Fourier Transform Infrared (DRIFT) spectroscopy has been applied to investigate various photocatalytic reactions at the gas/solid interfaces of pristine and platinized TiO_2. It was found that in the absence of O_2, addition of either H_2O or ethanol or a mixture of them when TiO_2 was irradiated causes progressive accumulation of trapped electrons on TiO_2 surface, suggesting the reduction reaction does not process steadily. The trapped electrons in return induce the re-dispersion of H_2O on the surface. O_2, as an efficient electron scavenger, is able to consume the trapped electrons and causes oxidation of ethanol on TiO_2 surface, with acetaldehyde and acetate as the intermediates and CO_2 and H_2O as the final products. By using ethanol as hole-scavenger, photo-generated electrons could also be used to deposite metallic Pt nanoparticles on TiO_2 surface.

Chapter 5. Investigation of Photocatalytic Reactions at the Liquid/Solid Interface by ATR-FTIR

In Chapter 4, interaction and reaction of gaseous simple molecules such as H_2O, O_2 and ethanol on TiO_2 surface have been studied by DRIFTS. However, despite its immediate relevance to science and industry, the liquid/solid interface has been much less studied due to lack of commercial accessories. In the IR region, a recent method emerging for *in situ* measurement of species at the solid/liquid interface is Attenuated Total Reflection Fourier Transform Infrared (ATR-FTIR) spectroscopy.[104] While changes in the electronic state of TiO_2 induced by UV illumination using *in-situ* ATR-FTIR has just been reported,[78] to the best of our knowledge its correlation with photocatalytic activity and the effect of metallization, as described herein, is new.

Interest in this project centers on the photocatalytic reforming of simple alcohols like methanol[69] and ethanol.[105-107] Such compounds, if derived from biomass, may be considered as high-density storage forms of renewable hydrogen. While DRIFTS (vapor/solid) investigations of ethanol photo-oxidation have been reported,[66,70,72] adventitious oxidation of ethanol in the condensed (dilute aqueous) phase is of more concern in practice, since most bio-ethanol is worked up from fermentation broth in just such a form.

In this chapter, we apply *in-situ* ATR-FTIR spectroscopy to study the photo-oxidation of dilute aqueous ethanol, including direct tests on probable intermediates, acetaldehyde and acetic acid, over pristine and platinized Degussa P25 TiO_2. As compared to pristineTiO_2, which was barely active, simultaneously accumulating electronic charge, platinization enhanced the photo-reduction process by acting as an

electron “sink” and more effectively activating dioxygen for mineralization. Ethanol is oxidized (photo-dehydrogenated) initially to acetaldehyde, and then to acetic acid. Evidence for C–C bond cleavage is also shown by the appearance of metal-adsorbed CO. However, the mineralization of acetic acid (as sorbed acetate) was very slow, suggesting it is the rate-determining step in ethanol photo-mineralization.

5.1. Adsorption from aqueous ethanol on thin-layers of pristine & platinized P25 TiO_2 in the dark.

The IR spectrum of a typical deposited layer of TiO_2 is shown in Figure 5-1. The pronounced absorption below 1000cm^{-1} is characteristic of the intense TiO_2 lattice phonon. This was used as a “gauge” in preliminary work to arrive at a suitable layer thickness (4-5 μm) with acceptably high spectral contrast.

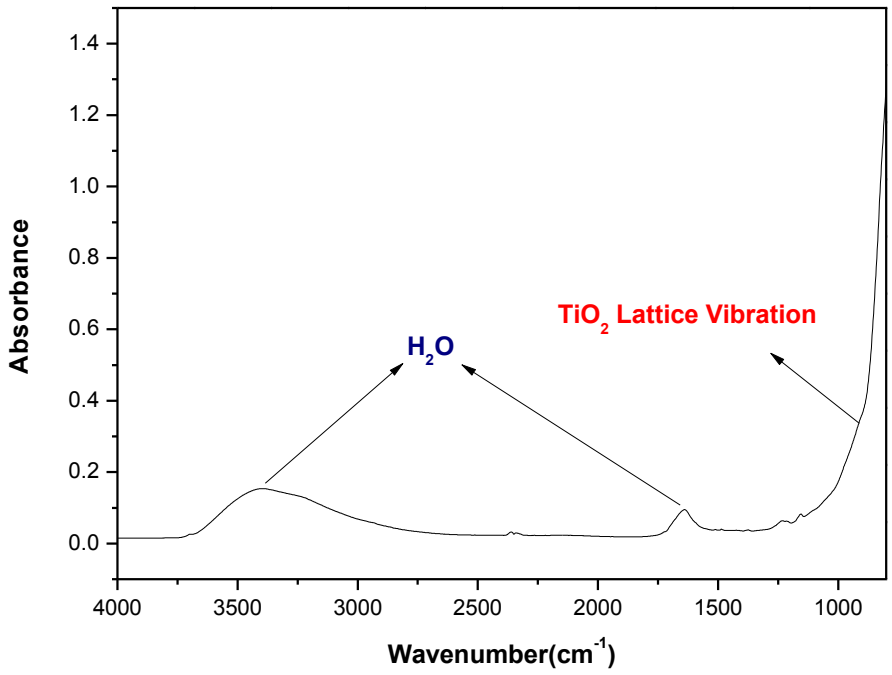

Figure 5-1 ATR-FTIR spectrum of TiO_2 thin film deposited on ZnSe crystal (Density: 5 mg cm^{-2} TiO_2; spectral background obtained from dry ZnSe)

In the first of a series of control experiments, Fig. 5-2 shows spectral changes on the P25 TiO_2 surface when 0.86M EtOH solution (O_2-free) was circulated into the ATR cell in the dark after pre-conditioning in DI water. Displacement of water from the TiO_2 surface is indicated by two broad negative H_2O bands, respectively at 3600~3000cm^{-1} (ν_{OH}) and 1700~1500cm^{-1} (δ_{OH}), while positive bands emerged characteristic of ethanol around 3000~2800,1400~1300, and 1100-1000 cm^{-1} (band assignments as indicated in Fig.5-2). It is difficult to distinguish between molecularly- and dissociatively-adsorbed ethanol (ethoxide) (as shown in Figure S5-1 in appendix).

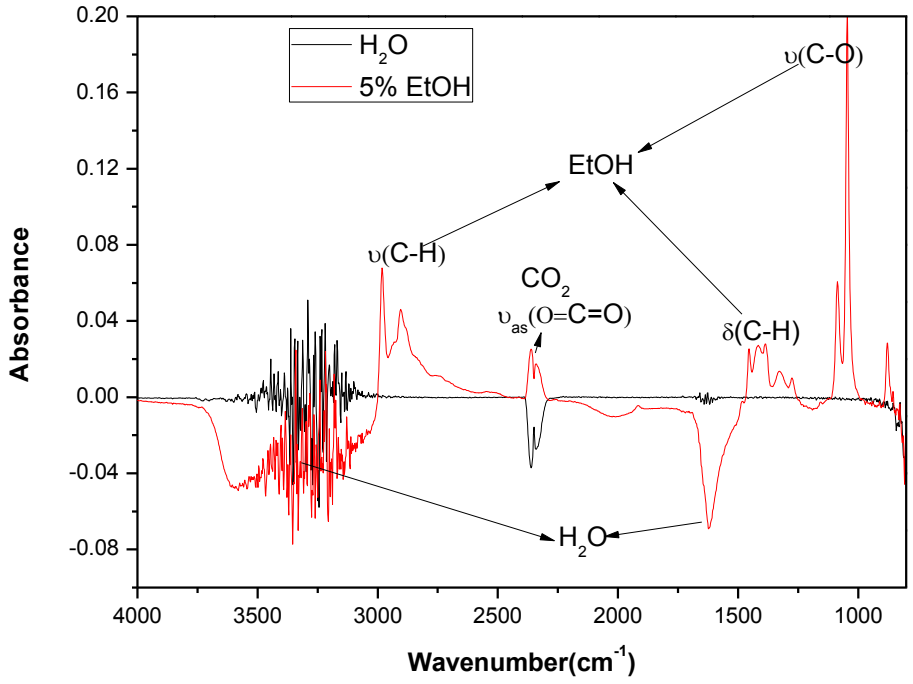

Figure 5-2 Adsorption of ethanol on P25 TiO_2 (TiO_2 thin film density = 5 mg cm^{-2}; background spectrum was obtained from the fresh sample immersed in DI water).

A similar competition between alcohol and water for adsorption sites on P25 TiO_2 has already been seen for methanol by DRIFTS in this laboratory.[69] Various reports have shown that simple monobasic alcohols adsorb on anatase and rutile surfaces in both molecular and heterolytically dissociated forms.[108-110] For ethanol, dissociation results in sorbed ethoxide groups atop a Lewis acidic Ti^{4+} centre (monodentate) or between two Ti^{4+} centers (bidentate), while the H from the alcohol associates with a neighbouring basic surface O to form an OH group.[108,110] The possibility of detecting ethanolic species on the metal component is extremely low in view of the small Pt loading and the relatively weak interaction. Indeed, very little difference can be seen between spectra taken either in the presence or absence of the photocatalyst layer. Thus, the ATR-FTIR set-up in this case (ethanol in the dark) samples mainly bulk species. The small change in absorption at 2350 cm^{-1} is an instrumental artifact associated with the FTIR spectrometer. Slow and periodic micro-changes in the compressed dry air purge quality protecting the KBr beamsplitter result in a slightly varying level of gaseous CO_2.

5.2 Ethanol photo-oxidation over pristine TiO_2.

Figures 5-3a and 5-3b show the ATR-FTIR raw and difference spectra, respectively, recorded during the photo-oxidization of EtOH over pristine P25 TiO_2. The most striking feature here is the initially rapid upward shift in the baseline, evidently more pronounced in the low-wavenumber range, peaking at around 1000 cm^{-1}. There is also a progressive and contemporaneous weakening of the deformation band due to adsorbed water at ~1625 cm^{-1}.

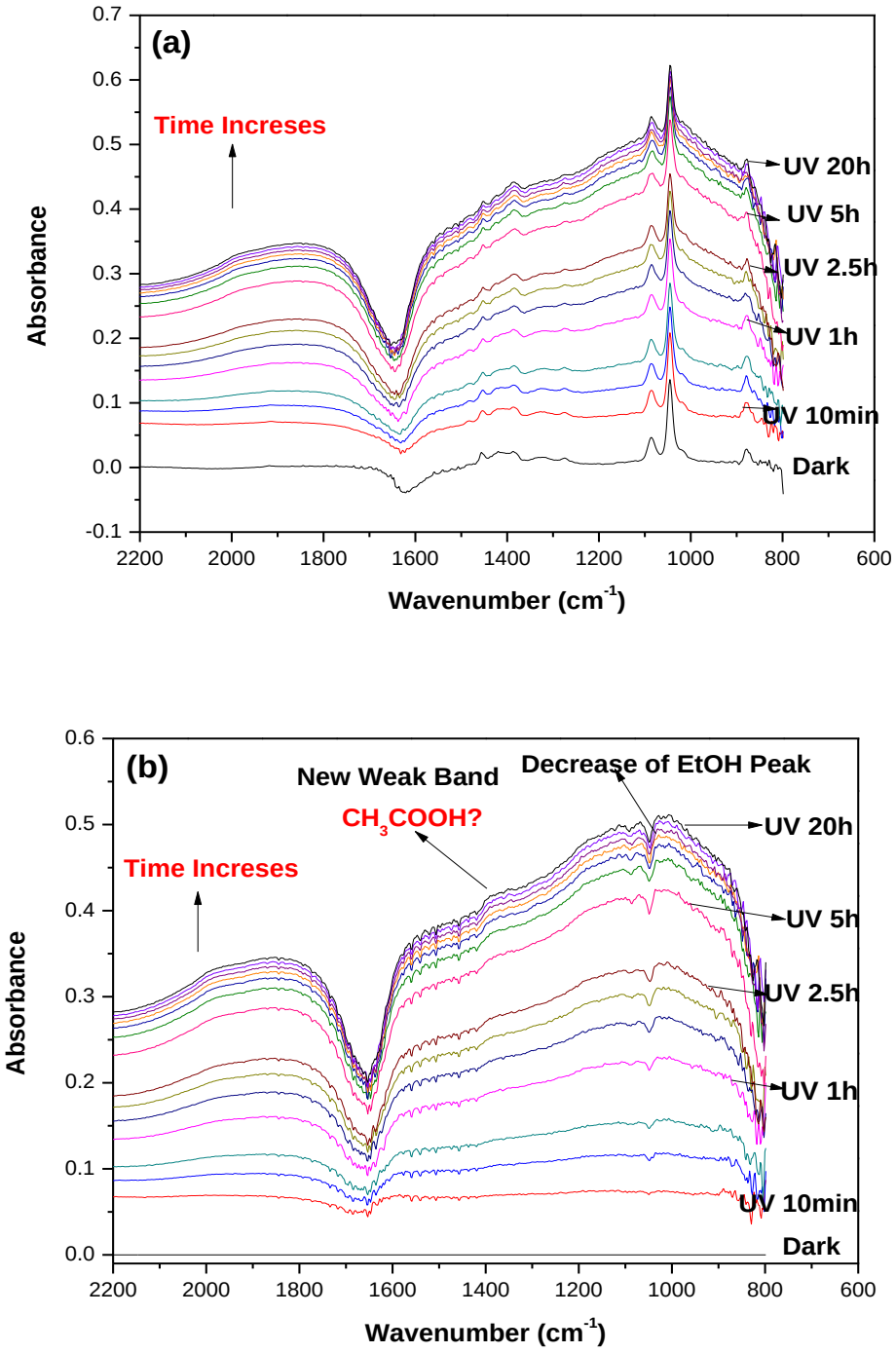

Figure 5-3 ATR-FTIR spectra during photo-oxidization of 0.86 M ethanol over pristine P25 TiO_2: (a) raw spectra (vs. TiO_2/H_2O reference); (b) difference spectra (vs. $EtOH/H_2O$ reference- dark).

Coincidentally, we have just become aware of independent ATR-FTIR studies reporting very similar features for TiO_2 in aqueous oxalate environment.[78] Whereas these authors attribute the water loss to hole-induced photo-dissociation into surface OH groups, we think this is not very likely in the presence of ethanol, which is by far the superior hole-scavenger. However, there is another key difference in reaction conditions. Whereas in Fig. 5-3 the background absorption (and water loss) develops under oxygenated conditions, *Savory et al.* worked under anaerobic conditions and effected rapid elimination of these spectral features by introduction of air. This sensitivity to O_2, which can ionosorb as superoxide (O_2^-) and/or act as a recombination centre, is consistent with previous literature.[71] Pioneering DRIFTS studies by Hoffmann et al [55,62] are the original source of the continuum mid-IR absorption (due to long-lived charge carriers) seen over O_2-free hydroxylated TiO_2, which they convincingly demonstrated was associated with photo-generated electrons filling (energetically) deep or shallow surface traps. Prior to this work, pump-probe UV-Vis-NIR photoacoustic spectroscopy was used to study the analogous photochromism in P25 TiO_2 (small polaron absorption, peaking in the near IR region), again illustrating the importance of having moist O_2-free conditions to best visualize this feature.[61,103] Otherwise, there are only minor spectral changes in Fig. 5-3, suggesting that photo-mineralization of aqueous ethanol is severely impaired over pure TiO_2. There is slow conversion of EtOH, as indicated by the gradual appearance of negative peaks around 1050 cm^{-1} due to the C–O stretch. However, the decrease in integrated area of this band suggests just a few percent of conversion after illumination for more than 20 hours. Acetaldehyde and acetic acid are both known intermediates of ethanol photo-oxidation in the vapor phase.[66,70,72,111,112] However, the

$\nu_{C=O}$ band of acetaldehyde, expected at ~1715cm^{-1}, is obscured by the relatively strong negative δ_{H-O-H} band at ~1630 cm^{-1}. Similarly, while there is a weak development of broad features in the range 1500-1300 cm^{-1}, where the doublet due to adsorbed acetate would be expected, the strong background absorption renders them insufficiently defined for any confident assignment. Accordingly, little or no difference was seen in ATR-FTIR between aerated and de-aerated solution.

5.3 Ethanol photo-oxidation over platinized TiO_2.

From control tests under both dark/aerated and UV/de-aerated (photo-reforming) conditions, little or no change was observed in the ATR-FTIR spectra when aqueous ethanol was equilibrated over a deposited layer of 0.5wt% Pt/TiO_2 for 15-20 hours (as shown in Figures S5-2 and S5-3 in appendix). Figures 5-4 & 5-5 show the ATR-FTIR difference spectra recorded under photo-oxidizing (UV/aerated) conditions and the changes of respective bands with time. The first substantial difference with pristine TiO_2 is the only slight build-up in background absorption over many hours. In addition, absorption bands characteristic of acetaldehyde (carbonyl stretch, $\nu_{C=O}$, at 1715 cm^{-1}) and acetate [asymmetric and symmetric stretch of the carboxylate moiety (ν_{OCO}) at 1550 & 1415 cm^{-1}, respectively], were seen already within the first few hours of illumination and continued to grow overnight. The identities of these intermediates were confirmed in separate experiments by their direct contact with the fresh catalyst, as described later (*vide infra*).

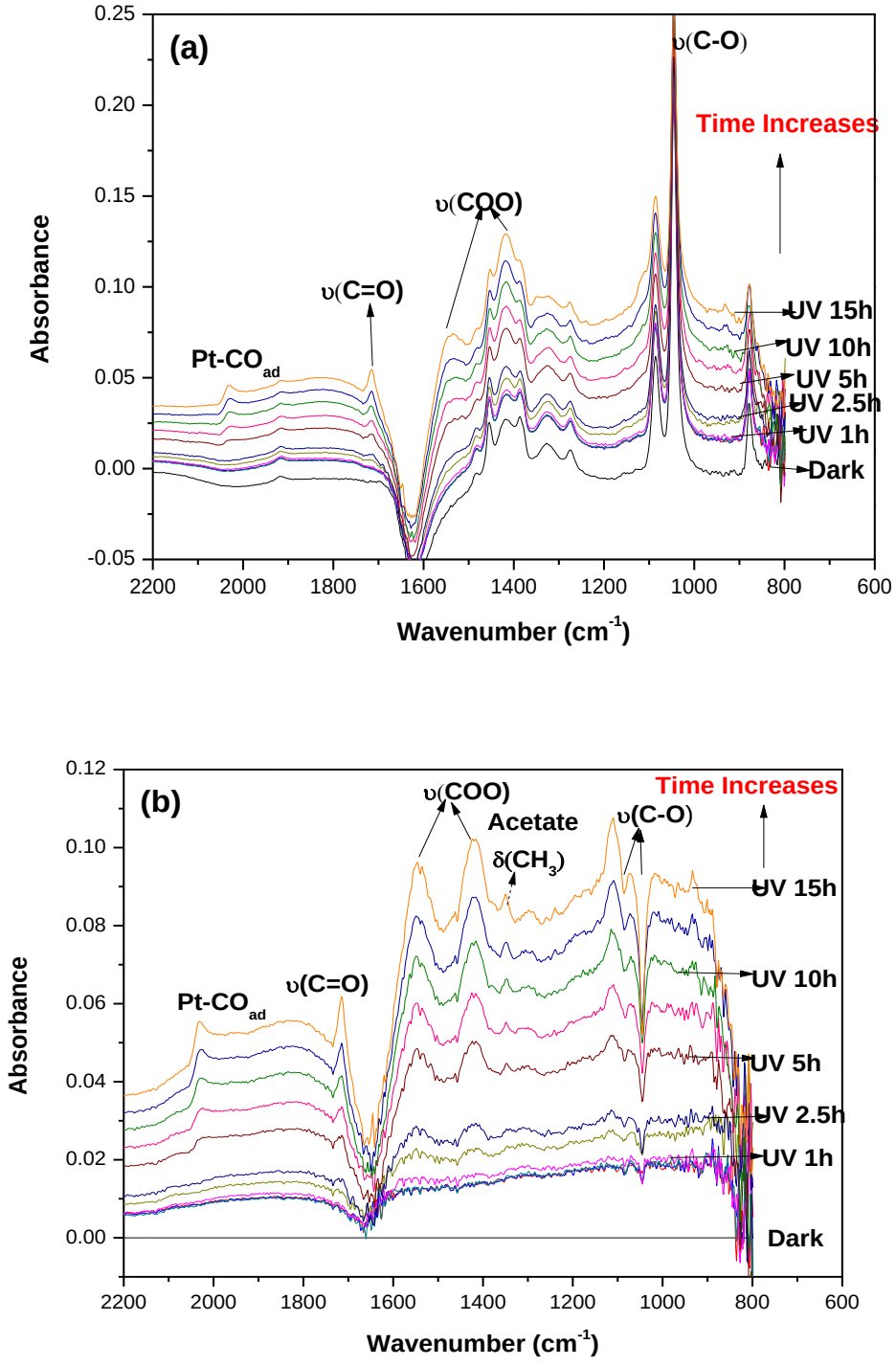

Figure 5-4 ATR-FTIR spectra during photo-oxidization of 0.86 M ethanol over 0.5wt% Pt /P25 TiO_2: (a). raw spectra (vs. TiO_2/H_2O reference); (b). difference spectra (vs.$EtOH/H_2O$ reference- dark).

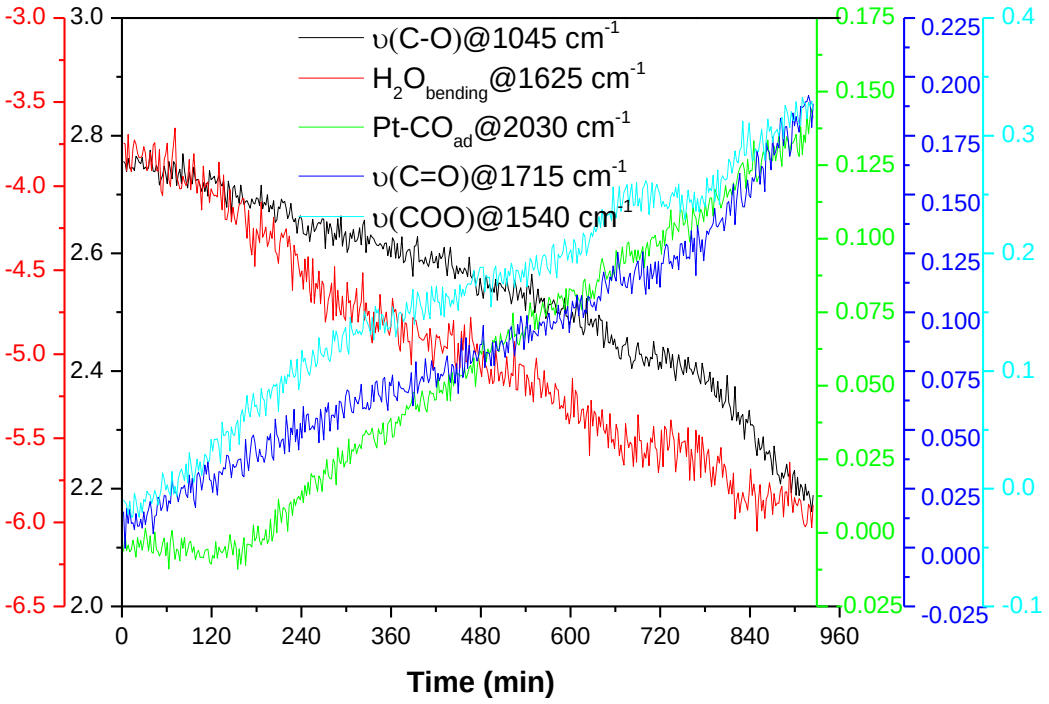

Figure 5-5 Spectral marker response: photo-oxidation of 0.86 M ethanol over 0.5% Pt/P25 TiO_2

The most likely sequence is that EtOH in aqueous solution over the platinized sample first undergoes photo-dehydrogenation (PDH) to acetaldehyde, which is in turn oxidized to acetic acid. According to Pichat,[113] the production of aldehydes from alcohols over Pt/TiO_2 involves a combination of dissociative adsorption in the dark and H abstraction from the adsorbed alkoxy group by a photo-generated hole, as shown schematically for ethanol in equations 5.1 & 5.2:

$$CH_3CH_2OH \longrightarrow CH_3CH_2O - Ti_s + O_s - H \qquad (5.1)$$

$$CH_3CH_2O - Ti_s + h^+ \longrightarrow CH_3CHO + H\cdot \qquad (5.2),$$

where Ti_s and O_s are surface ions (formal charges omitted for clarity). PDH is completed by proton discharge and H atom recombination over Pt:

$$H^+ + H\cdot + e^- \xrightarrow{Pt} H_2 \quad (5.3)$$

The summation of equations 1-3 corresponds to ethanol PDH:

$$CH_3CH_2OH \longrightarrow CH_3CHO + H_2 \quad (5.4)$$

which, while efficient ($\Phi \approx 0.5$), is also endergonic (thermodynamically uphill),[114] with an enthalpy increase of 86 $kJ \cdot mol^{-1}$. Under the static, ambient (equilibrium) conditions applied here, there is a strong likelihood of thermodynamic control, i.e., back-reaction between acetaldehyde and hydrogen. This would explain why no clear evidence was seen for acetaldehyde in the photo-reforming control test (see Fig. S5-3 in appendix). Nevertheless, extended illumination eventually gave rise to very slight bubbling, which was identified as H_2 gas by MS in separate experiments. Thus, evidence of more acetaldehyde production under photo-oxidative conditions can only be rationalized as "oxidative dehydrogenation", i.e., any H atoms are rapidly scavenged by dioxygen to produce water.

Extended illumination gradually gave rise to an additional band around 2050 cm^{-1}, which is characteristic of CO adsorbed on Pt in the "on-top" position.[102,115-117] It appeared initially at ca. 2030 cm^{-1} but progressively shifted to higher frequency due to the coverage-dependent dipolar coupling effect. Identical features have already been observed over Pt/TiO_2 by DRIFTS during photo-reforming of methanol vapour.[69] However, it is a surprising observation insofar as, from our previous work on methanol photo-reforming, adsorbed CO on Pt was extremely reactive with ambient air even in the dark. Furthermore, previous independent ATR-FTIR studies of CO oxidation over Pt/Al_2O_3 emphasize that the liquid environment has a dramatic influence on the rate, being accelerated in pure water,[118,119] but markedly hindered in ethanol[120], as compared to the gas-phase. So although the cause of the growth of the

Pt-CO_{ad} species is unclear at this stage, it inevitably raises concerns as to the maintenance of O_2 supply over the entire experiment. One potential source of CO is decarbonylation of acetaldehyde:

$$CH_3CHO \longrightarrow CO + CH_4 \quad (5.5)$$

Although it is difficult to identify products in the gas phase by the ATR technique, CH_4 has been detected by *in situ* DRIFTS during ethanol photo-reforming at elevated temperature.

Despite the aforementioned concerns, the acetate bands continued to grow alongside Pt-CO_{ad}, indicating that acetic acid is, at least partially, derived from the *Cannizzaro* disproportionation, which does not formally require dioxygen, water acting as oxidant instead:

$$2CH_3CHO + H_2O \longrightarrow CH_3CH_2OH + CH_3COOH \quad (5.6)$$

This is the analogous process identified as the source of formate from methanol in photo-reforming.[69] Early studies of ethanol reforming in thermal heterogeneous catalysis led to a similar conclusion, although temperatures close to 100 °C were required to develop adsorbed acetate bands from the aldehyde over a Co/Cu/MgO catalyst.[106]

5.4 Acetaldehyde and acetic acid photo-oxidation over platinized TiO_2.

Having verified the identities of two key intermediates in ethanol conversion, viz., acetaldehyde and acetic acid, their independent and direct photo-oxidation on platinized TiO_2 was also of interest to propose a plausible mechanistic scheme. Figures 5-6 & 5-7 show ATR-FTIR spectra and functional group marker response, respectively, recorded during the photo-oxidation of acetaldehyde over platinized

TiO_2. Consumption of the aldehyde is seen most clearly as the progressive weakening (shift to more negative values) of the diagnostic carbonyl stretch, $\nu_{C=O}$, at 1720 cm^{-1}.

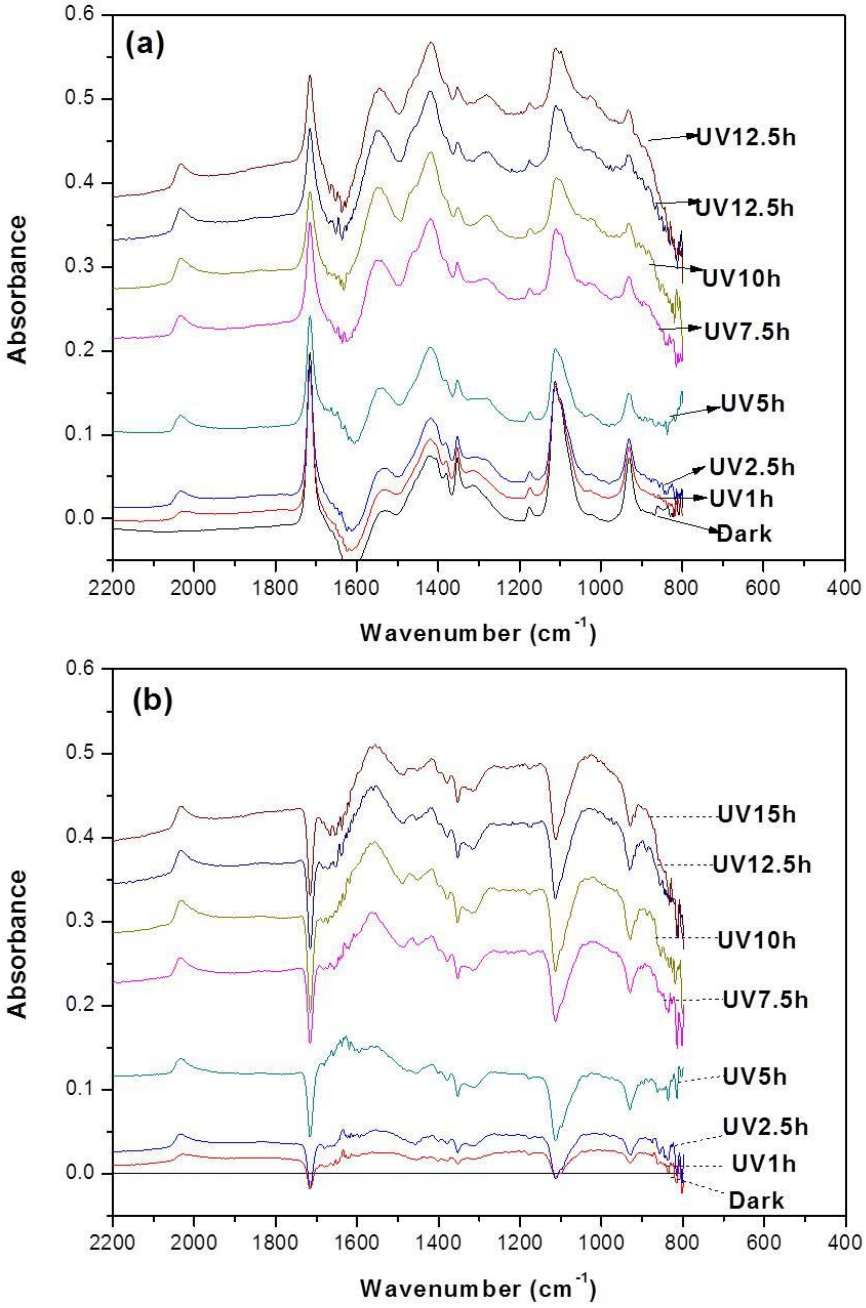

Figure 5-6 ATR-FTIR spectra during photo-oxidation of 0.89 M acetaldehyde over 0.5% Pt/P25 TiO_2: (a). raw spectra (vs. TiO_2/H_2O reference); (b).difference spectra (vs. acetaldehyde/H_2O reference- dark).

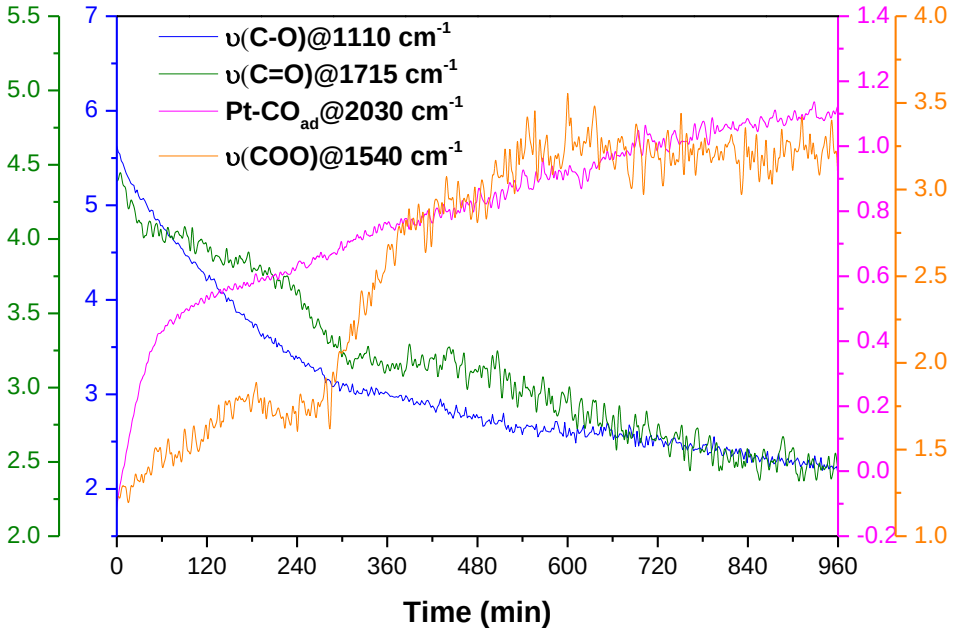

Figure 5-7 Spectral marker response: photo-oxidation of 0.89 M CH_3CHO over 0.5% Pt/P25 TiO_2

Figure 5-6 & 5-7 also show that the bands of acetate (asymmetric and symmetric stretch of the carboxylate moiety, ν(OCO), around 1550 & 1415 cm^{-1}, respectively) grew with time, thus, acetaldehyde is gradually converted to acetic acid in a parallel process to decarbonylation.

The gradual appearance of Pt-CO_{ad} proves that the aldehyde is indeed one source of CO. However, unless conditions are well-controlled and rates carefully compared, this does not rule out an additional route to CO from ethanol in which the C–C bond is cleaved *before* dehydrogenation.[121,122] To evaluate this, Figure 5-8 compares the growth curves for Pt-CO_{ad} derived from the aldehyde (Figure 5-6) and from the alcohol (Figure 5-4) under otherwise equivalent conditions. These show that CO is

generated immediately and initially faster from acetaldehyde. The delay in appearance of CO from ethanol can be interpreted as a sensitivity issue, i.e., the time required for sufficient build-up of aldehyde level, it being mechanistically the most immediate, and apparently the sole, source of CO. Decarbonylation of acetaldehyde is evidently *photo-activated* as no adsorbed CO band developed over several hours in the dark prior to illumination.

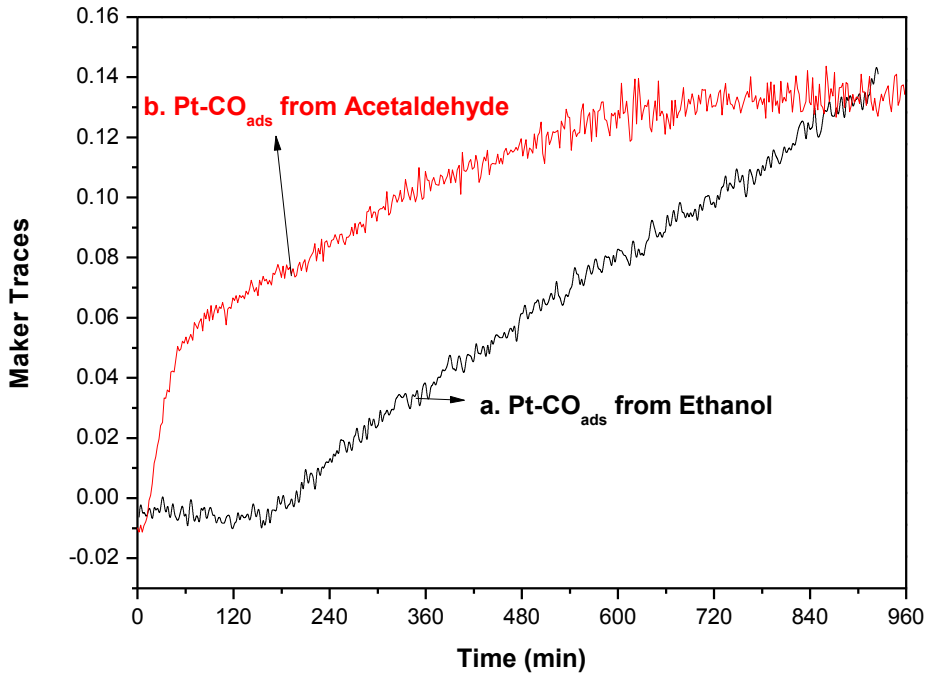

Figure 5-8 Spectral marker response showing growth of Pt-CO_{ads} during photo-reaction: (a) from 0.86M ethanol (black); (b) from 0.89M acetaldehyde (red)

The direct photo-oxidation of acetic acid was also carried out under the same conditions, and ATR-FTIR difference spectra are shown in Figure 5-9.

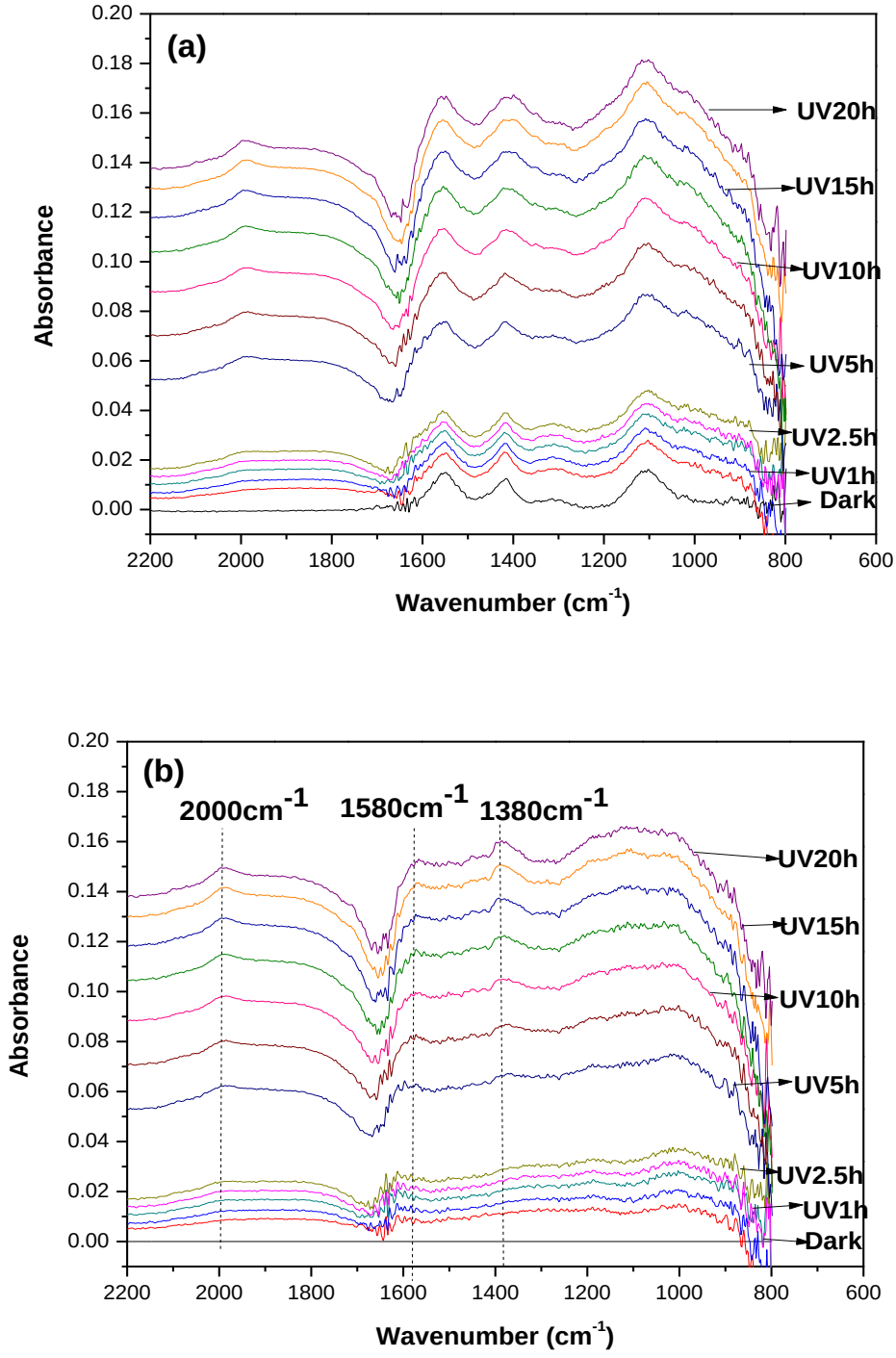

Figure 5-9 ATR-FTIR spectra during photo-oxidation: 1mM acetic acid on 0.5wt.% Pt/P25 TiO_2 a. raw spectra (vs. TiO_2/H_2O reference); b. difference spectra (vs.$EtOH/H_2O$ reference- dark).

1mM acetic acid solution was illuminated for more than 15 hours but the diagnostic bands of acetic acid did not even become weaker. Furthermore, the background absorption remained low, suggesting that the acetate species is not an efficient hole scavenger, unlike the analogous (C_2) alcohol, probably due to the absence of sufficiently photo-labile H.[123,124] A weak band of Pt-CO_{ad} appeared eventually at ~2000 cm^{-1}, similar to those observed from ethanol and acetaldehyde, suggestive of decarbonylation:

$$CH_3COO^-_{ad} \longrightarrow CH_3O^-_{ad} + CO \qquad (5.7),$$

but a putative methoxy group as product would be difficult to distinguish from acetate due to near coincidence in the C-H stretching and bending vibrations of the common methyl group.

Acetate decarbonylation is rather surprising since CO_2 is a more likely product via simple photo-hole-stimulated decarboxylation, or possibly along with CH_4 and C_2H_6 via a Photo-Kolbe coupling mechanism.[125] An additional indirect test for any CO_2 was made. *In-situ* production was simulated by sparging CO_2 through liquid water, with the aim of forming a bulk bicarbonate species readily detectable by ATR-FTIR. The spectral signature (see Figure S5-4 in appendix), against both pure water and the platinized catalyst is consistent, showing two bands of similar intensity close to 1575 and 1325 cm^{-1}, assigned as the asymmetric and symmetric stretch of the bicarbonate moiety.[85] The other two weak bands growing at 1580 cm^{-1} and 1380cm^{-1} in Figure 5-9 can be tentatively assigned to adsorbed carbonate species.[126]

Evidently, the photo-mineralization of acetic acid is very slow indeed and the integrated areas of the acetate bands in the raw spectra even increased slightly, and unexpectedly, under illumination, similar with that Bahnemann et al.[82] reported for

oxalate on TiO_2 during UV illumination. The increase of acetate adsorption here is more likely due to the photo-induced desorption of water from the TiO_2 surface, as indicated by the negative band around 1630 cm^{-1} under illumination. Thus, further acetate adsorption becomes possible. Nevertheless, these slight changes do not obscure or fully explain the growth of bands (and the 1380 cm^{-1} band in particular) in the difference spectra which can be taken as evidence for adsorbed carbonate.

The underlying difficulty in activating adsorbed acetate is not yet clear, but it is not altogether surprising since it has also been identified as the rate-determining step (RDS) by various groups studying ethanol reforming in thermal heterogeneous catalysis.[106,127-129] It may be due to the lack of sufficient oxidant O_2 in liquid phase, because photo-mineralization of acetate in the presence of rich O_2 at the gas/solid interface proceeds steadily (see Fig. 4-10). In any event, the evidence suggests that the rate-determining step in ethanol photo-oxidation over platinized TiO_2 is the activation and mineralization of acetic acid.

5.5 Photocatalyst charging under band-gap excitation and its correlation with photo-activity

As shown in Figure 5-10, the continuum growth or "charging" curve in pristine TiO_2 appears almost exponential with an asymptote, consistent with Hoffmann's view of progressive filling of a fixed number of electron trap states.[22-23]

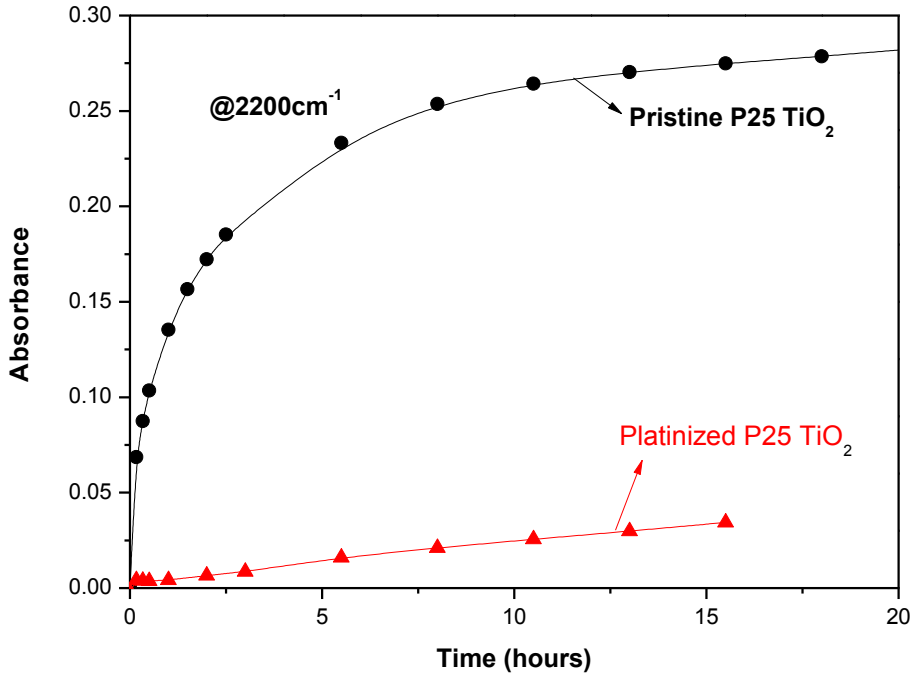

Figure 5-10 Growth curves for continuum absorption (at 2200 cm^{-1}) during photo-oxidation of aqueous ethanol solution over pristine and platinized TiO_2

The build-up of long-lived electronic charge confirms efficient hole scavenging by ethanol, as expected. However, it also suggests that the complementary process to sustain a photo-oxidation cycle, viz., activation of molecular oxygen via ionosorption to form adsorbed superoxide, peroxide, (a 4 electron transfer process overall):

$$O_2 + e^- \rightarrow O^-_{2\,ad} + e^- \rightarrow O^{2-}_{2\,ad} \rightarrow 2O^-_{ad} + 2e^- \rightarrow 2O^{2-}_{ad} \qquad (5.8),$$

occurs only slowly; a situation that cannot be sustained indefinitely. The accumulation of excess negative charge on the catalyst surface will impede hole-induced chemistry by progressively increasing the probability of electron/hole recombination. Consistent with this view, TiO_2 *per se* appears a poor catalyst for ethanol photo-oxidation. In contrast, the presence of Pt suppresses dramatically the charging effect in TiO_2, and at the same time promotes much higher photo-activity. Pt should act as an efficient

electron sink and mediator regardless of the identity of the electron acceptor(s) present at the surface. For good photo-oxidation activity, O_2 must compete with H^+ and $H^\bullet$ for adsorption sites on Pt. Provided there is a good supply of oxidant, there is little reason to doubt this since the kinetics of Pt-catalyzed H_2 oxidation (to water) are well-known.[130] Indeed, this has been indirectly verified here in the fact that O_2 promotes aldehyde production. Furthermore, Pt remains the best cathode material for the O_2 electro-reduction reaction (ORR) in PEM fuel cells.[131,132] Any aldehyde-derived CO which becomes bound to Pt should also be readily converted to CO_2, but the stable CH_4 co-product is undesirable as it is a potent greenhouse gas. For more complete mineralization of the organic carbon, the pre-activated oxidant must migrate or "spill over" to intermediate(s) with the C-C bond still intact , i.e., adsorbed ethoxy, aldehyde, or a derivative species like the acetyl radical ($CH_3CO\bullet$), all of which will be bound predominantly to the oxide surface. Evidence for such oxygen spillover has been reported.[133] Although dioxygen can be ionosorbed directly on TiO_2 as superoxide (O_2^-), there is little evidence for this on the pristine TiO_2 surface as studied here, otherwise it should have suppressed the growth of the IR continuum, notwithstanding any hindrance by the ethanol component (*vide ultra*). Additional electron trapping to form the peroxo species (O_2^{2-}), and/or irreversible dissociation into more highly activated O_{ad}^- species (see equation 5.8) seems much more probable on Pt.[130,131] Indeed, evidence for multiple electron transfer at Pt, e.g., direct formation of peroxide, provides the only plausible explanation for sustained photo-oxidation of organic compounds over Pt/WO_3. In this case, the reduction potential at the conduction band edge of the oxide is insufficiently negative to generate superoxide in

a single electron transfer step.[134] This is also a topical issue in view of growing interest in the direct synthesis of H_2O_2 from H_2 and O_2.[135]

5.6 Water interaction with the TiO_2 surface studied by ATR-FTIR

This section is a more dedicated study of the interaction of water with the TiO_2 surface, stimulated by accumulating evidence, including previous sections in this thesis, showing that band-gap irradiation of TiO_2 perturbs the infrared band intensities of ambient water. It was of particular interest to establish if these spectral effects are one manifestation of "superhydrophilicity" (SHP), a phenomenon that promises a range of technical application. SHP was discovered by Fujishima et al. in 1997.[97] UV irradiation of a glass-supported TiO_2 film in the presence of liquid water causes the droplets to spread and merge into an extended film, such that the previously opaque substrate becomes transparent. Since UV-irradiation evidently improves the wettability of the TiO_2 surface, as supported by contact angle measurements, [97] it was initially rationalized in terms of photo-degradation of adsorbed organic (hydrophobic) contaminants, However, there is growing evidence that SHP is fully-reversible, albeit slowly, in the dark. This casts serious doubt on the "cleaning" mechanism, which is irreversible by definition.[32,38] Current interpretations generally fall into three categories:[38] (1) reductive mechanism; (2) oxidative mechanism; (3) combined redox mechanism. Despite extensive investigation in the last decade, the issue is still not resolved and more surface science studies are needed.

Regarding the effect of UV irradiation on TiO_2, there is now a wealth of evidence, including spectroscopic experiments in this thesis (DRIFTS section-Chapter 4.1, ATR-FTIR –in this part) that it causes progressive, but temporary, accumulation of trapped electrons (and presumably holes) on the TiO_2 surface. This reversible "surface

charging" effect may be responsible for reversible chemical and/or physical changes in ambient molecules. The enhancement of the "electron" spectrum by water, and its suppression by O_2 is already established in the vapour state (see Chapter 4.1).

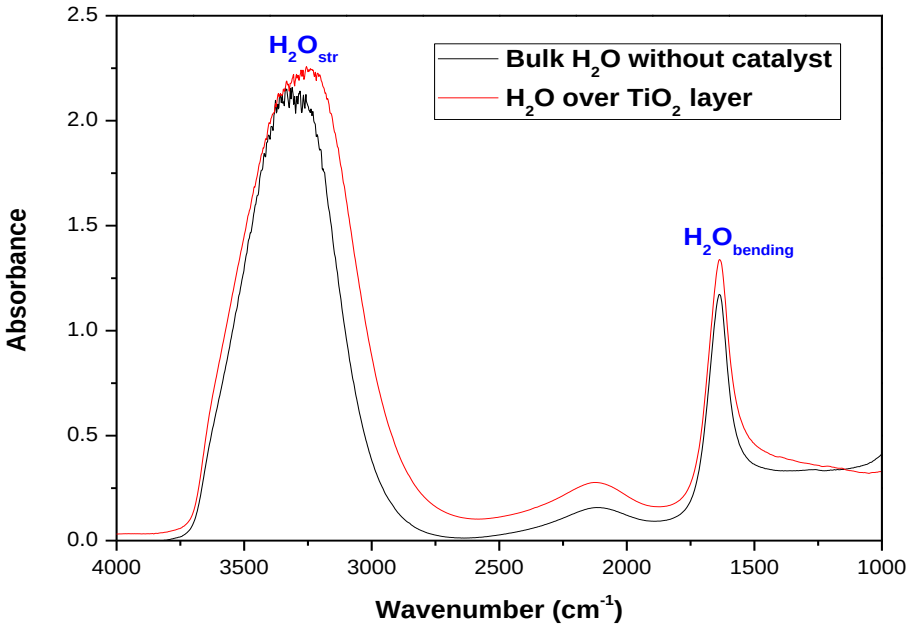

Figure 5-11 ATR-FTIR spectrum of liquid water alone (vs. ZnSe) and in the presence of a 4 μm thick layer of P25 TiO_2 (vs. TiO_2/ZnSe).

Figure 5-11 compares ATR-FTIR spectra of bulk water (vs. dry ZnSe crystal as reference) and over a pre-deposited layer of P25 TiO_2 (vs TiO_2 layer as reference). Liquid H_2O shows three main bands in the mid-IR region, assigned to the stretching (~3300 cm^{-1}), bending (~1635 cm^{-1}), and combination (~2120 cm^{-1}) modes. In the presence of TiO_2 in the dark, these bands are hardly perturbed except for a slight red-shift of the stretching band, suggestive of greater H-bonding at the TiO_2 surface.[136] When this immersed TiO_2 layer was exposed to UV-Vis irradiation, the familiar growth of the IR background spectrum was observed, peaking at 1000 cm^{-1}. Bearing

in mind that the reference spectrum was taken from the same (liquid water) system in the dark condition, the contemporaneous weakening of the H_2O bands, most notably the bending vibration at ~1650 cm^{-1}, suggests an overall lowering of areal or volumetric density in the vicinity of the illuminated TiO_2 surface.

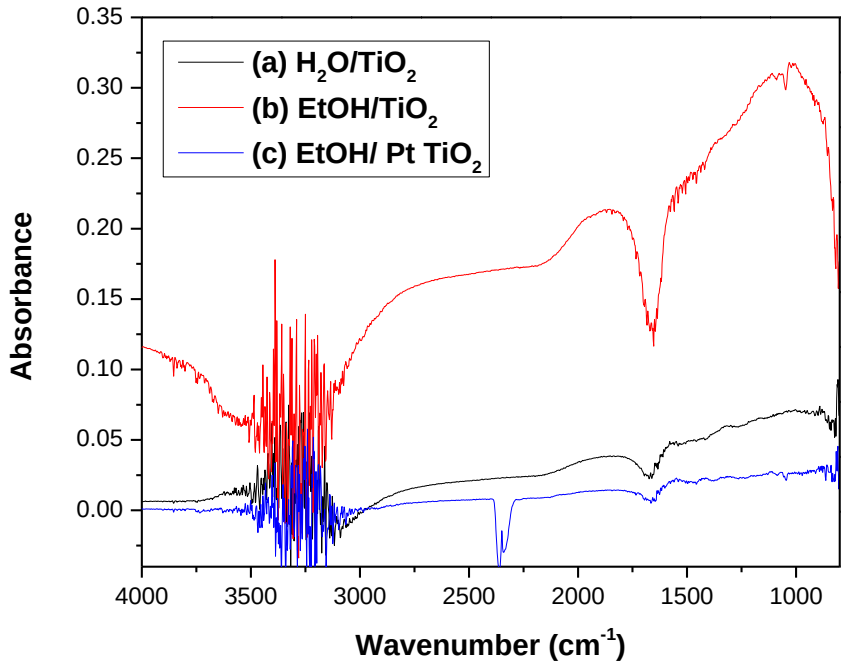

Figure 5-12 (a) ATR-FTIR Spectrum of (a) bulk H_2O over pristine TiO_2, (b) EtOH solution over pristine TiO_2 and (c) EtOH solution over platinized TiO_2 illuminated for 2 hours.

To enhance the build-up of charge and evaluate the effect more definitively, 0.86M ethanol was also introduced. Its role as hole scavenger has already been demonstrated (see Fig. 5-3). As shown in Fig. 5-12b, the background intensified in dilute ethanol while the negative-going H_2O bands were even more striking.[23] In related gas/solid DRIFTS studies, both here (Chapter 4) and elsewhere,[55,62] the spectral continuum is associated with photo-generated electrons filling (energetically) deep or shallow

surface traps. As already reported in Chapter 4, platinization efficiently promotes the consumption of electrons, e.g., by ionosorption of dissolved O_2 as superoxide (O_2^-), and reduction of protons to H_2.[137] Figure 5-12c shows the dramatic suppressive effect of Pt on both the background continuum and any disruptive effect on water band intensities. The small change in absorption at 2350 cm^{-1} is an instrumental artifact associated with the FTIR spectrometer. Slow and periodic micro-changes in the compressed dry air purge quality protecting the KBr beamsplitter result in a slightly varying level of gaseous CO_2.

Several explanations for photo-induced displacement of water as observed here are possible: (1) **photo-induced local heating of TiO_2 surface**. Thermal desorption of adsorbed water by heating, as studied by, e.g., DRIFTS is well-known.[73] A UV light source generates an associated local heating effect in TiO_2 due to non-radiative recombination of charge carriers. However, for water in the liquid phase, there is no possibility of net desorption, only a re-distribution in adsorbed states and/or disruption (expansion) of a compact overlayer due to less effective H-bonding; (2) competitive **adsorption of reaction intermediates**. Ethanol photo-oxidation produces intermediates such as acetaldehyde and acetic acid. The latter is adsorbed on TiO_2 and may displace water. However, we have already seen (Fig. 5.4) that photo-oxidation only proceeds at a significant rate over platinized TiO_2, where water bands are hardly affected; (3) **photo-dissociation of H_2O to OH groups.** Savory et al.[78] attribute similar observations in their ATR-FTIR work to photo-dissociation of H_2O into surface OH groups, an oxidation process at surface-trapped holes. This conclusion was reached because whereas the H_2O bending vibration weakened with time under illumination, the intensity of the OH stretching band envelope was hardly affected. However, this will be highly unlikely in the presence of ethanol, which is by far the

superior hole-scavenger. Ethanol will be preferentially photo-oxidized to the exclusion of water, even if the latter is present in excess.

The only convincing explanation is that disruption of the adsorbed water layer is due to the build-up of trapped charges on the TiO_2 surface. Figure 5-13 shows the progressive filling of surface (electron) trap states and the contemporaneous change in band intensities of adsorbed water.

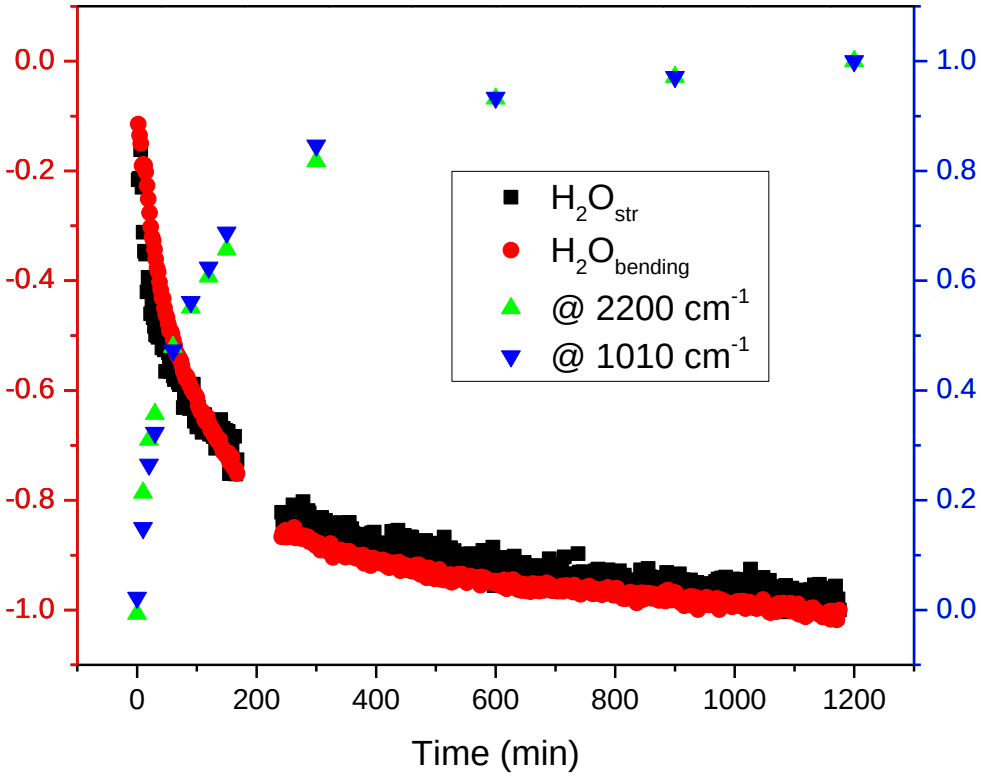

Figure 5-13 Correlation of trapped electron level (signal at 2200 and 1010 cm^{-1}) and intensity of water bands (marker response) on normalized scales.

The normalized change in signals at two locations, viz., 2200 cm^{-1} and 1010 cm^{-1}, exactly match, confirming that they have a common origin. These increase almost exponentially with an asymptotic approach to steady-state after 5 hours. In contrast,

the H_2O bands at 3300 cm^{-1} and 1650 cm^{-1} show a clear anti-correlation, decreasing progressively at the same rate and also leveling out after 5 hours.

The change in band intensity is reversible. After a long illumination for 20 hours, a switch to dark conditions caused the background to weaken somewhat. At the same time, the negative water band recovered (becoming less negative) by almost 60% relative (as shown in Figure 5-14).

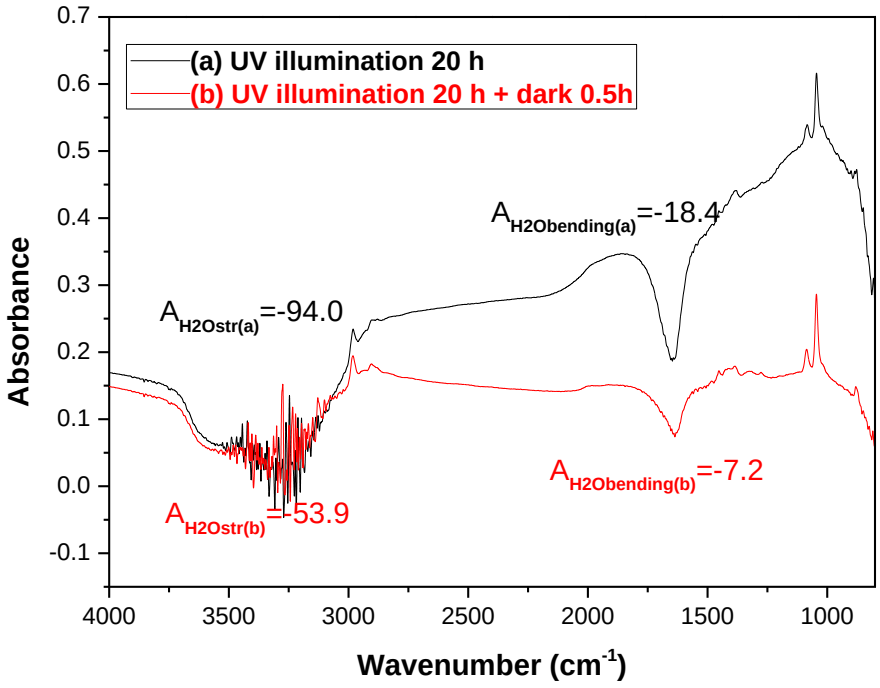

Figure 5-14 Reversibility of photo-induced band changes in the dark (post illumination).

Inclusion of an electron-acceptor (Fe3+) in solution, in the absence of ethanol, impeded development of the background under illumination, and completely suppressed the (negative) band response of water (as shown in Figure 5-15). This is also observable in the spectra of Nakato et al.,[79,80] obtained during O_2 photo-reduction

experiments although no explicit statement was made in their paper. In this situation, photo-generated electrons will be consumed by Fe^{3+}:

$$Fe^{3+} + e^{-} \rightarrow Fe^{2+} \qquad (5.9),$$

while the holes are involved in oxidative processes. Once again, the simultaneous suppression of both features of accumulation of trapped electrons and the decrease in intensities of H_2O bands indicates that surface-trapped electrons effectively repel water, or drastically weaken its binding to the TiO_2 surface. Calculations on Ti^{n+} (n =4, 3, 2) hydrate complexes appear to support this observation, a drastic lowering of the enthalpy of hydration being reported when Ti^{4+} is replaced by Ti^{3+}. [138]

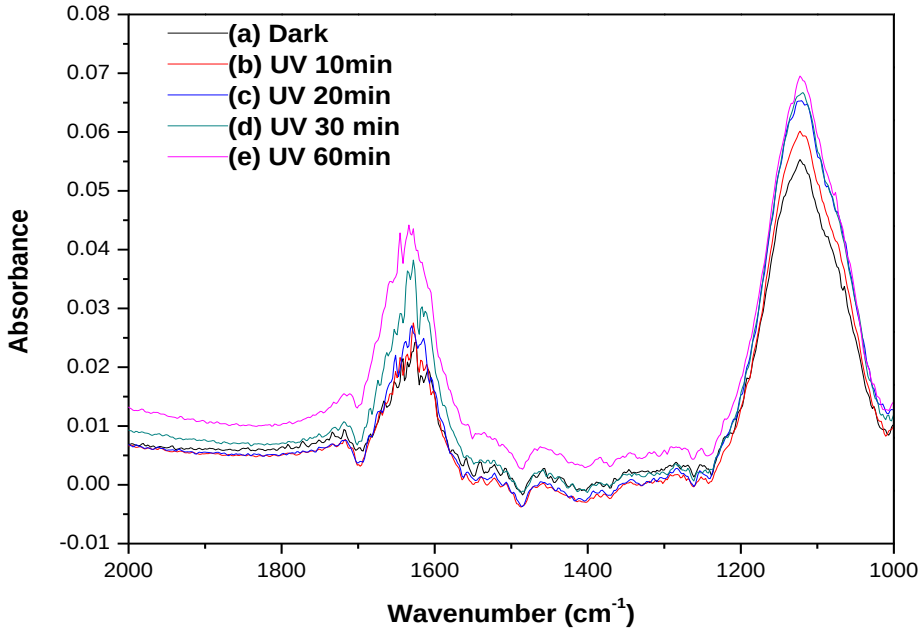

Figure 5-15 H_2O band changes over irradiated TiO_2 in the presence of 10 mM Fe^{3+}.

At the first glance, this phenomenon seems contrary to the superhydrophilic effect, i.e., an attraction or build-up of (adsorbed) water. However, it is now clear that SHP is only observed on the irradiated TiO_2 surface *in the presence of oxygen (air).*[139,140]

Quenching of the electron spectrum by O_2 has already been seen in DRIFTS (see Chapter 4). This re-establishes or maintains Ti^{4+} ions at the surface even under illumination. It should also be borne in mind that the original report of Fujishima et al. [98]claimed superhydroam*philicity*, in which interpenetrating nanodomains of hydrophilic and hydrophobic properties are generated together under irradiation. Furthermore, the presence of water vapour promotes generation of the electron spectrum (see Chapter 4), presumably by stabilizing surface-trapped holes. This is reasonable because water is an electron donor rather than acceptor.

A tentative mechanism, based mainly on data reported in this thesis, is that surface charging by both electrons and holes disrupts the local ordering of water overlayers,[141] repelling and attracting, water molecules, respectively. However, in the presence of O_2 the repulsive effect is suppressed, such that the *net observable* is an increase in coverage by adsorbed water attracted by the holes. In ATR-FTIR, where excess water is present, and access of O_2 (in liquid water) to the TiO_2 surface is impeded, the net observable is repulsion. Similarly, the observations in DRIFTS at high humidity may be considered to represent a balance between (DRIFTS at) low humidity, where more water can be attracted to the surface, and the other extreme of submersion in liquid water, as studied here by ATR-FTIR.

5.7 Summary

The present work demonstrates the feasibility of *in situ* ATR-FTIR spectroscopy, adapted for optical pumping, to investigate not only the reaction pathway, but also the change in electronic state of the photocatalyst under *operando* conditions and its relation to activity.

As model reactions, the photo-oxidation of ethanol, acetaldehyde, and acetic acid have been studied. These show that photo-oxidation of aqueous ethanol solution over pristine TiO_2 is quite slow. Band-gap excitation causes the accumulation of free electrons with their associated quasi-continuum absorption, implying that photo-reductive activation of dioxygen does not proceed at a significant rate in aerated aqueous ethanol. Platinization results in a dramatic increase in activity with only slight build-up of negative charge. This supports the view that the noble metal serves as a "reactive sink" for electrons, thereby promoting ionosorption of dioxygen, a key initial step. Photo-oxidation of dilute aqueous ethanol proceeds through acetaldehyde and acetic acid as intermediates. Mineralization of acetic acid (acetate) is very slow and constitutes the rate-determining step. Clear mechanistic parallels between gas- and liquid-phase ethanol photo-processes lead to the conclusion that, depending on the availability of the chemical oxidant (a function of both experimental design and identity of the substrate molecule), photo-oxidation and photo-reforming can occur in parallel. In the case of ethanol, acetaldehyde is a common intermediate in both processes, and its formation is promoted by O_2. However, other important features of this work, viz., charging of TiO_2 and growth of metal-adsorbed CO on the platinized catalyst, both under aerated conditions, raise concerns as to the efficacy of photo-

oxidation processes over submerged or suspended catalysts unless due attention is given to supply (mass transfer) limitations of the oxidant in particular.

As regards the ATR-FTIR technique, as currently practiced, a number of limitations have been made evident. Probably the most serious of these is its inability to track and identify gaseous products except where speciation into the bulk liquid is possible, as with CO_2 in water. Dominance of spectral response by the bulk liquid is still a problem although a more shallow penetration depth is, in principle, achievable by using a crystal with higher refractive index, e.g., Ge, albeit at the expense of sensitivity. Finally, just as in the case of DRIFTS, there remain urgent fundamental developments to make the ATR-FTIR technique more *quantitative*.

The present work also demonstrates that disruption of the adsorbed water layer(s) on TiO_2 surface is related to the accumulation of surface-trapped electrons. This effect is accentuated by addition of ethanol as hole scavenger, and eliminated when Fe^{3+} is present as electron acceptor. Based on cross-referral to the relevant DRIFTS studies, the predominant repulsive effect seen in ATR-FTIR is rationalized and can be integrated into the general view of the superhydrophilic effect, or more accurately, superhydro*amphilicity* as originally claimed.

Chapter 6. Investigation of Visible Light Active Photocatalysts

Due to prior emphasis on technique development and methodology, the last two chapters focused on *in-situ* FTIR studies at the gas- and liquid- interface to pristine and metalized Degussa P25, an established photocatalyst with quite predictable behavior. To the best of our knowledge, *in situ* investigation of photocatalytic reactions has primarily focused on pristine TiO_2 to date. In view of the recent trend towards photocatalysts active in the visible region for practical application under sunlight, two groups of candidate samples were prepared and tested in both methyl orange(MO) photo-degradation and ethanol photo-oxidation. These comprised a) melon sensitized titanate/TiO_2 and b) Ag nanoparticle decorated titanate/TiO_2, characterized by various bulk techniques including DRIFTS both for verification of surface/overlayer structure and to obtain mechanistic information by tracing intermediates generated under UV & visible irradiation *in-situ*.

6.1 Melon-modified titanate/TiO_2

6.1.1 Introduction

Titanium dioxide (TiO_2) is the most widely used photocatalyst so far, but it suffers from its large band gap (3.2 ev for anatase TiO_2), which only allows utilization of 4~5 % solar irradiation. To make use of solar energy effectively, a key topic in photocatalysis research now is to confer visible absorption, either by shifting the absorption edge suitably, or by sensitizing TiO_2 for visible photo-activity with surface additives. Doping with anionic elements, such as carbon, nitrogen, sulfur, etc, appears to be a more promising method to “engineer the band gap” of the semiconductor, as compared to cationic (transition metal) colour centers as formerly explored but with

only limited success. Since the pioneering work on anion doping by Asahi et al.,[21] the field has undergone prolific growth, with particular emphasis on nitrogen-doped TiO_2. Asahi et al[21] initially proposed that N 2p level mixing with the valence band of TiO_2, which is mainly from O 2p orbital contribution, leads to the narrowing of the band gap. However, this view was soon challenged, one alternative interpretation being that N-doping introduces localized mid-gap states, and that these are responsible for the visible absorption. While evidence has steadily accumulated that visible activity in TiO_2 does result by introducing N, bulk-doping is a complex process, and coloration due specifically to N is not easy to prove because oxygen vacancies are created simultaneously to maintain charge balance. Furthermore, recent work focusing on cheaper wet-chemical methods, typically based on urea, triethylamine, etc., as nitrogen source, has met with some success even after mild calcination of the impregnated material, where substantial bulk (ionic) diffusion is unlikely. Consequently, some researchers even doubt that doped- or surface states of N exist as such[47,48] and the term "N-modification" is generally preferred. Starting from urea, there is now strong evidence that "melon-like" surface layers are obtained. [47,48]

6.1.2 Characterization of hydrogen titanate (HT)

Typical TEM images of the titanate are shown in Figure 6-1a and 6-1b respectively. Their morphologies are highly dependent on the hydrothermal temperature. Titanate nanotubes (TNTs or HT 150) synthesized at 150 °C have lengths up to hundreds of nanometers, outer diameters around 10 nm, and inner diameters around 5 nm, while titanate nanobelts (TNBs or HT 200) synthesized at 200 °C have lengths from hundreds of nanometers to a few millimeters and widths of tens of nanometers. The interlayer spacing of the layered TNTs is approximately 0.8 nm, which is slightly less

than that indicated from the XRD peak position at 2θ ~10°, corresponding to d ~0.96 nm (Figure 6-1c). This deviation is probably due to dehydration of titanate under ultrahigh vacuum during TEM observation. Since TNBs were synthesized at a higher temperature, their crystallinity is much better and more XRD peaks were observed as compared to the TNTs.

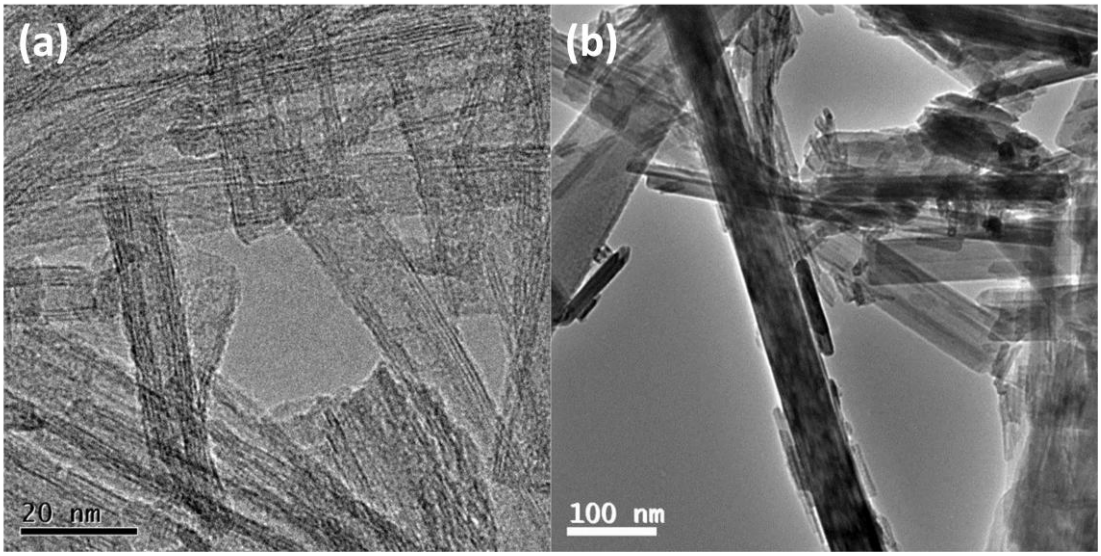

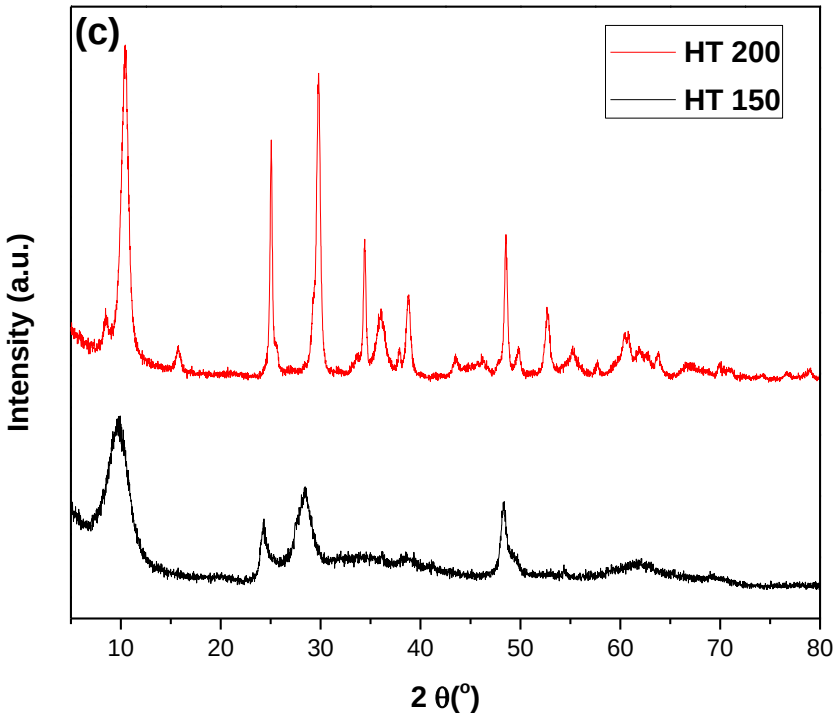

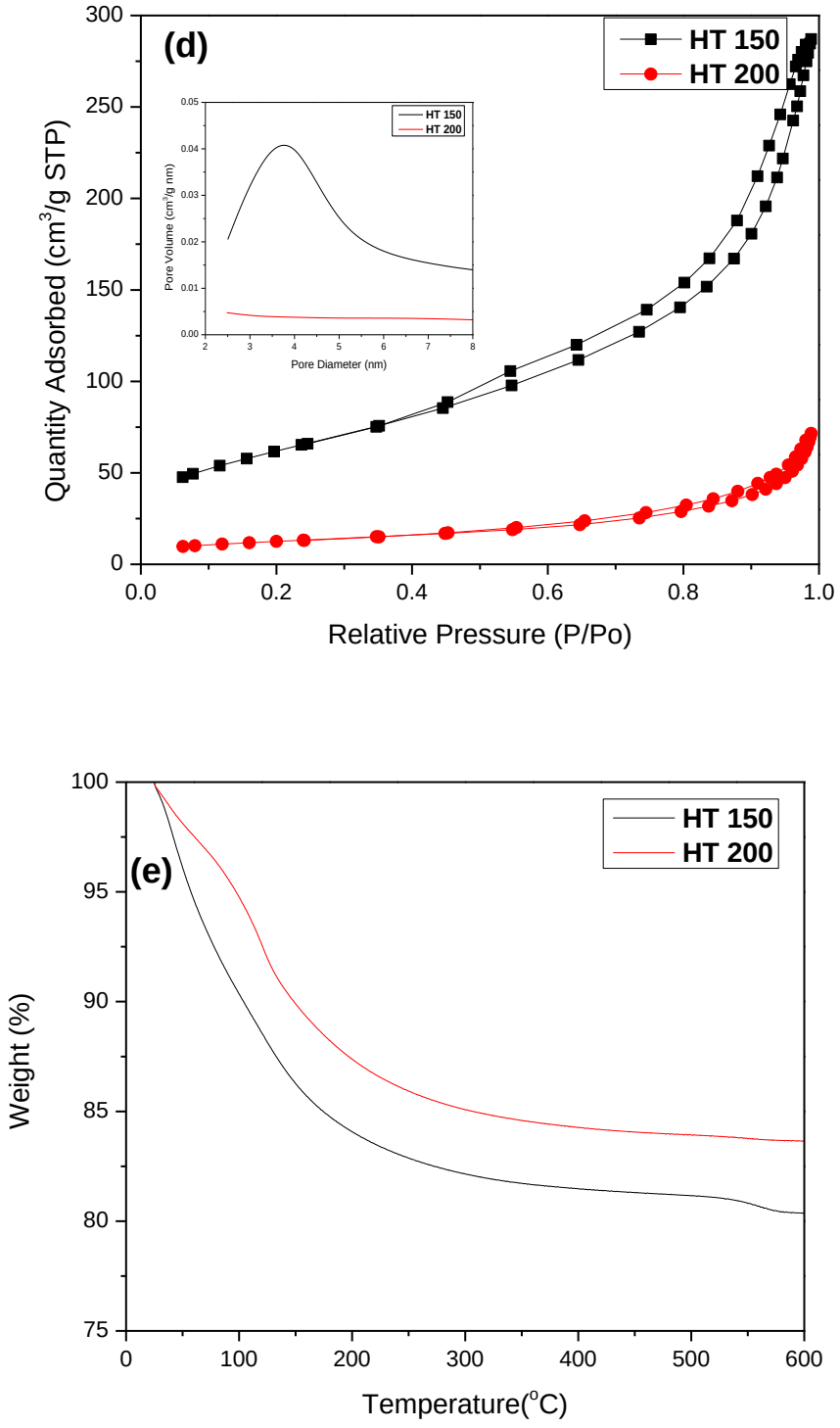

Figure 6-1. Characterization of titanates: TEM images of (a) HT 150 and (b) HT 200; (c) XRD patterns; (d) N_2 sorption isotherm (inset - pore volume distribution); (e) TGA curve measured at 10 °C/min from RT to 600 °C in N_2 flow.

Due to their tubular structure, TNTs have a large surface area, around 224 m^2 g^{-1}, and the pore diameter is around 4 nm (see Figure 6-1d inset), close to the inner diameter of the tubes observed by TEM. TNBs have a relatively small surface area, around 45 m^2 g^{-1}, only 1/5 of that of the TNTs.

Both TNTs and TNBs were thermally unstable. The TGA curves (Figure 6-1e) show that they started to lose weight even from room temperature (RT) and levelled out by 300 °C. This is associated initially with removal of physically-adsorbed water, followed by the phase transformation from titanates to TiO_2 where crystal (structural) water is lost. [142,143]

6.1.3 Formation of melon from urea on titanate/TiO_2

Urea is widely used a nitrogen source for TiO_2 doping. In this work, it was mixed with either titanate or TiO_2 in a weight ratio of 2:1 and then annealed in ambient air or N_2 gas. The residual surface deposits were analyzed by various methods.

XRD patterns of the mixtures annealed in ambient (static) air and in nitrogen flow up to 400 ℃ are shown in Figure 6-2. For HT150 (air) phase transformation from titanate to anatase phase was observed, whereas HT200 (air) transformed to the TiO_2(B) phase. P25 was unaffected by calcination in air, remaining as a mixture of anatase and rutile TiO_2. The anatase phase may have undergone slight conversion to rutile. Similar XRD patterns were observed for samples calcined in nitrogen gas. However, it is notable that HT150 (N_2) did not fully transform to anatase, possibly because the steady state temperature under forced gas flow kept the sample slightly below the control temperature of 400 °C.

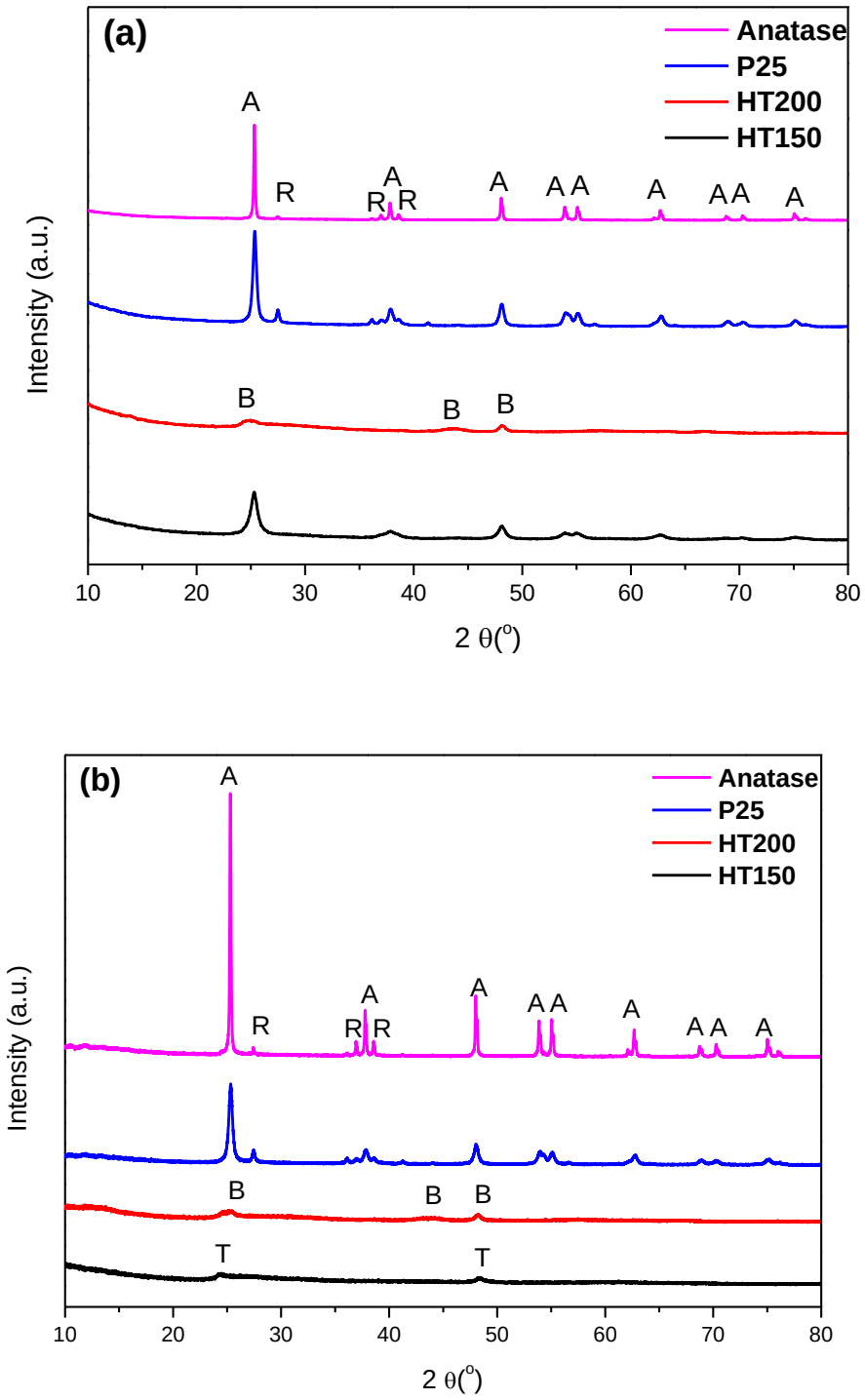

Figure 6-2. XRD patterns for melon modified titanate/TiO_2: (a) annealed in air and (b) annealed in nitrogen flow at 400 °C. A denotes anatase phase TiO_2, R denotes rutile phase TiO_2, B denotes TiO_2(B) phase and HT denotes titanate phase TiO_2.

Elemental analysis (EA) provided essential information about the deposited surface products. Tables 6-1 and 6-2 show results for modified titanate/TiO_2 samples calcined in ambient air and nitrogen gas, respectively.

Table 6-1 Elemental analysis results of melon modified titanate/TiO_2 samples calcined at 400 °C in ambient air.

Samples (Air)	**H**	**C**	**N**	**C/N**
	(wt.%)	**(wt.%)**	**(wt.%)**	**(mole ratio)**
Melon-HT150	0.69	0.17	0.15	1.32
Melon-HT200	0.62	3.40	6.15	0.645
Melon-P25	0.15	0.09	0	-
Melon-Anatase	0.04	0.13	0	-

Table 6-2 Elemental analysis results of melon modified titanate/TiO_2 samples calcined at 400 °C in N_2 gas

Samples (N_2)	**H**	**C**	**N**	**C/N**
	(wt.%)	**(wt.%)**	**(wt.%)**	**(mole ratio)**
Melon-HT150	1.72	6.55	11.45	0.667
Melon-HT200	0.86	5.45	10.57	0.602
Melon-P25	0.24	1.91	3.6	0.619
Melon-Anatase	0.12	1.56	2.32	0.784

Except for sample HT 200, low values of wt% C and wt% N were measured on samples annealed in air. However, much higher values were obtained for all samples when annealed in nitrogen gas, presumably due to restricted oxidation. The atom

ratios of C to N were also calculated as shown in the far right column. There are 18 carbon atoms and 27 nitrogen atoms in a single formula unit of melon (see also Fig. 2-3), so the theoretical atom ratio of C to N is 0.667. The C/N ratios of the samples prepared in nitrogen gas were fairly close to theoretical. It is also interesting to note that more surface species were formed on HT 150 and HT 200, as compared to P25 and anatase TiO_2, implying that the titanates have a chemical functionality, possibly the rich surface OH groups, that promotes the conversion/polymerization of urea into melon. This is evidently not only due to textural effects *per se* because the loading on HT 200 (after calcination in N_2) was only slightly lower than that on HT 150 despite having only a fifth of the surface area. The formation of melon from urea is initiated by reaction with surface OH groups (see Eqn. 2.9 & 2.10). Figure 6-3 compares DRIFT spectra of HT150, HT 200 and P25 TiO_2. At room temperature (RT), the absorption band at 3300 cm^{-1} is due to both surface OH stretching and adsorbed water. After heating at 200 °C to remove the latter, the isolated surface OH groups around 3700 cm^{-1} were revealed for HT 150. There are clearly more surface OH groups on HT 150 and 200, as compared to P25.

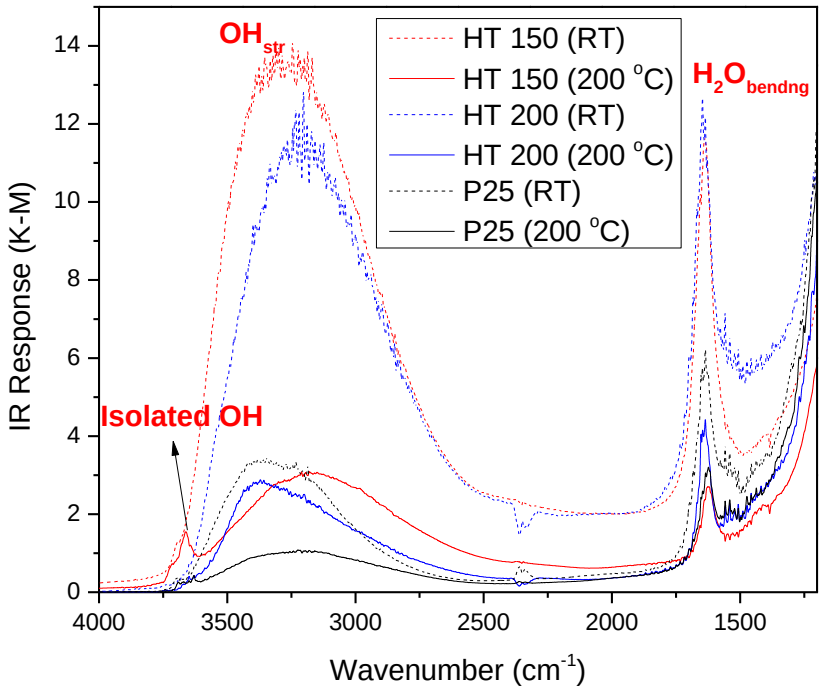

Figure 6-3 DRIFT spectra of HT 200 and P25 TiO_2 at different temperatures

The morphologies of melon modified titanate/TiO_2 in N_2 are shown by TEM in Figure 6-4. HT150 kept its tubular structure and polymeric melon could also be spotted. The morphology of HT 200, P25 and anatase TiO_2 did not change much, and melon could not be seen clearly on their surfaces. Their surface areas were slightly smaller than unmodified ones (as shown in Table 6-3), possibly because melon blocks some pores.

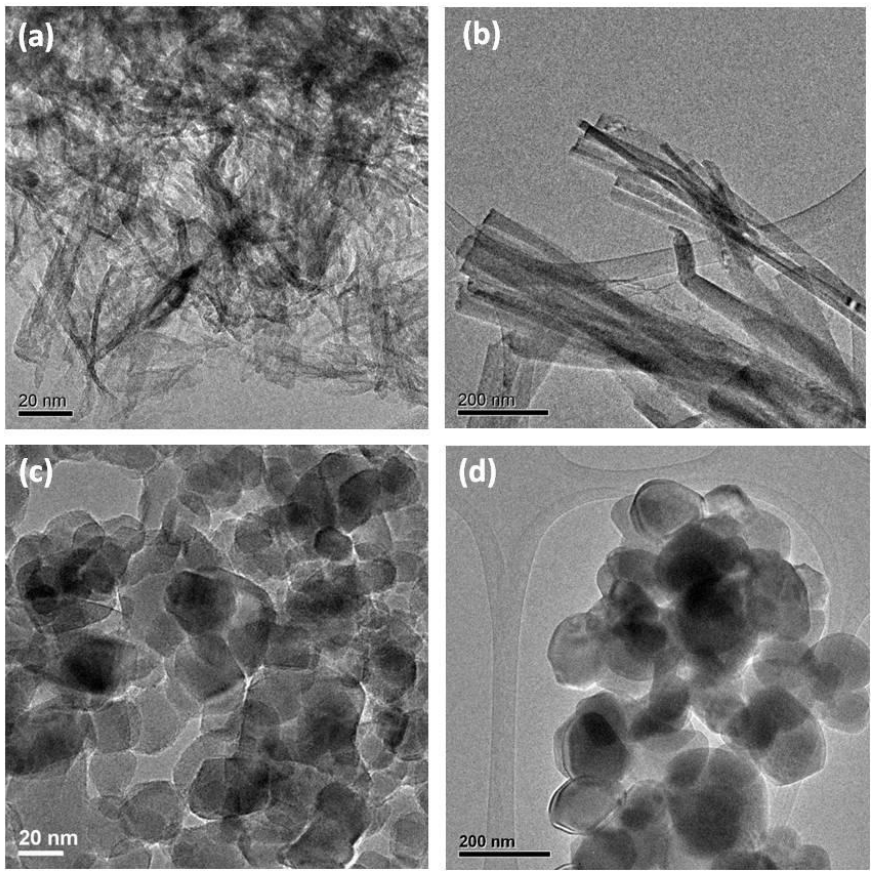

Figure 6-4 TEM micrographs of melon modified titanate/TiO_2 samples calcinated at 400 °C in nitrogen gas (a) HT 150; (2) HT 200; (3) P25; (4) Anatase

Table 6-3 BET surface area analysis of melon modified titanate/TiO_2 samples calcinated at 400 °C in static air and nitrogen flow

Samples	**BET Surface Area (m^2/g)**	
	Air	**Nitrogen**
Melon-HT150	175.51	132.56
Melon-HT200	34.81	22.25
Melon-P25	44.09	51.05
Melon-Anatase	8.82	12.02

The surface species after calcination in N_2 were also examined by ^{13}C solid state nuclear magnetic resonance (NMR). As seen in Figure 6-5, three resonances were evident for HT 150 and HT 200 at ~165 ppm, 163 ppm, and 156 ppm, linked with heptazine units,[144] whereas there was only a weak singlet at ~165 ppm for modified P25 and anatase.

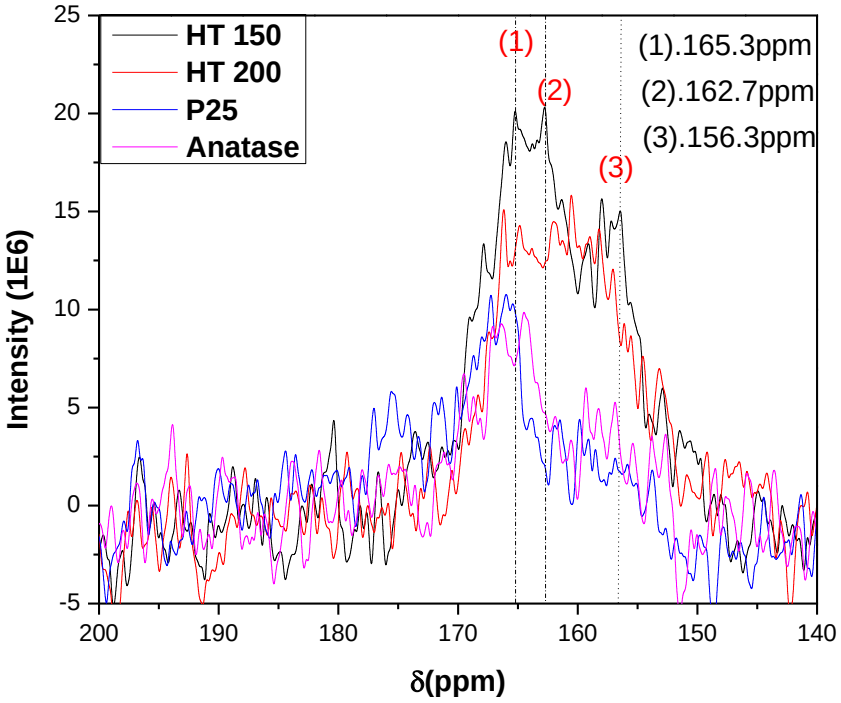

Figure 6-5 Solid state ^{13}C NMR spectra of melon modified titanates and TiO_2 in N_2

Optical properties of the melon-modified samples calcined in air and N_2 were examined by diffuse reflectance (DR) UV-visible spectroscopy as shown in Figs 6-6a and 6-6b, respectively.

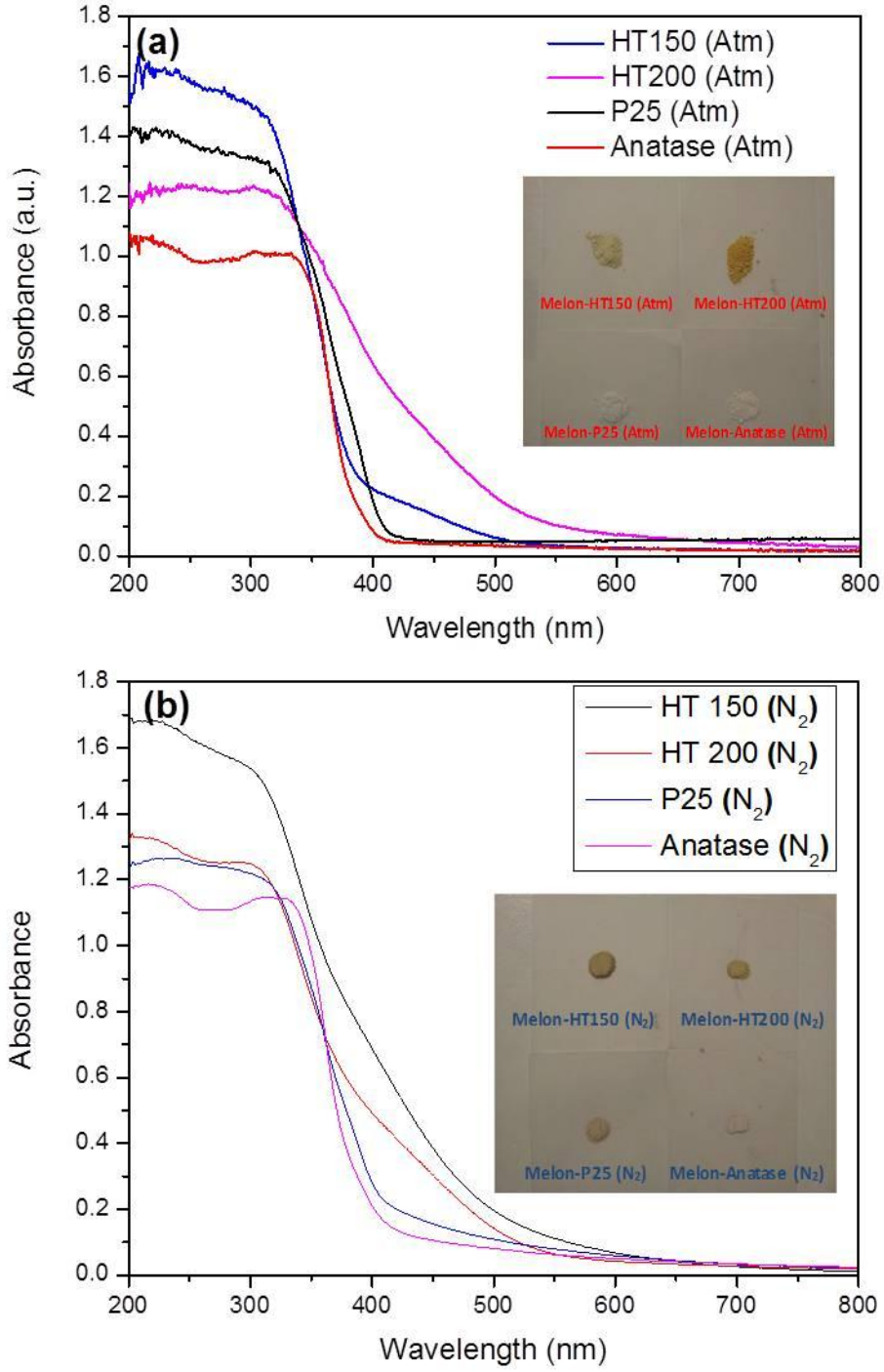

Figure 6-6. Diffuse reflectance UV–Vis spectra of melon modified titanates and TiO_2 calcined at 400 °C in (a) static air; (b) N_2 (Inset: digital photos)

Melon modified titanate samples HT 150 and HT 200 had more intense visible light absorption compared to Melon-P25 and Melon-Anatase, showing broad tails extending beyond 500 nm. This correlates with the higher loadings of melon as indicated by EA and NMR. Accordingly, the titanates were yellow-brown in appearance, as compared to a pale yellow hue in P25 and anatase TiO_2.

Melon formed on the surface could be removed by thermal oxidation. TGA curves in Figure 6-7 shows the weight changes of melon modified titanate/TiO_2 (N_2) samples heating in air up to 800 °C. The furnace temperature was firstly heated up to and maintained at 100 °C for 40 minutes to remove physically-adsorbed moisture for better estimation of melon amount and reactivity. After pre-drying, the furnace was ramped to 800 °C at 10 °C/min. A sharp decrease in weight was observed in all cases just above 400 C, suggesting depolymerization, oxidation and volatilization. All samples reached a steady weight by 500 °C, suggesting complete removal of melon. The "dry" weight loss was 24 % for Melon-HT 150, 12 % for Melon-HT 200 and ~5 % for both Melon-P25 and Melon-Anatase. These values correspond well to the sum of weight percentages of hydrogen, carbon and nitrogen from elemental analysis for Melon-TiO_2 (N_2), seen in Table 6-2.

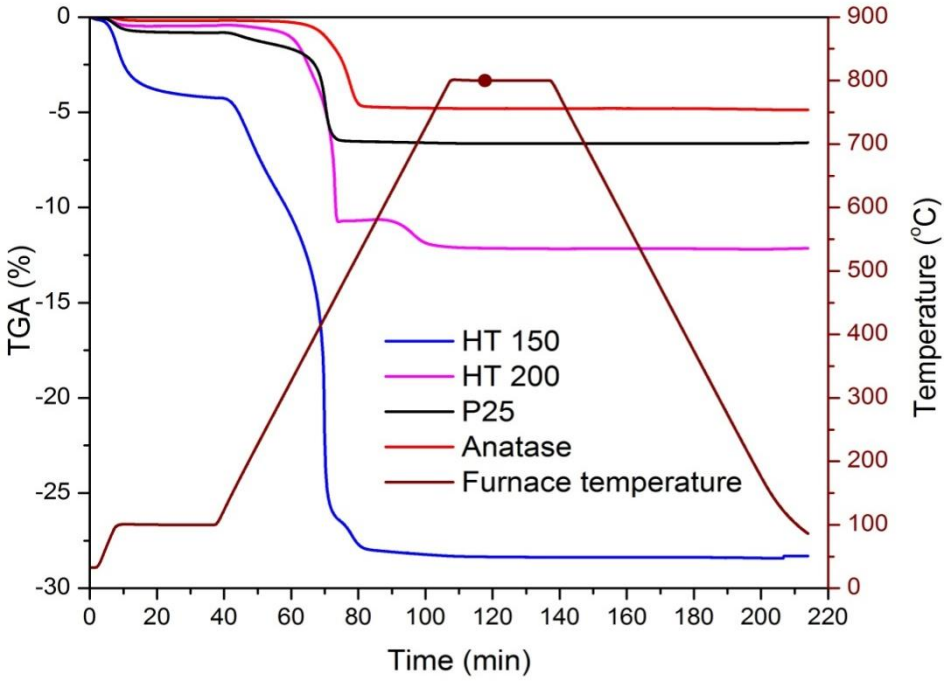

Figure 6-7 Relative weight changes of melon modified titanate/TiO_2 (N_2) samples when heating up to 800 °C in air

After this severe oxidation treatment, the optical absorption was also checked, as shown in Figure 6-8. Except for P25, all previous visible absorption was removed, confirming the residues were back in the virgin (oxide) state. The slight extension in absorption for P25 beyond 400 nm was found to be due to generation of rutile from the predominantly anatase phase, as expected.

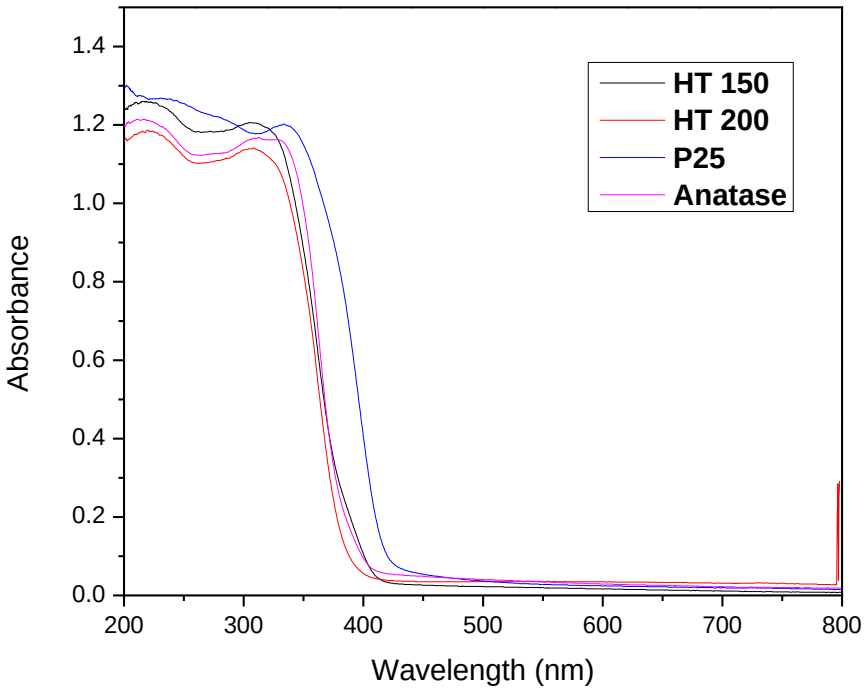

Figure 6-8 Diffuse-reflectance UV–Vis spectra of Melon-TiO_2 samples after calcination in air up to 800 °C

6.1.4 Surface species identification and photo-stability by DRIFTS

Figure 6-9a compares the DRIFT spectra of modified titanate/TiO_2 against unsupported melon as reference, whose peaks have been assigned elsewhere as follows:[145] 810 cm^{-1} – 6-membered ring out of plane bending; 1250 cm^{-1} and 1324 cm^{-1} – $\nu(C\text{-}N)_{chain}$ between the heptazine ring and NH group; 1414 cm^{-1} – $\delta(NH)$; 1468 cm^{-1} – $\nu(ring)$; 1640 cm^{-1} – $\delta(NH_2)$ conjugated with heptazine ring; 3190 cm^{-1} and 3300 cm^{-1} – $\nu(NH)_{symmetric/asymmetric}$. The most distinct melon bands were also evident in the modified titanate/TiO_2 samples, viz., 1640, 1414, 1468, 3190 and 3300 cm^{-1}.

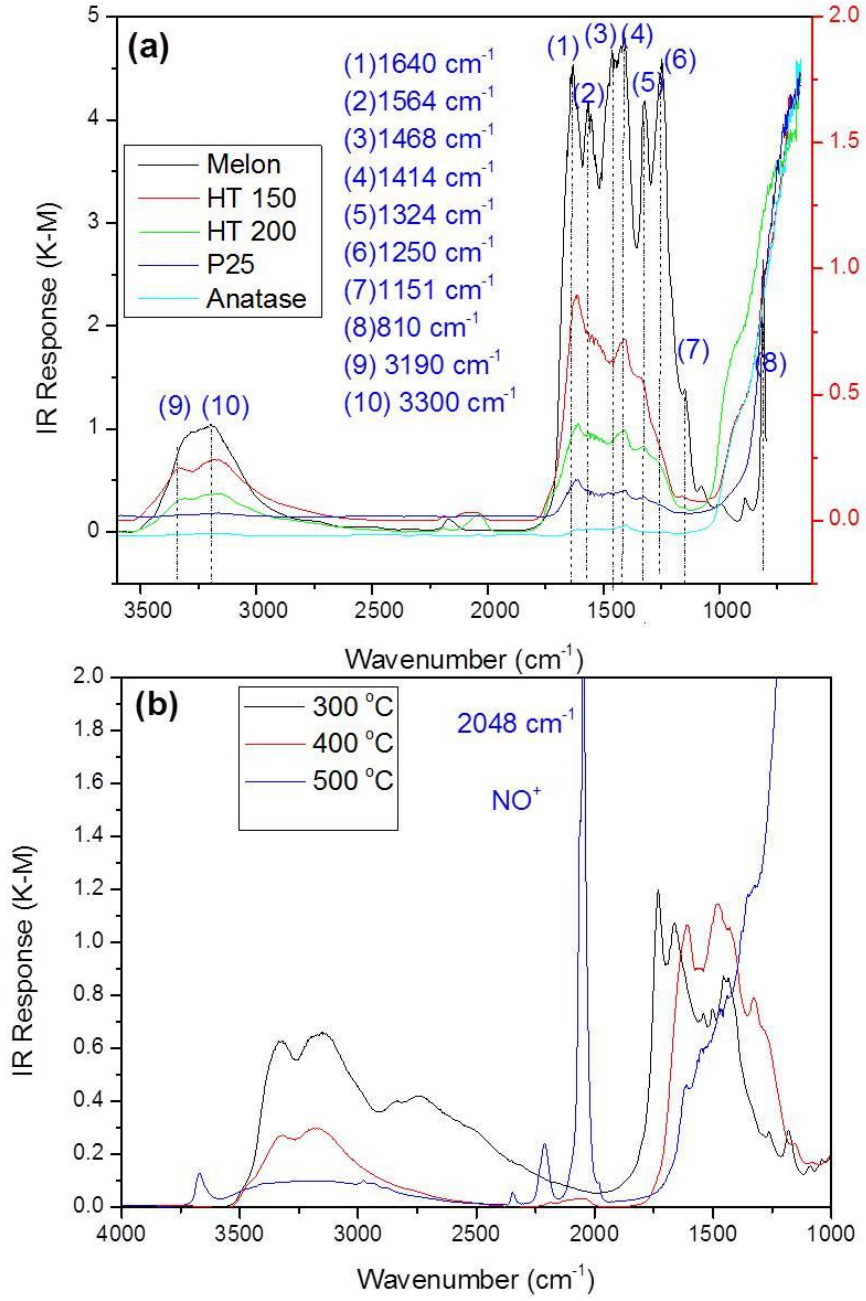

Figure 6-9. DRIFT spectra of (a) melon and modified titanate/TiO_2 calcined in N_2 at 400 °C; (b) mixture of urea and HT 200 calcined in air at different temperatures （To improve spectral quality, samples were diluted to 5wt.% in KBr and spectra were collected after pre-drying at 200 °C in N_2)

The existence of these IR bands strongly supports the formation of melon on titanate/TiO_2 surface, with intensities in proportion to the loading as determined by EA analyses. Recalling the EA data from Table 6-2, suggesting the presence of melon on HT 200 even in air, its optimal formation conditions were evaluated. Figure 6-9b shows DRIFT spectra of a mixture of HT 200 and urea in a ratio of 1:2 in weight percentage calcinated in air at different temperatures. At 300 °C, all the IR bands could be assigned to un-converted urea. By 400 °C, melon was clearly formed on the surface. However, by 500 °C, all of the melon bands were replaced by a strong band at 2048 cm^{-1} diagnostic of the NO group.

For surface sensitized photocatalysts, the stability of the sensitizer under applied conditions is essential. It is well known that organic dyes and pollutants like methylene blue and methyl orange are photo-degraded under UV light. Before using melon as an organic polymeric sensitizer, it was important to verify its photo-stability. Figure 6-10 shows DRIFT spectra of melon-HT 150 (N_2) collected after various exposure times under UV-Vis irradiation.

For neat melon-HT 150 (N_2), the intensity of IR response was very strong but the characteristic bands of melon were still distinguishable. During photo-irradiation up to 16 hours, the bands remained virtually unaffected, indicating that melon is a photo-stable visible light sensitizer.

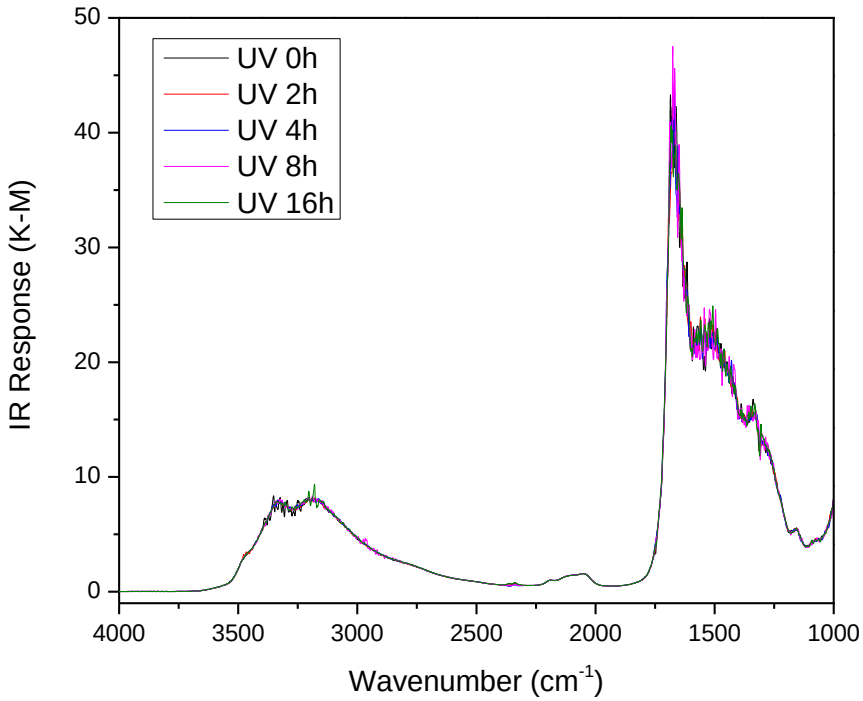

Figure 6-10 DRIFT spectra of melon-HT 150 (N_2) under UV-Vis irradiation for 16 hours

6.1.5 Photocatalytic reactor tests of melon-modified titanate/TiO_2

6.1.5.1 Photo-degradation of methyl orange under visible light irradiation

Methyl orange (MO) dye was selected as a model for the photocatalytic performance test. MO is a pollutant found in waste water from the textile industry and is unaffected by direct photolysis. Pristine titanate and anatase TiO_2 have been extensively studied in our group, and none of them shows photocatalytic activity under visible light (>385 nm). Figure 6-11 shows the effect on MO of visible light irradiation in the presence of suspended particles of melon-modified titanate/TiO_2 (N_2). Adsorption of MO by TiO_2 under dark was negligible.

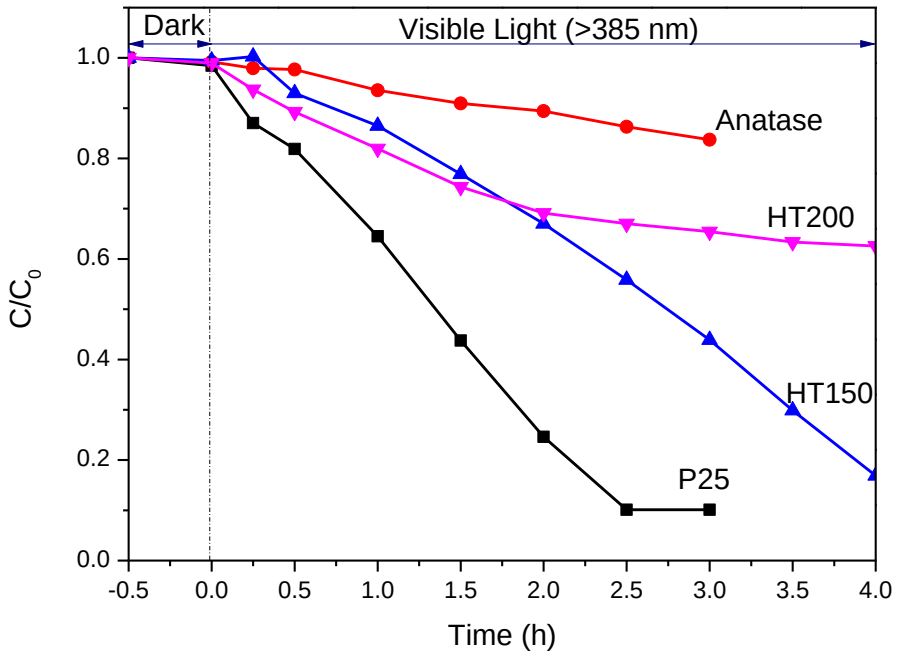

Figure 6-11. Photocatalytic degradation of MO solution (5 ppm) by melon-modified titanates and TiO_2 under visible light irradiation (>385 nm)

It was found that Melon-P25 (N_2) degraded roughly 90% of MO within 2.5 hours, Melon-HT150 (N_2) shows around 80% degradation within 4 hours, while Melon-HT200 (N_2) and Melon-Anatase (N_2) exhibited only about 30% and 10% degradation respectively. Visible light photo-activity is clearly conferred by the presence of melon. However, it is somewhat surprising that P25, with a low loading of melon, is the most active catalyst. It might be due to the presence of rutile phase in P25, which has a lower band gap (3.0 eV) thus responsive to the visible light.

6.1.5.2 Photo-oxidation of ethanol under visible light irradiation

Ethanol photo-oxidation on P25 TiO_2 under UV-Vis irradiation was extensively reported in the last two chapters. Insofar as it is colorless, ethanol is an even more valuable probe molecule for tests under visible light because direct photolytic degradation is impossible. Figure 6-12 shows the DRIFT spectra recorded during photo-oxidation of ethanol vapor by Melon-HT150 (N_2). Although the reaction is quite slow, the spectroscopic behavior was similar to that observed over P25 TiO_2 under UV-visible irradiation (see Chap. 4). Key intermediates acetaldehyde and sorbed acetate species were detected and grew over time at the expense of the C–H stretching band envelope of the ethyl moiety.

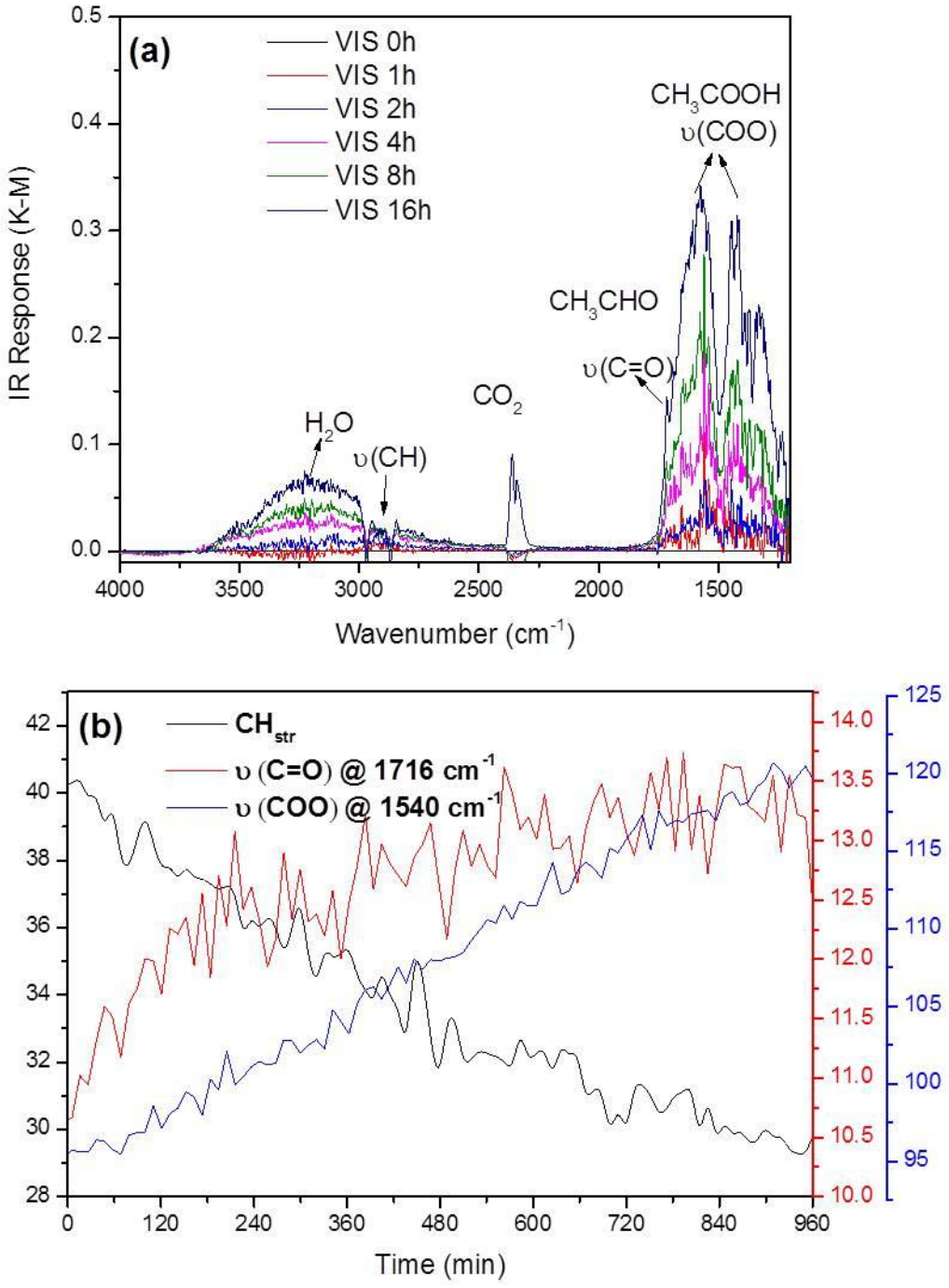

Figure 6-12 Photo-oxidation of ethanol vapor in air over melon- HT 150 (N_2) under visible light irradiation (>400 nm)

6.1.6 Discussion of the mechanism

Graphitic carbon nitride (g-C_3N_4) has the same heptazine units as melon, but only with a higher polymerization degree, thus a group of g-C_3N_4 modified TiO_2 samples were also studied to further clarify the mechanism, which were prepared through heating mixture of pre-formed C_3N_4 with HT 150 in air up to 400 °C (see Chapter 3.). All the samples show anatase TiO_2 phase with minority of C_3N_4, as indicated by the XRD patterns of the mixtures in Figure 6-13a. Compared with un-modified TiO_2, g-C_3N_4 modified TiO_2 samples show a small tail to visible region (as shown in Fig. 6-13b). DRIFT spectrum of g-C_3N_4 modified sample is very similar with melon-modified ones, indicating the structure similarity of melon and g-C_3N_4 (Fig. 6-13c). The absence of N-H bands at 3190 cm^{-1} and 3300 cm^{-1} suggests the high polymerization degree of g-C_3N_4 in comparison with melon. Figure 6-14 shows their photocatalytic performance for MO degradation. Either un-modified TiO_2 or g-C_3N_4 shows minimal photoactivity, but all of g-C_3N_4 modified TiO_2 samples can degrade MO under visible irradiation (>385 nm), with an optimal loading of 10 wt.%.

Melon or g-C_3N_4 acts as visible light sensitizer for titanate/TiO_2. As they are narrow gap semiconductor (2.8 eV),[50] visible light-induced interband transitions are excited just as in TiO_2, then the photo-generated electrons can transfer to the conduction band of titanate/TiO_2 for oxygen activation (superoxide formation). The hole left in the valence band of melon may be sufficient to react with adsorbed ethanol (or ethoxy) to promote H atom abstraction and ultimately dehydrogenation to produce acetaldehyde.

Compared with melon-modified samples with the same loading, g-C_3N_4 modified samples show a better performance for MO degradation. This is possibly due to the better crystallinity of g-C_3N_4, which reduces the probability of charge recombination.

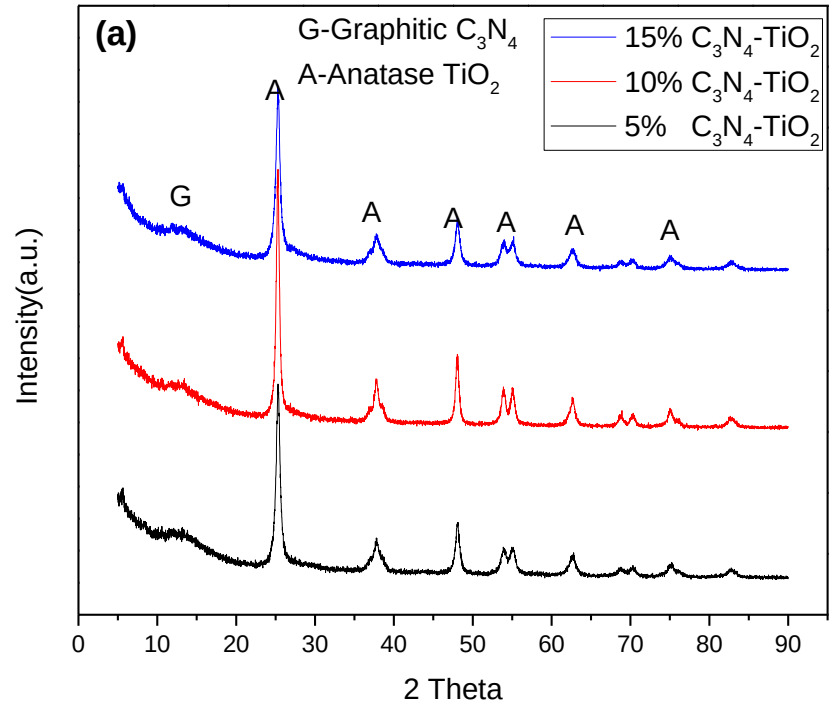
(a)
G-Graphitic C_3N_4
A-Anatase TiO_2
15% C_3N_4-TiO_2
10% C_3N_4-TiO_2
5% C_3N_4-TiO_2
A
G
A
A
A
A
A
Intensity(a.u.)
0
10
20
30
40
50
60
70
80
90
2 Theta

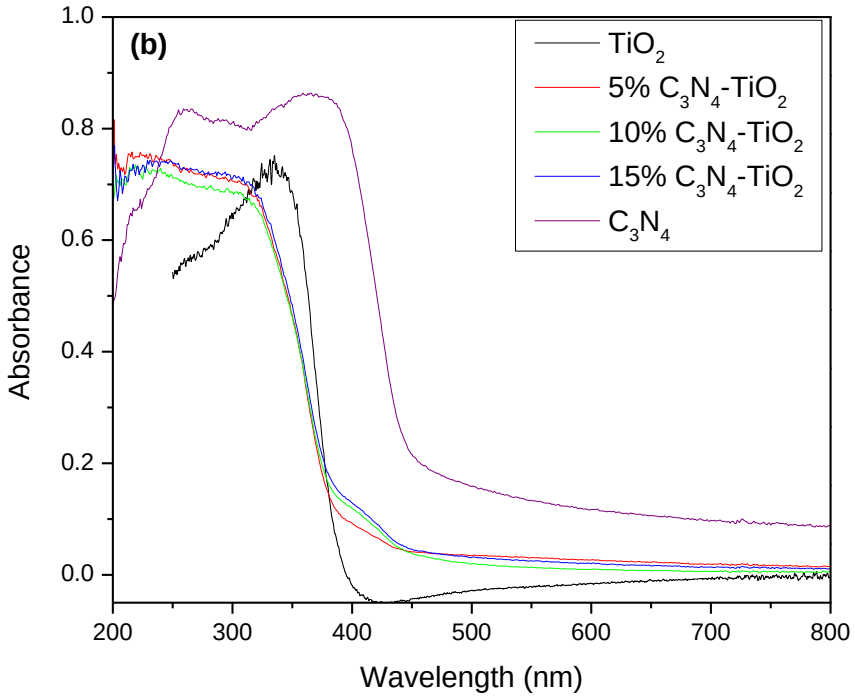
(b)
TiO_2
5% C_3N_4-TiO_2
10% C_3N_4-TiO_2
15% C_3N_4-TiO_2
C_3N_4
Absorbance
1.0
0.8
0.6
0.4
0.2
0.0
200
300
400
500
600
700
800
Wavelength (nm)

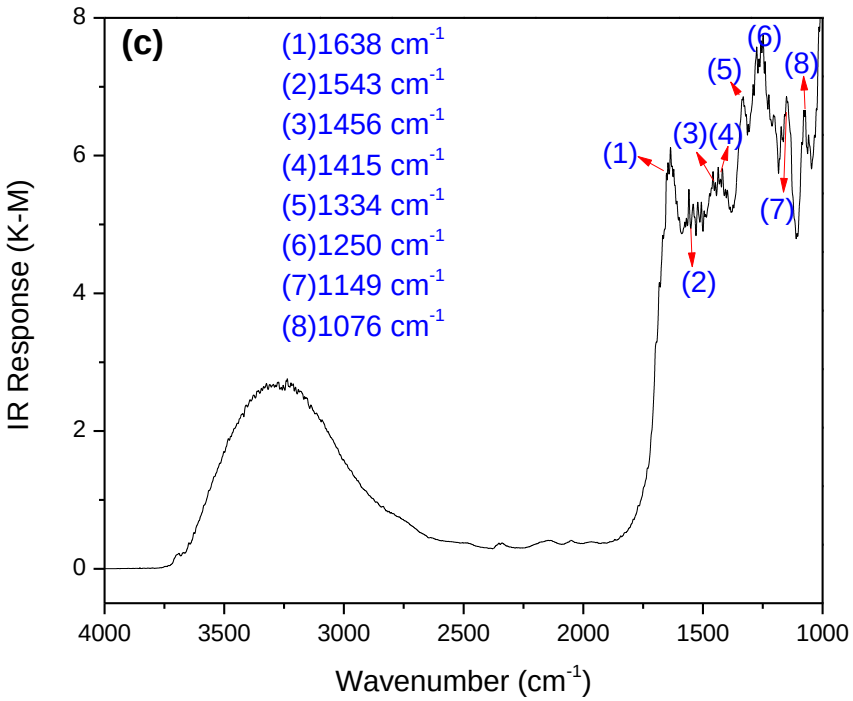

Figure 6-13. Characterization of g-C_3N_4 modified TiO_2 samples: (a) XRD patterns; (b) Diffuse Reflectance UV-Vis spectra and (c) DRIFT spectrum of 10 wt.% g-C_3N_4 modified TiO_2

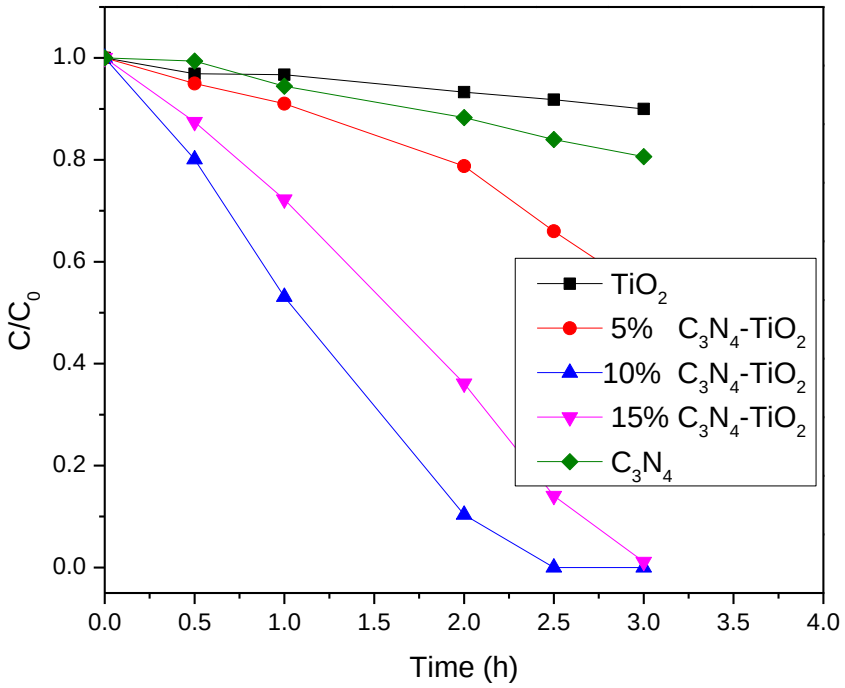

Figure 6-14. Photodegradation of MO by g-C_3N_4 modified TiO_2 samples under visible light (>385 nm) compared with un-modified TiO2 and g-C_3N_4 itself

6.1.7 Short summary

When urea is mixed with titanate/TiO_2 and heated to 400 °C, melon, a polymeric narrow band gap semiconductor is formed on the surface and acts as a visible light sensitizer. The rich surface group of titanate promotes the formation of melon on its surface compared with TiO_2. Different with other organic dyes, melon is also photo-stable under UV-Vis irradiation. Melon-modified titanate/TiO_2 is able to degrade methyl orange dye and to oxidize ethanol vapor under visible light irradiation. Graphitic carbon nitride (g-C_3N_4), having the similar structure with melon, also can be used as visible light sensitizer.

6.2 Ag nanoparticle-decorated titanate/TiO_2

6.2.1 Introduction

Besides sensitization of TiO_2 by narrow band gap semiconductors like melon, decoration of noble metal nanoparticles is another method to extend its light absorption to visible range. Nano-structured layered titanates are of great interest for catalytic purposes. Their large surface areas and ion-exchange properties provide the possibility to achieve uniform and high loading of the active noble metal in highly-dispersed form on the surface.[96,142] They also provide a good platform for delicate phase- and morphological tailoring, by annealing [16,143] or wet chemistry reaction [146,147], to obtain various TiO_2 or controlled mixed-phase nanostructures. Although it has been reported that protonated titanate can be photocatalytic under UV irradiation,[148-150] the efficiency is usually low due to the poor crystallinity and wide band gap (3.4 ev).

Here, we report the synthesis of titanate/titania nanostructures decorated with silver nanoparticles that show remarkable photocatalytic performance under visible irradiation. The preparation consisted of three stages: hydrothermal modification of anatase powder, photo-reductive deposition of Ag, and post-annealing. It was found that the trends in visible activity of these photocatalysts mimic those seen by irradiation in the UV, where only the support oxide absorbs. This is consistent with the view that visible activity arises via metal-to-support electron transfer, and a mechanism is proposed.

6.2.1 Phase transformation of hydrogen titanates and Ag-titanates

As stated in Chapter 6.1.1, hydrogen titanate transforms to TiO_2 during heating. XRD (Figure 6-15a) confirmed the progressive transformation from monoclinic hydrogen titanate (HT 150) to anatase TiO_2. This was essentially complete at 350 °C.

At higher temperature, the tetragonal anatase pattern became sharper indicative of growing crystallinity.

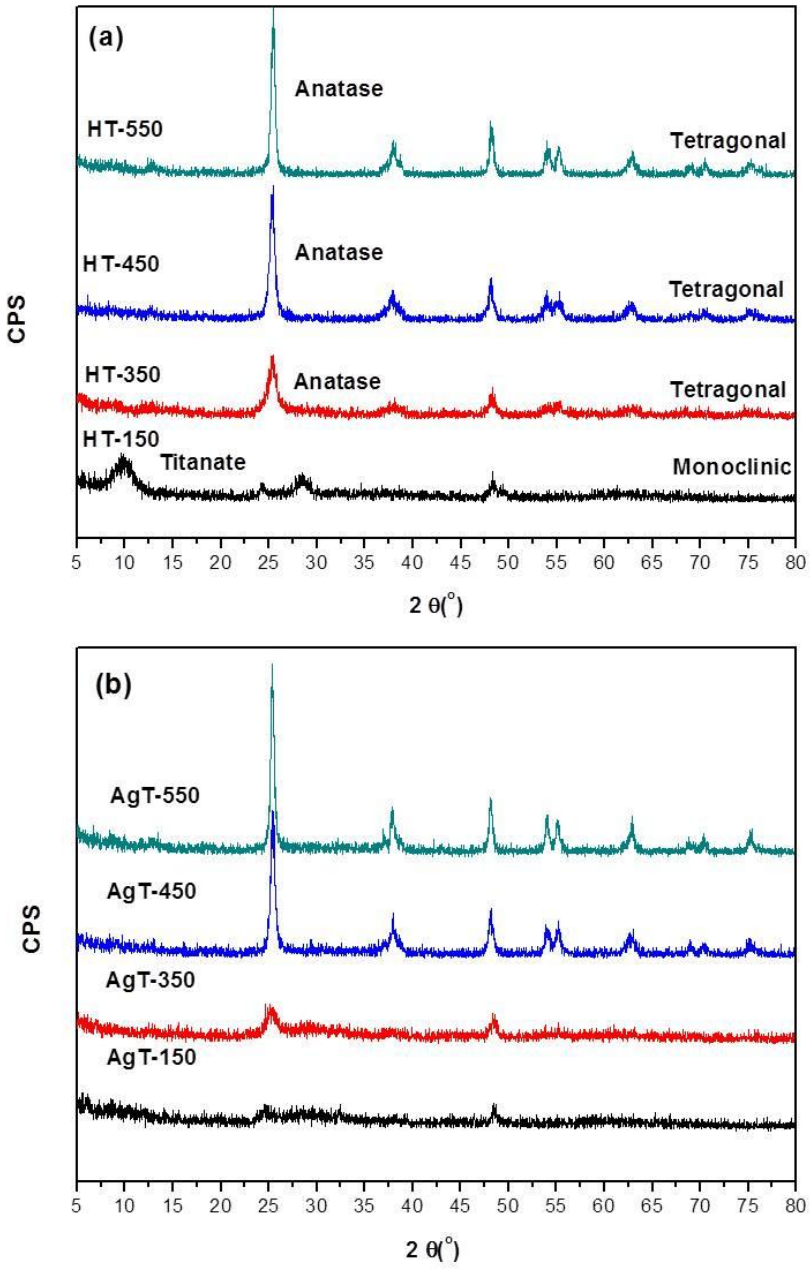

Figure 6-15 XRD patterns of (a) pristine hydrogen titanates and (b) Ag-decorated titanates annealed at different temperatures in air.

The phase transformation sequence of Ag decorated TNTs was similar, although apparently somewhat hindered by the presence of Ag (Figure 6-15b). The XRD pattern AgT 150 is much weaker and less ordered compared with HT 150, suggesting that ion-exchange of H^+ by Ag^+ disrupts the well-defined layered structure of the TNT. The transformation to anatase TiO_2 was partial up to 350 °C and complete only by 450 °C.

Figure 6-16 shows the TEM images of Ag TNTs heated at different temperatures. At 350 °C, they still retained the tubular structure, although with signs of re-structuring. At higher temperature, the crystallites were more rounded, signifying conversion to nanoparticulate anatase TiO_2. The size of the Ag nanoparticles was initially ca. 3~4 nm and these appeared uniformly dispersed. Although 10 wt% Ag (by calculation) was loaded onto the TNTs [11.7% Ag confirmed by energy dispersive X-ray spectroscopy (EDS) for AgT 150], neither metallic Ag nor Ag_2O was found in the XRD pattern, presumably due to their high dispersion. However, metallic Ag reflections (not shown) became visible for loadings over 20 wt%, with no evidence for Ag oxide forms. Thus, it can be inferred that the Ag was also present in the metallic form at the lower loadings of interest here.

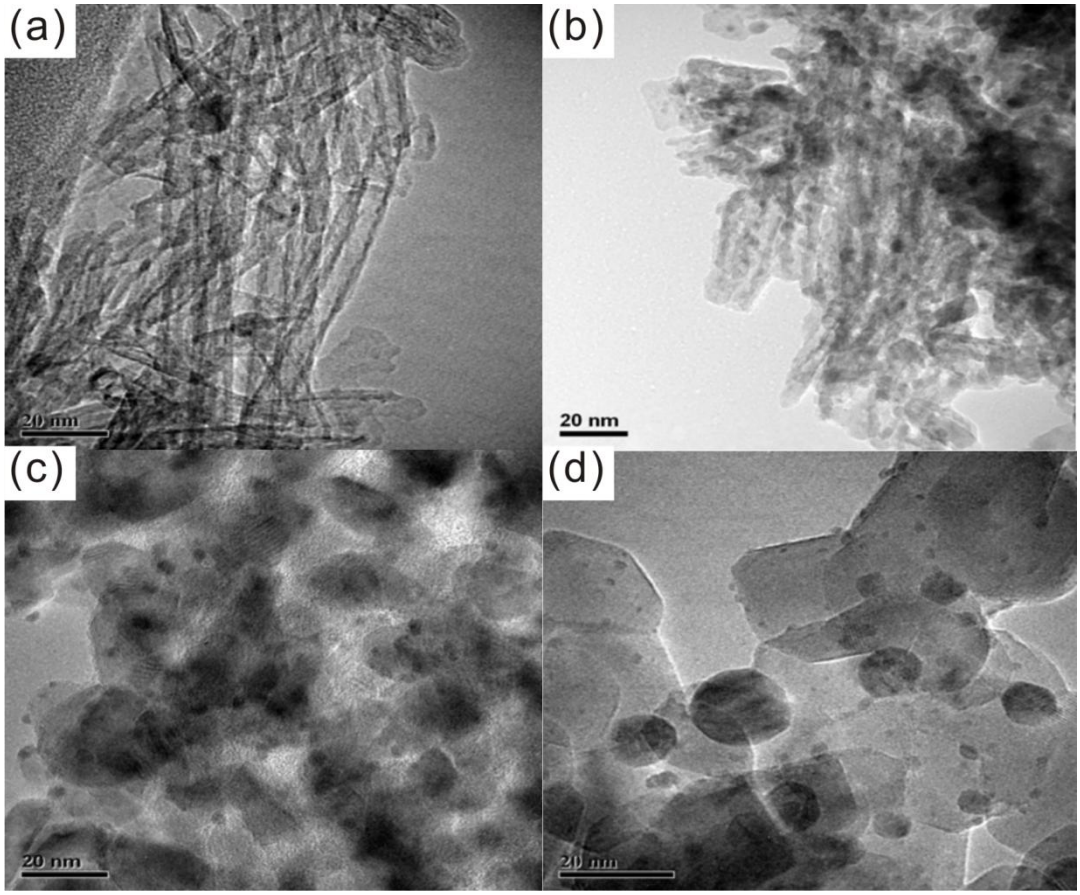

Figure 6-16 TEM images of Ag-decorated titanates annealed at different temperatures (a) 150 °C; (b) 350 °C; (c) 450 °C; (d) 550 °C

Annealing at high temperature leads to a progressive decrease in the surface area of the support, i.e., sintering, as seen in the N_2 isotherms (Figure 6-17) and surface area values given in Table 6-4.

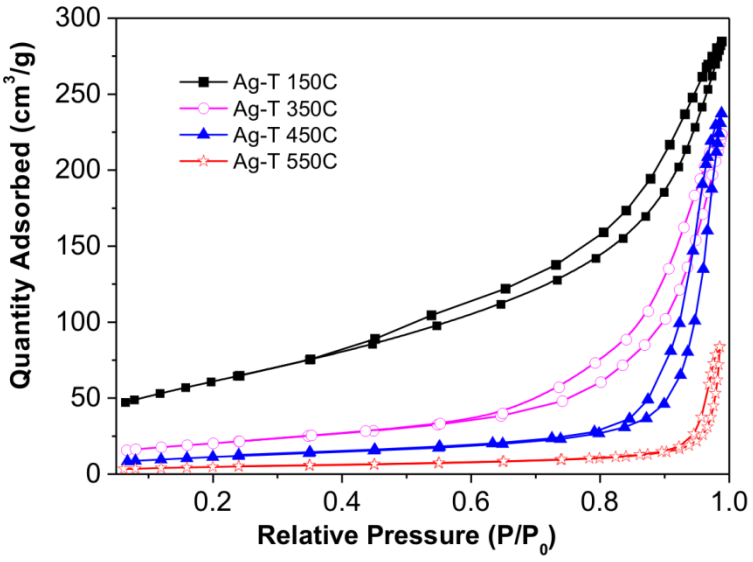

Figure 6-17 N_2 sorption isotherms on Ag-decorated titanate annealed at different temperatures.

Table 6-4 BET surface area of (Ag, H) titanates annealed at different temperatures

Samples	*BET surface area(m^2/g)*
HT 150	224.48
AgT 150	221.13
AgT 350	73.59
AgT 450	41.76
AgT 550	17.74

6.2.2 Optical properties of hydrogen/Ag titanates

Figure 6-18a shows the DR UV-VIS spectra of TNTs and anatase TiO_2 (obtained from TNTs heated at 450 °C). It is well known that anatase TiO_2 is a wide band-gap semiconductor (3.2 eV) such that it is only active under UV light (λ < 385nm). TNTs can be considered as comprising isolated layers of TiO_6 octahedra intercalated with cations. Due to the quantum size effect, the band gap of pristine hydrogen titanate (ca. 3.4 eV) is even wider than anatase, consistent with the data reported by others. [96,142]After incorporation of Ag nanoparticles, visible light absorption was already evident in AgT 15O and AgT 350 but more pronounced in AgT 450 and AgT 550, a strong and broad absorption being observed over the entire visible range due to the surface plasmon resonance effect of Ag nanoparticles (as shown in Figure 6-18b).

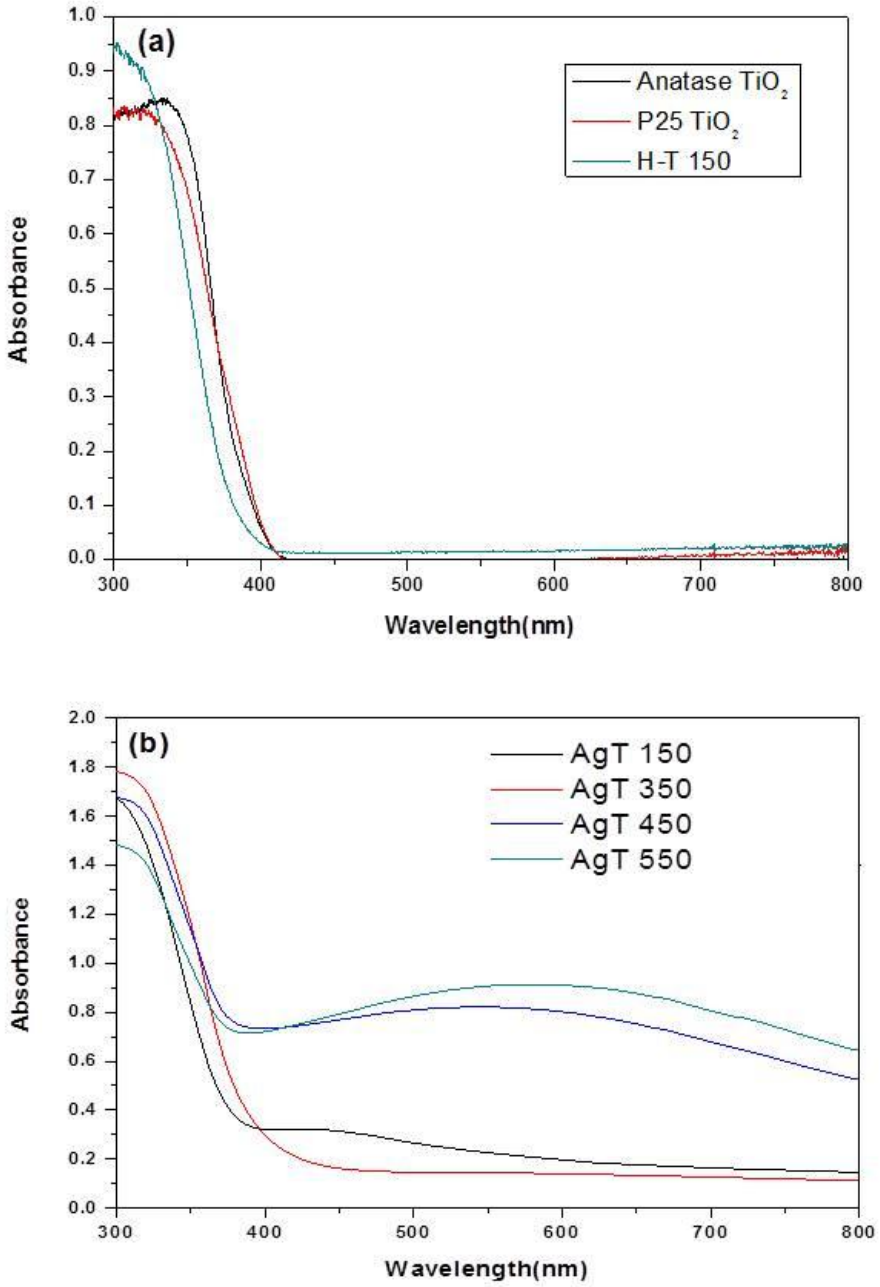

Figure 6-18 Diffuse Reflectance UV-Vis Spectra of (a) anatase TiO_2, P25 TiO_2, HT150 and (b) Ag-decorated titanates annealed at different temperatures.

6.2.3 Photo-degradation of methyl orange under UV-Visible irradiation

The adsorption of MO on both pristine titanate and anatase TiO_2 in the dark was negligible (as shown in Figure S6-1 in appendix). Results of photo-reactor tests on pristine titanate and anatase TiO_2 in MO photo-degradation is shown in Figure 6-19. The titanate itself was scarcely active under UV illumination although it has band gap absorption in this range. This can be attributed to its poor crystallinity (cf. the broad XRD reflections in Figure 6-1), tending to increase the number of surface defects that act as electron-hole recombination centers. In contrast, annealing improved performance significantly, and for sample HT 450 in particular. As shown in Figure 6-19b, visible light activity was poor, as expected since neither the hydrogen titanate nor anatase TiO_2 absorb visible light ($\lambda > 420$ nm - cf. Figure 6-18a).

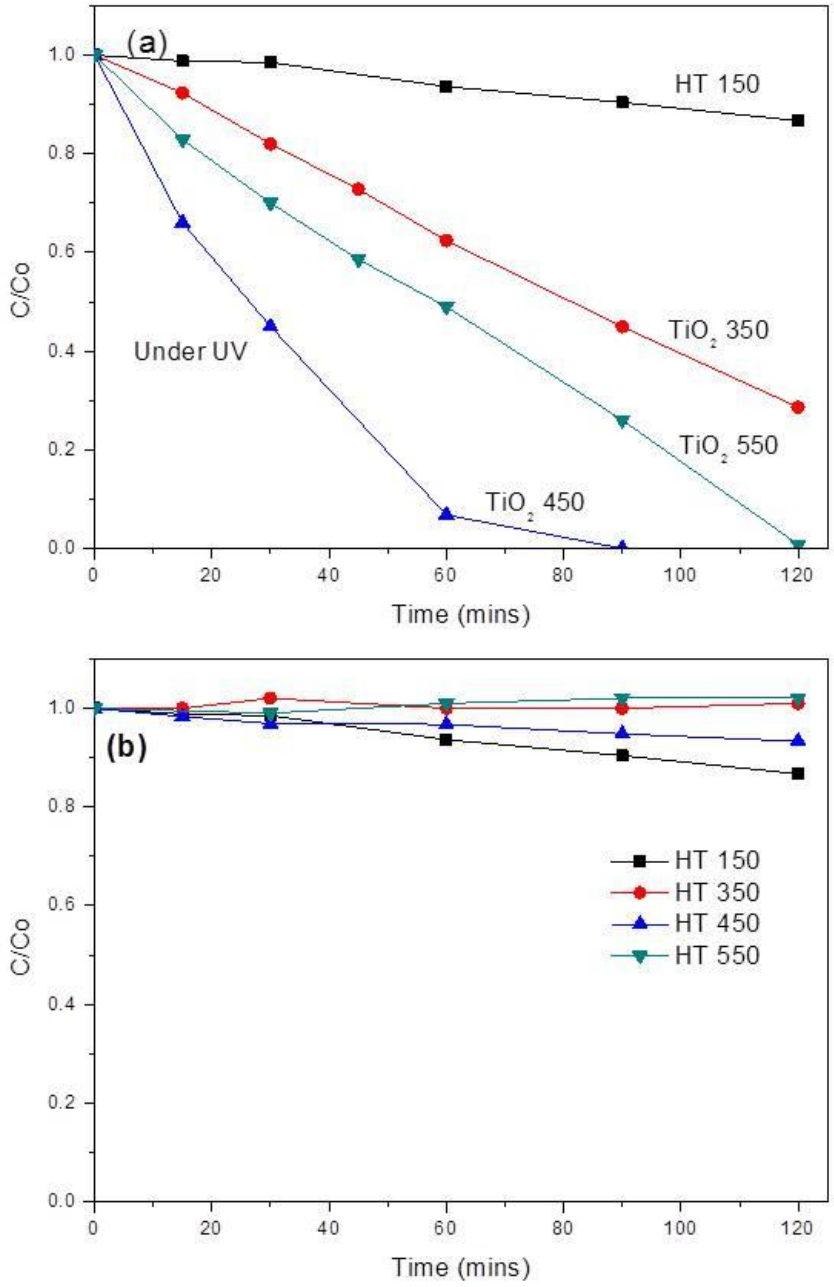

Figure 6-19 Degradation of Methyl Orange by pristine hydrogen titanate annealed at different temperatures under (a) UV-Vis; (b) Vis (>420nm)

Compared with pristine samples, pronounced visible light activity was observed for Ag-decorated samples, as shown in Figure 6-20. The best performance was found for AgT 450, where more than 80% MO was degraded within 2 hours. It is probably not coincidental that the same annealing temperature resulted in the best UV performance for anatase derived from the pristine titanate (cf. Fig. 6-19a), and this may be taken as indirect evidence for involvement of the support in the visible-stimulated process with Ag (*vide infra*). The overall order of performance of was AgT 450 > AgT 550 >>AgT 350 >AgT 150.

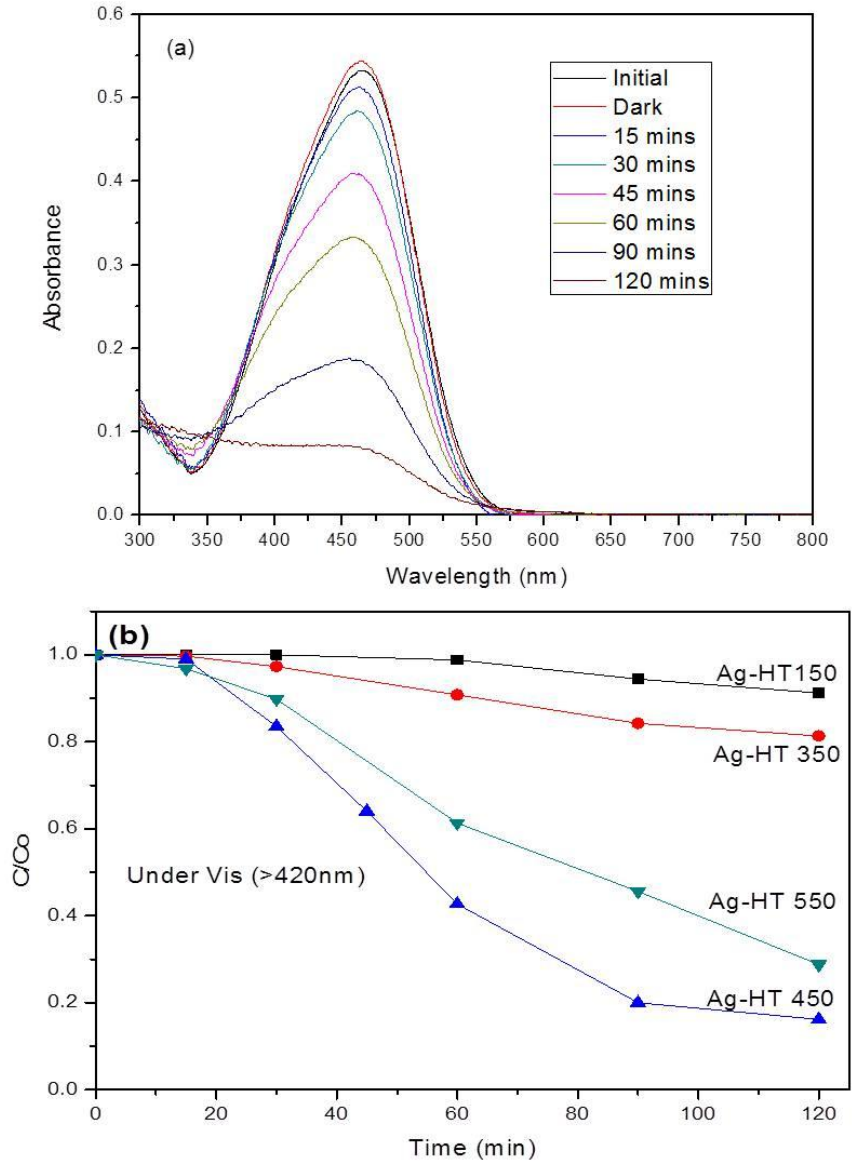

Figure 6-20 (a) Sequential absorption spectra showing degradation of Methyl Orange by Ag-HT 450 under visible light (b) comparison of visible activities of Ag-decorated titanates annealed at different temperatures.

6.2.4 Photo-oxidation of ethanol vapor in air under visible light

Figure 6-21 shows the DRIFT spectrum of Ag loaded TiO_2 (10%Ag-HT 450). Curiously, unlike the case of Pt (see Fig. 4-11b), no absorption tail linked to the

plasmon resonance was observed above 4000 cm^{-1}. Only bands due to adsorbed H_2O and the TiO_2 lattice vibration were evident.

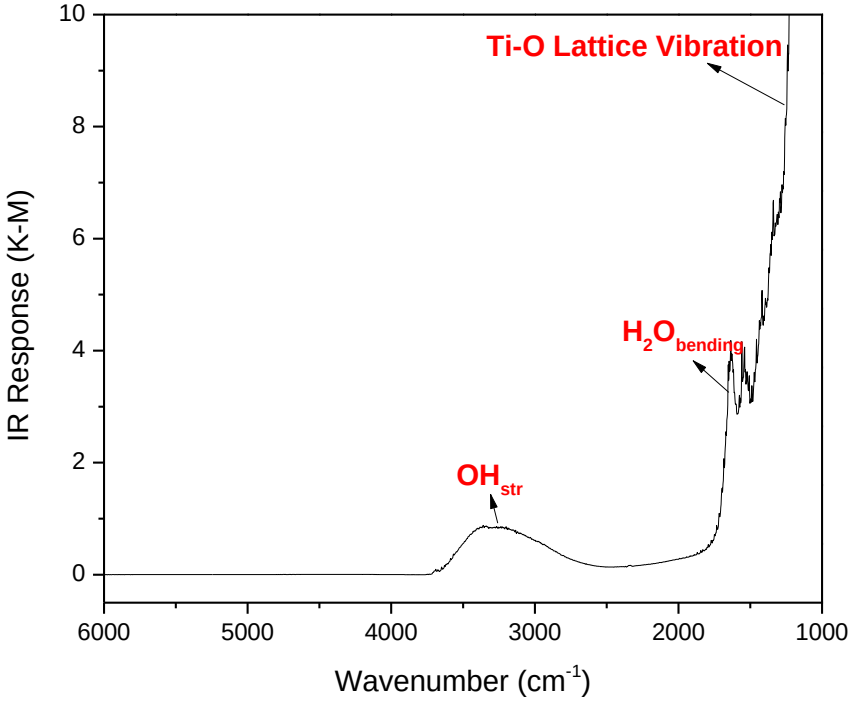

Figure 6-21 DRIFTS spectrum of 10% Ag-HT 450

Since Ag decorated titanate/TiO_2 is active for MO photo-degradation under visible light, it was of interest to extend the study to ethanol, a colorless probe molecule. Figure 6-22 shows the spectra of ethanol photo-oxidation by Ag-HT 450 under visible light (>400 nm).The growth of adsorbed acetate was observed, but unlike for P25 under UV irradiation (see Fig. 4-9a), no evidence was seen for acetaldehyde, as would be indicated by the carbonyl stretch at 1720 cm^{-1}. Ag is known to be inferior to Pt as a dehydrogenation catalyst.[39] It is possible that the photo-oxidation of ethanol on Ag-decorated TiO_2 under visible light is mainly via O-insertion (after dioxygen photo-activation as superoxide), or when the ethanol was oxidized to acetaldehyde by holes, that was quickly oxidized to acetate in the presence of Ag.

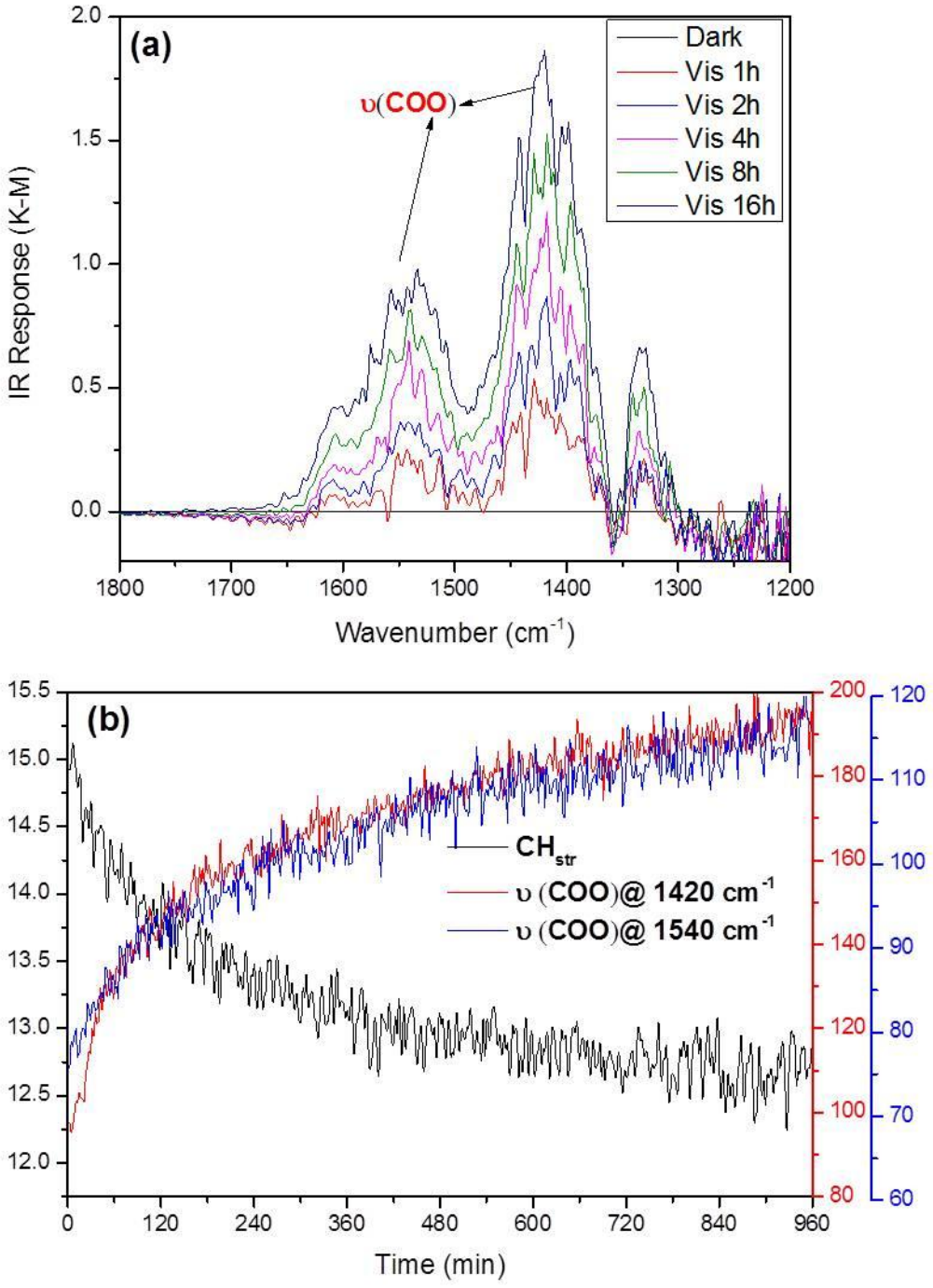

Figure 6-22 (a). DRIFT spectra (detail) collected during photo-oxidation of ethanol vapor by 10% Ag-HT 450 under visible irradiation (>400 nm); (b). marker traces: CH_{str} -ethyl group and ν(COO) – acetate.

6.2.5 Discussion of the mechanism

Although Au nanoparticles loaded on insulators (SiO_2, Al_2O_3, etc.) have been reported as visible light active photocatalysts, [40] better performance is obtained for Au on TiO_2, which suggests that the support also plays a key role in the reaction mechanism.[151]

In our case, it is quite clear that AgT 450 and AgT 550, have stronger and broader absorption properties in the visible, and consequently, show much better visible light activity than AgT 150 and AgT 350. A proposed reaction mechanism is shown in Scheme 6-1. When Ag nanoparticles are under visible illumination, the metallic electrons must be excited from ground states to higher energy states via the surface plasmon resonance (SPR) effect and possibly injected into the conduction band(s) of the supports (titanate and anatase in this case). At the metal-semiconductor interfacial region, an element of band-bending in the TiO_2 states due to the space charge layer, coupled with the strong (negative) electric field induced by SPR may favor charge injection into the semiconductor.[25,26,152] A well-crystallized support could reduce the charge recombination thus enhancing the lifetime of charge carriers and leading to better performance. Other plasmon-induced visible light photocatalysts have also been reported, such as Ag-AgCl,[153,154] Ag-AgBr, [155,156]Ag-AgI,[157] and claimed to work on similar principles.

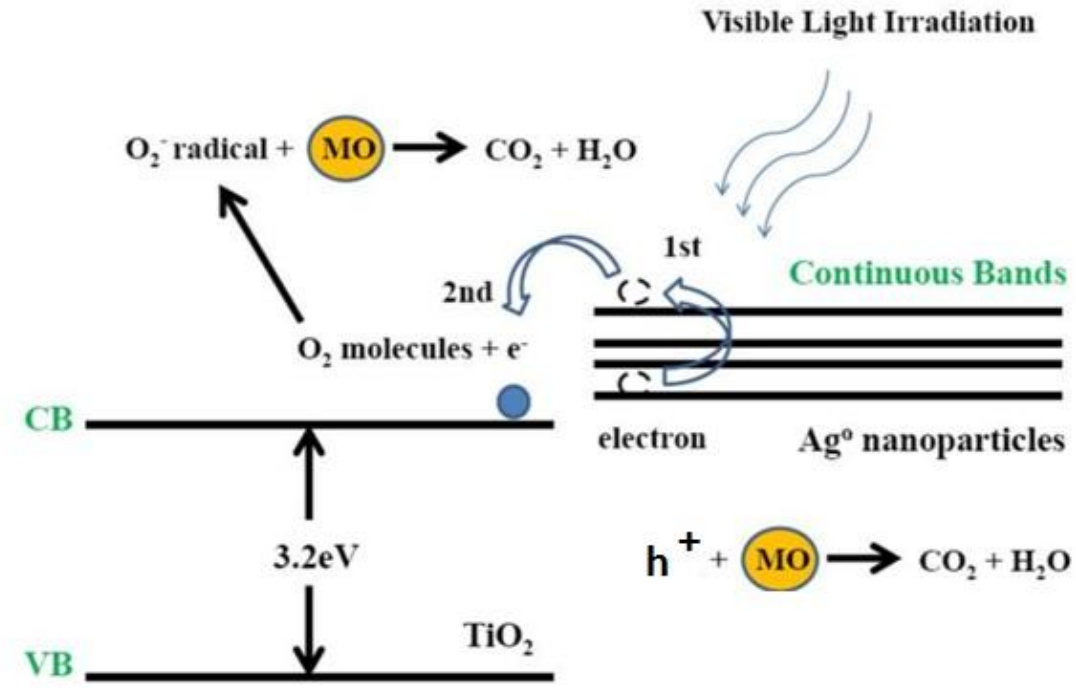

Scheme 6-1 Proposed reaction mechanism for Ag-decorated titanate/titania[158]

Although both AgT 450 and AgT 550 are well crystallized and have similar visible light absorption, AgT 450 shows better activity than AgT 550. The principal difference between them is the higher surface area in the former sample showing that, as in many heterogeneous catalytic processes, access to the surface by reactants is often rate-controlling. This includes adsorption of superoxide or other intermediates generated from O_2 and/or hole trapping by MO, a complex process that requires further work to unravel. That the optimum performance under both UV and visible irradiation results after annealing at 450 °C shows the importance of the semiconductor and adds support to the view that electrons are transferred from the metal to the titanate/anatase under visible irradiation. The well-recognized fact [159] that annealing simultaneously introduces beneficial (higher crystallinity) and deleterious effects (sintering) on the photocatalyst is also evident.

6.2.6 Short summary

In this section, a photo-deposition/ post-annealing method was employed to decorate Ag nanoparticles onto titanate nanotubes and anatase TiO_2. Although titanate itself is scarcely active even under UV illumination, anatase TiO_2 obtained by calcination shows efficient MO photo-degradation and ethanol photo-oxidation. It was found that the support also play a key role in the photocatalytic process, probably by accepting electrons from Ag under visible light excitation, via the surface plasmon resonance effect, and promoting longer-lived charge carrier states. An optimal annealing temperature for both pristine and Ag titanate was found to be 450 °C due to the inevitable compromise between improved crystallinity and loss of surface area due to heat treatment.

6.3 Summary

In this chapter, we have investigated two groups of in-house prepared visible light active photocatalysts. It is found that:

1. When urea is mixed with titante/TiO_2 and heated to 400 °C, melon, a polymeric narrow band gap semiconductor is formed on the surface as a sensitizer. Compared with other organic dyes, melon is photo-stable under UV-Vis irradiation. It is also found that the rich surface OH groups on titanate surface promote the formation of melon compared with TiO_2. Melon-modified titanate/TiO_2 is able to degrade methyl orange dye and oxidize ethanol vapor under visible light irradiation, similar with the g-C_3N_4 modified samples.

2. Decoration of TiO_2 with Ag nanoparticles can extend the absorption range to visible light due to the surface plasmon effect of metal nanoparticles. Silver decorated titanate and TiO_2 nanomaterials are active for methyl orange degradation and ethanol photo-oxidation under visible light irradiation.

Chapter 7. Conclusions and Outlook

In this thesis, *in situ* infrared spectroscopy was used to investigate model and in-house -prepared materials for UV- and visible-light driven photocatalytic processes. Diffuse Reflectance Infrared Fourier Transform (DRIFT) was used to provide fundamental and mechanistic information at the gas/solid interface, while Attenuated Total Reflection (ATR) FTIR spectroscopy was developed to provide related information at the liquid/solid interface.

The main findings listed below are brief summaries of Chapters 4, 5, and 6, respectively.

1. Photocatalysis at the Gas/Solid Interface: DRIFTS studies were made initially on commercial P25 TiO_2 to establish the changes in state under illumination and its relation with the ambient gas environment, H_2O vapour and O_2 in particular. Earlier reports of long-lived and reversible photochromism due to free charge carriers (electrons) were confirmed, and a detailed study made of the conditions that optimize this effect. The photo-generated charge carriers recombine quickly in dry inert atmosphere (N_2), but are stabilized in the presence of H_2O vapor. Under inert gas, and depending on the humidity level, photo-adsorption of water is promoted by surface-trapped holes and repelled (or substantially weakened) by surface-trapped electrons. Oxygen acts as a charge-recombination center and rapidly quenches the electron spectrum in a reversible manner. Addition of ethanol, a more powerful (sacrificial) hole-scavenger, results in the accumulation of excess electrons due to irreversible oxidation. These migrate to the surface and effect photo-metallization, viz., reduction of adsorbed metal ions, such as Pt^{4+}, to deposit metallic Pt nanoparticles. In an O_2-rich

atmosphere, ethanol is effectively mineralized over TiO_2, i.e., photo-oxidized to CO_2 and H_2O, via acetaldehyde and acetic acid (acetate) intermediates.

2. Photocatalysis at the Liquid/Solid Interface: ATR-FTIR spectroscopy was applied to liquid-phase photo-oxidation of ethanol over P25 TiO_2, both in the pristine and metalized form. Just as in DRIFTS, development of a continuum background (due to electron absorption) was seen in pristine TiO_2 but was barely visible in the platinized sample. Photo-oxidation of ethanol solution over pristine TiO_2 is slow, as indicated by low levels of intermediates and the accumulation of trapped electrons. Pt efficiently promotes the necessary electron transfer processes, e.g., ionosorption of dioxygen and/or proton reduction. Ethanol is initially oxidized to acetaldehyde and then to acetate, but the further mineralization of acetate is the rate-limiting step in liquid phase. It was also found that that disruption of the adsorbed water layer(s) on TiO_2 surface is related to the accumulation of surface-trapped electrons, where holes are efficiently consumed by ethanol.

3. Photocatalysis under Visible Light.

Melon-modified titanate/TiO_2: When urea is mixed with titanate/TiO_2 and heated to 400 °C, a polymeric narrow band-gap semiconductor called melon is formed on the surface as a sensitizer. Compared with other organic dyes, melon is photo-stable under UV-Vis irradiation. The abundance of surface OH groups on titanate surface promote the formation of melon, as compared with TiO_2. Melon-modified titanate/TiO_2 is able to degrade methyl orange dye in solution, and oxidize ethanol vapor under visible light irradiation.

Ag nanoparticle-decorated titanate/TiO_2: Ag nanoparticles can extend the optical absorption of the composite into the visible due to the surface plasmon effect. Both

titanate and regular TiO_2 decorated with Ag are active for methyl orange dye degradation and ethanol photo-oxidation under visible light irradiation.

The key advances in photocatalysis reported in this thesis, based on *in-situ* infrared spectroscopy, are as follows:

1. The development of the electron spectrum is an important marker of (and screening tool for) limitations in the composition of new photocatalysts, e.g., inadequate chemical reduction half-cycle), and/or difficulties in application, e.g., restricted access of O_2 to the surface in immersed samples.

2. An intimate relation has been found between surface charging and the structure of the adsorbed water overlayer. This is the first successful demonstration of a spectroscopic analogy to (manifestation of) the superamphiphilic effect, with implications for a wide range of applications.

3. A variety of novel ways to sensitize TiO_2 for photocatalysis in the visible region have been demonstrated.

Recommendations for future work.

1. Towards quantitative reflection infrared spectroscopy: While good experimental design enables control of reactant supply, analytical determination of the (normally low) levels of intermediates, and to some extent, those of desorbed products remains problematic. For adsorbed species, advances must be made in calibration of infrared band area vs. concentration, e.g., by pulse methods. Quadrupole mass spectrometry is vital in gas-phase product analysis, especially when dealing with molecules that are not infrared-active, e.g., H_2, and O_2. For the liquid phase, micro-loop sampling chromatography is indicated.

2. *Alternatives to titania-based photocatalysts*: While developments in visible-light sensitized TiO_2 remain very important, a better solution may ultimately be found in

narrow band-gap semi-conductors provided they are active, environmentally benign, cheap, and photo-stable. These are key practical reasons why TiO_2-based materials have still not been superseded. The Graetzel team is exploring nano-particulate haematite (Fe_2O_3) with some success, while the "cobalt phosphate" electrode of Nocera (for O_2 evolution from water) appears promising but must be linked to a PV cell. Other possibilities are manganese oxide-based materials, inspired by the Mn_4O_4Ca cluster in Photosystem II in plants. However, even Nature prefers not to "burden" any single compound with too many functions, achieving efficient visible light absorption and charge transfer via a chlorophyll antenna mechanism.

List of Publications

Journal Publications：

(1)**D. G. Gong**, W. C. J. Ho, Y. X. Tang, Q. L. Tay, Y. K. Lai, J. G. Highfield, Z. Chen "Silver Decorated Titanate/Titania Nanostructures for Efficient Solar Driven Photocatalysis", *Journal of Solid State Chemistry*, 2012, Vol. 189, pp. 117-122

(2)**D. G. Gong**, V. P. Subramaniam, J. G. Highfield, Y. X. Tang, Y. K. Lai, Z. Chen "In Situ Mechanistic Investigation at the Liquid/Solid Interface by ATR-FTIR: Ethanol Photo-oxidation over Pristine and Platinized TiO_2(P25)", *ACS Catalysis*, 2011, Vol. 1 (8), pp. 864-871

(3)D. G. Gong, Y. X. Tang, S. Z. Ng, Q. L. Tay, J. G. Highfield, Z. Chen "Melon-modified Titanate/Titania Nanomaterials for Visble Light Photocatalysis", *In Preparation.*

(4) **D. G. Gong**, S. O. Pekhonen, J. G. Highfield, Z. Chen "Photo-induced Redispersion of Molecular Water Overlayers on Pristine Degussa P25 TiO_2 by In-situ FTIR Spectroscopy ", *In Preparation.*

(5)Y. X. Tang, P. X. Wee, Y. K. Lai, X. P. Wang, **D. G. Gong**, P. D. Kanhere, T. T. Lim, Z. L. Dong, Z. Chen "Hierarchical TiO_2 Nanoflakes and Nanoparticles Hybrid Structure for Improved Photocatalytic Activity",*The Journal of Physical Chemistry C*, 2012, Vol. 116, pp. 2772-2780

(6)Y. X. Tang, Z. L. Jiang, J. Y. Deng, **D. G. Gong**, Y. K. Lai, H. T. Tay, I. T. K. Joo, T. H. Lau, Z. L. Dong, Z. Chen "Synthesis of Nano-Structured Silver/Silver Halides on Titanate Surfaces and Their Visible Light Photocatalytic Performance", *ACS Applied Materials & Interfaces*, 2012, Vol. 4, pp. 438-446

(7)Y. K. Lai, Y. X. Tang, J. J. Gong, **D. G. Gong**, L. F. Chi, C. J. Lin, Z. Chen "Transparent Superhydrophobic/Superhydrophilic TiO_2-based Coatings for Self-cleaning and Anti-fogging", *Journal of Materials Chemistry*, 2012, Vol. 22, pp. 7420-7426

(8)Y. K. Lai, Y. X. Tang, J. Y. Huang, H. Wang, H. Q. Li, **D. G. Gong**, X. B. Ji, J. J. Gong, C. J. Lin, L. Sun, Z. Chen "Multi-functional Hybrid Protonated Titanate Nanobelts with Tunable Wettability", *Soft Matter*, 2011, Vol. 7, pp. 6313-6319

(9)Y. X. Tang, V. P. Subramaniam, T. H. Lau, Y. K. Lai, **D. G. Gong**, P. D. Kanhere, Y. H. Cheng, Z. Chen, Z. L. Dong "In situ Formation of Large-scale Ag/AgCl Nanoparticles on Layered Titanate Honeycomb by Gas Phase Reaction for Visible Light Degradation of Phenol Solution", *Applied Catalysis B: Environmental*, 2011, Vol. 106, pp. 577-585

(10)Y. H. Cheng, Y. Z. Huang, P. D. Kanhere, V. P. Subramaniam, **D. G. Gong**, S. Zhang, J. Highfield, M. K. Schreyer, Z. Chen "Dual phase titanate/anatase with nitrogen doping for enhanced degradation of organic dye under visible light", *Chemistry – A European Journal*, 2011, Vol. 17, pp. 2575-2578

(11)Y. X. Tang, **D. G. Gong**, Y. K. Lai, Y. Q. Shen, Y. Y. Zhang, Y. Z. Huang, J. Tao, C. J. Lin, Z. L. Dong, Z. Chen "Hierarchical Layered Titanate Microspherulite: Formation by Electrochemical Spark Discharge Spallation and Application in Aqueous Pollutant Treatment", *Journal of Materials Chemistry*, 2010, Vol. 20 (45), pp. 10169-10178

(12)Y. X. Tang, Y. K. Lai, **D. G. Gong**, K. H. Goh, T. T. Lim, Z. L. Dong, Z. Chen "Ultrafast Synthesis of Layered Titanate Micro-Spherulite Particles by Electrochemical Spark Discharge Spallation", *Chemistry – A European Journal*, 2010, Vol. 16, pp. 7704-7708

(13)Y. K. Lai, J. Y. Huang, H. F. Zhang, V. P. Subramaniam, Y. X. Tang, **D. G. Gong**, L. Sundar, L. Sun, Z. Chen, C. J. Lin "Nitrogen-doped TiO_2 nanotube array films with enhanced photocatalytic activity under various light sources", *Journal of Hazardous Materials*, 2010, Vol. 184, pp. 855-863

(14)Y. K. Lai, H. F. Zhuang, K. P. Xie, **D. G. Gong**, Y. X. Tang, L. Sun, C. J. Lin, Z. Chen "Fabrication of Ag/TiO_2 nanotube array structures with enhanced photoelectrochemical performance", *New Journal of Chemistry*, 2010, Vol. 34, pp. 1335-1340

(15)Y. K. Lai, Y. C. Chen, Y. X. Tang, **D. G. Gong**, Z. Chen, C. J. Lin "Electrophoretic Deposition of Titanate Nanotube Films with Extremely Large Wetting Contrast", *Electrochemistry Communications*, 2009, Vol. 11, pp. 2268-2271

Conference Presentations：

(1) **D. G. Gong**, S. Z. Ng, Y. X. Tang, Q. L. Tay, J. G. Highfield, Z. Chen "Melon-modified Titanate/Titania Nanomaterials for Visble Light Photocatalysis", International Conference of Young Researchers on Advanced Materials 2012, Singapore, 1 to 6 July, 2012.

(2) **D. G. Gong**, W. C. J. Ho, Y. X. Tang, Q. L. Tay, Y. K. Lai, J. G. Highfield, Z. Chen. "Silver Decorated Titanate/Titania Nanostructures for Efficient Solar Driven Photocatalysts", International Conference on Materials for Advanced Technologies 2011, Singapore, 26 June to 1 July, 2011.

(3) **D. G. Gong**, V. P. Subramaniam, J. G. Highfield, Y. X. Tang, Y. K. Lai, Z. Chen. "In Situ ATR-FTIR Study of Photocatalytic Reactions at Liquid/Solid Interface", The 15^{th} International Conference on TiO_2 Photocatalysis: Fundamentals and Applications, San Diego, CA, USA, Nov 15-18, 2010.

References

(1) Kudo, A.; Miseki, Y., *Heterogeneous Photocatalyst Materials for Water Splitting.* Chemical Society Reviews, **2009**, 38(1): 253.

(2) Fujishima, A.; Honda, K., *Electrochemical Photolysis of Water at a Semiconductor Electrode.* Nature, **1972**, 238(5358): 37.

(3) Chen, X.; Mao, S. S., *Titanium Dioxide Nanomaterials: Synthesis, Properties, Modifications, and Applications.* Chemical Reviews, **2007**, 107(7): 2891.

(4) Fujishima, A.; Rao, T. N.; Tryk, D. A., *Titanium Dioxide Photocatalysis.* Journal of Photochemistry and Photobiology C: Photochemistry Reviews, **2000**, 1(1): 1.

(5) Zhang, H. Z.; Banfield, J. F., *Understanding Polymorphic Phase Transformation Behavior during Growth of Nanocrystalline Aggregates: Insights from TiO_2.* Journal of Physical Chemistry B, **2000**, 104(15): 3481.

(6) Ranade, M. R.; Navrotsky, A.; Zhang, H. Z.; Banfield, J. F.; Elder, S. H.; Zaban, A.; Borse, P. H.; Kulkarni, S. K.; Doran, G. S.; Whitfield, H. J., *Energetics of Nanocrystalline TiO_2.* Proceedings of the National Academy of Sciences of the United States of America, **2002**, 99: 6476.

(7) Yang, H. G.; Sun, C. H.; Qiao, S. Z.; Zou, J.; Liu, G.; Smith, S. C.; Cheng, H. M.; Lu, G. Q., *Anatase TiO_2 Single Crystals with a Large Percentage of Reactive Facets.* Nature, **2008**, 453(7195): 638.

(8) Alivov, Y.; Fan, Z. Y., *A Method for Fabrication of Pyramid-Shaped TiO2 Nanoparticles with a High {001} Facet Percentage.* Journal of Physical Chemistry C, **2009**, 113(30): 12954.

(9)Chen, D. H.; Huang, F. Z.; Cheng, Y. B.; Caruso, R. A., *Mesoporous Anatase TiO_2 Beads with High Surface Areas and Controllable Pore Sizes: A Superior Candidate for High-Performance Dye-Sensitized Solar Cells.* Advanced Materials, **2009**, 21(21): 2206.

(10)Dai, Y. Q.; Cobley, C. M.; Zeng, J.; Sun, Y. M.; Xia, Y. N., *Synthesis of Anatase TiO2 Nanocrystals with Exposed {001} Facets.* Nano Letters, **2009**, 9(6): 2455.

(11)Han, X. G.; Kuang, Q.; Jin, M. S.; Xie, Z. X.; Zheng, L. S., *Synthesis of Titania Nanosheets with a High Percentage of Exposed (001) Facets and Related Photocatalytic Properties.* Journal of the American Chemical Society, **2009**, 131(9): 3152.

(12)Liu, G.; Yang, H. G.; Wang, X. W.; Cheng, L. N.; Lu, H. F.; Wang, L. Z.; Lu, G. Q.; Cheng, H. M., *Enhanced Photoactivity of Oxygen-Deficient Anatase TiO2 Sheets with Dominant {001} Facets.* Journal of Physical Chemistry C, **2009**, 113(52): 21784.

(13)Liu, G.; Yang, H. G.; Wang, X. W.; Cheng, L. N.; Pan, J.; Lu, G. Q.; Cheng, H. M., *Visible Light Responsive Nitrogen Doped Anatase TiO2 Sheets with Dominant {001} Facets Derived from TiN.* Journal of the American Chemical Society, **2009**, 131(36): 12868.

(14)Yang, H. G.; Liu, G.; Qiao, S. Z.; Sun, C. H.; Jin, Y. G.; Smith, S. C.; Zou, J.; Cheng, H. M.; Lu, G. Q., *Solvothermal Synthesis and Photoreactivity of Anatase TiO_2 Nanosheets with Dominant {001} Facets.* Journal of the American Chemical Society, **2009**, 131(11): 4078.

(15) Zheng, Z. K.; Huang, B. B.; Qin, X. Y.; Zhang, X. Y.; Dai, Y.; Jiang, M. H.; Wang, P.; Whangbo, M. H., *Highly Efficient Photocatalyst: TiO_2 Microspheres Produced from TiO_2 Nanosheets with a High Percentage of Reactive {001} Facets.* Chemistry-a European Journal, **2009**, 15(46): 12576.

(16) Yang, D. J.; Liu, H. W.; Zheng, Z. F.; Yuan, Y.; Zhao, J. C.; Waclawik, E. R.; Ke, X. B.; Zhu, H. Y., *An Efficient Photocatalyst Structure: TiO_2(B) Nanofibers with a Shell of Anatase Nanocrystals.* Journal of the American Chemical Society, **2009**, 131(49): 17885.

(17) Zheng, Z. F.; Liu, H. W.; Ye, J. P.; Zhao, J. C.; Waclawik, E. R.; Zhu, H. Y., *Structure and Contribution to Photocatalytic Activity of the Interfaces in Nanofibers with Mixed Anatase and TiO_2(B) Phases.* Journal of Molecular Catalysis a-Chemical, **2010**, 316(1-2): 75.

(18) Linsebigler, A. L.; Lu, G. Q.; Yates, J. T., *Photocatalysis on TiO_2 Surfaces - Principles, Mechanisms, and Selected Results.* Chemical Reviews, **1995**, 95(3): 735.

(19) Liu, G.; Wang, L. Z.; Sun, C. H.; Yan, X. X.; Wang, X. W.; Chen, Z. G.; Smith, S. C.; Cheng, H. M.; Lu, G. Q., *Band-to-Band Visible-Light Photon Excitation and Photoactivity Induced by Homogeneous Nitrogen Doping in Layered Titanates.* Chemistry of Materials, **2009**, 21(7): 1266.

(20) Umebayashi, T.; Yamaki, T.; Itoh, H.; Asai, K., *Analysis of Electronic Structures of 3d Transition Metal-doped TiO_2 Based on Band Calculations.* Journal of Physics and Chemistry of Solids, **2002**, 63(10): 1909.

(21) Asahi, R.; Morikawa, T.; Ohwaki, T.; Aoki, K.; Taga, Y., *Visible-Light Photocatalysis in Nitrogen-Doped Titanium Oxides.* Science, **2001**, 293(5528): 269.

(22) Hoyer, P.; Konenkamp, R., *Photoconduction in Porous TiO_2 Sensitized by PbS Quantum Dots.* Applied Physics Letters, **1995**, 66(3): 349.

(23)Fitzmaurice, D.; Frei, H.; Rabani, J., *Time-resolved Optical Study of the Charge-carrier Dynamics in a TiO_2/AgI Sandwich Colloid.* Journal of Physical Chemistry, **1995**, 99(22): 9176.

(24)Vogel, R.; Hoyer, P.; Weller, H., *Quantum-sized PbS, CdS, Ag_2S, Sb_2S_3, and Bi_2S_3 Particles as Sensitizers for Various Nanoporous Wide-bandgap Semiconductors.* Journal of Physical Chemistry, **1994**, 98(12): 3183.

(25)Tian, Y.; Tatsuma, T., *Plasmon-induced Photoelectrochemistry at Metal Nanoparticles Supported on Nanoporous TiO_2.* Chemical Communications, **2004**(16): 1810.

(26)Tian, Y.; Tatsuma, T., *Mechanisms and Applications of Plasmon-induced Charge Separation at TiO_2 Films Loaded with Gold Nanoparticles.* Journal of the American Chemical Society, **2005**, 127(20): 7632.

(27)Zhu, A. W.; Luo, Y. P.; Tian, Y., *Plasmon-Induced Enhancement in Analytical Performance Based on Gold Nanoparticles Deposited on TiO2 Film.* Analytical Chemistry, **2009**, 81(17): 7243.

(28)Banfield, J. F.; Veblen, D. R.; Smith, D. J., *The Identification of Naturally-occuring TiO_2(B) by Structure Determination using High-resolution Electron-microscopy, Image Simulation, and Distance-least-square Refinement.* American Mineralogist, **1991**, 76(3-4): 343.

(29)Marchand, R.; Brohan, L.; Tournoux, M., *TiO_2(B) A New Form of Titanium-dioxide and the Potassium Titanate $K_2Ti_8O_{17}$.* Materials Research Bulletin, **1980**, 15(8): 1129.

(30)Ohno, T.; Sarukawa, K.; Tokieda, K.; Matsumura, M., *Morphology of a TiO_2 Photocatalyst (Degussa, P-25) Consisting of Anatase and Rutile Crystalline Phases.* Journal of Catalysis, **2001**, 203(1): 82.

(31)Ohno, T.; Tokieda, K.; Higashida, S.; Matsumura, M., *Synergism between Rutile and Anatase TiO_2 Particles in Photocatalytic Oxidation of Naphthalene.* Applied Catalysis a-General, **2003**, 244(2): 383.

(32)Henderson, M. A., *A Surface Science Perspective on TiO_2 Photocatalysis.* Surface Science Reports, **2011**, 66(6-7): 185.

(33)Xu, Q. A.; Ma, Y.; Zhang, J.; Wang, X. L.; Feng, Z. C.; Li, C., *Enhancing Hydrogen Production Activity and Suppressing CO Formation from Photocatalytic Biomass Reforming on Pt/TiO_2 by Optimizing Anatase-rutile Phase Structure.* Journal of Catalysis, **2011**, 278(2): 329.

(34)Gombac, V.; De Rogatis, L.; Gasparotto, A.; Vicario, G.; Montini, T.; Barreca, D.; Balducci, G.; Fornasiero, P.; Tondello, E.; Graziani, M., *TiO_2 Nanopowders Doped with Boron and Nitrogen for Photocatalytic Applications.* Chemical Physics, **2007**, 339(1-3): 111.

(35)Lu, N.; Zhao, H. M.; Li, J. Y.; Quan, X.; Chen, S., *Characterization of Boron-doped TiO_2 Nanotube Arrays Prepared by Electrochemical Method and Its Visible Light Activity.* Separation and Purification Technology, **2008**, 62(3): 668.

(36)Dong, F.; Zhao, W. R.; Wu, Z. B., *Characterization and Photocatalytic Activities of C, N and S Co-doped TiO_2 with 1D Nanostructure Prepared by the Nano-confinement Effect.* Nanotechnology, **2008**, 19(36): 10.

(37)Chen, X. B.; Burda, C., *The Electronic Origin of the Visible-light Absorption Properties of C-, N- and S-doped TiO_2 Nanomaterials.* Journal of the American Chemical Society, **2008**, 130(15): 5018.

(38)Fujishima, A.; Zhang, X. T.; Tryk, D. A., *TiO_2 Photocatalysis and Related Surface Phenomena.* Surface Science Reports, **2008**, 63(12): 515.

(39)Sclafani, A.; Mozzanega, M. N.; Pichat, P., *Effect of Silver Deposites on the Photocatalytic Activity of Titanium-dioxide Samples for the Dehydrogenation or Oxidation of 2-Propanol* Journal of Photochemistry and Photobiology a-Chemistry, **1991**, 59(2): 181.

(40)Chen, X.; Zhu, H. Y.; Zhao, J. C.; Zheng, Z. T.; Gao, X. P., *Visible-light-driven Oxidation of Organic Contaminants in Air with Gold Nanoparticle Catalysts on Oxide Supports.* Angewandte Chemie-International Edition, **2008**, 47(29): 5353.

(41)Chen, X.; Zheng, Z. F.; Ke, X. B.; Jaatinen, E.; Xie, T. F.; Wang, D. J.; Guo, C.; Zhao, J. C.; Zhu, H. Y., *Supported Silver Nanoparticles as Photocatalysts under Ultraviolet and Visible Light Irradiation.* Green Chemistry, **2010**, 12(3): 414.

(42)Gratzel, M., *Recent Advances in Sensitized Mesoscopic Solar Cells.* Accounts of Chemical Research, **2009**, 42(11): 1788.

(43)Yu, K. F.; Tian, Y.; Tatsuma, T., *Size Effects of Gold Nanaoparticles on Plasmon-induced Photocurrents of Gold-TiO_2 Nanocomposites.* Physical Chemistry Chemical Physics, **2006**, 8(46): 5417.

(44)Tian, Y.; Wang, X. T.; Zhang, D.; Shi, X.; Wang, S. L., *Effects of Electron Donors on the Performance of Plasmon-induced Photovoltaic Cell.* Journal of Photochemistry and Photobiology a-Chemistry, **2008**, 199(2-3): 224.

(45)Primo, A.; Corma, A.; Garcia, H., *Titania Supported Gold Nanoparticles as Photocatalyst.* Physical Chemistry Chemical Physics, **2011**, 13(3): 886.

(46)Mitoraj, D.; Kisch, H., *Surface Modified Titania Visible Light Photocatalyst Powders.* Solid State Phenomena, **2010**, 162: 49.

(47)Mitoraj, D.; Kisch, H., *On the Mechanism of Urea-Induced Titania Modification.* Chemistry-a European Journal, **2010**, 16(1): 261.

(48)Mitoraj, D.; Kisch, H., *The Nature of Nitrogen-Modified Titanium Dioxide Photocatalysts Active in Visible Light.* Angewandte Chemie-International Edition, **2008**, 47(51): 9975.

(49)Zhang, J. S.; Chen, X. F.; Takanabe, K.; Maeda, K.; Domen, K.; Epping, J. D.; Fu, X. Z.; Antonietti, M.; Wang, X. C., *Synthesis of a Carbon Nitride Structure for Visible-Light Catalysis by Copolymerization.* Angewandte Chemie-International Edition, **2010**, 49(2): 441.

(50)Wang, Y.; Wang, X. C.; Antonietti, M., *Polymeric Graphitic Carbon Nitride as a Heterogeneous Organocatalyst: From Photochemistry to Multipurpose Catalysis to Sustainable Chemistry.* Angewandte Chemie-International Edition, **2012**, 51(1): 68.

(51)Wang, X. C.; Maeda, K.; Thomas, A.; Takanabe, K.; Xin, G.; Carlsson, J. M.; Domen, K.; Antonietti, M., *A Metal-free Polymeric Photocatalyst for Hydrogen Production from Water under Visible Light.* Nature Materials, **2009**, 8(1): 76.

(52)Ibach, H., *Physics of Surfaces and Interfaces*. **2006**: Springer Berlin Heidelberg New York.

(53)Brown, G. E.; Henrich, V. E.; Casey, W. H.; Clark, D. L.; Eggleston, C.; Felmy, A.; Goodman, D. W.; Gratzel, M.; Maciel, G.; McCarthy, M. I.; Nealson, K. H.; Sverjensky, D. A.; Toney, M. F.; Zachara, J. M., *Metal Oxide Surfaces and Their Interactions with Aqueous Solutions and Microbial Organisms.* Chemical Reviews, **1999**, 99(1): 77.

(54)Fuller, M. P.; Griffiths, P. R., *Diffuse Reflectance Measurements by Infrared Fourier-transform Spectrometry.* Analytical Chemistry, **1978**, 50(13): 1906.

(55)Szczepankiewicz, S. H.; Moss, J. A.; Hoffmann, M. R., *Slow Surface Charge Trapping Kinetics on Irradiated TiO_2.* Journal of Physical Chemistry B, **2002**, 106(11): 2922.

(56)Burgi, T.; Baiker, A., *Attenuated Total Reflection Infrared Spectroscopy of Solid Catalysts Functioning in the Presence of Liquid-phase Reactants*, in *Advances in Catalysis, Vol 50*. **2006**. 227.

(57)McQuillan, A. J., *Probing Solid-Solution Interfacial Chemistry with ATR-IR Spectroscopy of Particle Films.* Advanced Materials, **2001**, 13(12-13): 1034.

(58)Mojet, B. L.; Ebbesen, S. D.; Lefferts, L., *Light at the Interface: the Potential of Attenuated Total Reflection Infrared Spectroscopy for Understanding Heterogeneous Catalysis in Water.* Chemical Society Reviews, **2010**, 39(12): 4643.

(59)Harrick, N. J., *Study of Physics and Chemistry of Surfaces from Frustrated Total Internal Reflections.* Physical Review Letters, **1960**, 4(5): 224.

(60)Harrick, N. J., *Surface Chemistry from Spectral Analysis of Totally Internally Reflected Radiation.* Journal of Physical Chemistry, **1960**, 64(9): 1110.

(61)Highfield, J. G.; Gratzel, M., *Discovery of Reversible Photochromism in Titanium-dioxide Using Photoacoustic Spectroscopy- Implications for the Investigation of Light-induced Charge-separation and Surface Redox Processes in Titanium-dioxide.* Journal of Physical Chemistry, **1988**, 92(2): 464.

(62)Szczepankiewicz, S. H.; Moss, J. A.; Hoffmann, M. R., *Electron Traps and the Stark Effect on Hydroxylated Titania Photocatalysts.* Journal of Physical Chemistry B, **2002**, 106(31): 7654.

(63)Kataoka, S.; Lee, E.; Tejedor-Tejedor, M. I.; Anderson, M. A., *Photocatalytic Degradation of Hydrogen Sulfide and In Situ FT-IR Analysis of Reaction Products on Surface of TiO_2.* Applied Catalysis B-Environmental, **2005**, 61(1-2): 159.

(64)Wu, J. C. S.; Cheng, Y. T., *In Situ FTIR Study of Photocatalytic NO Reaction on Photocatalysts under UV Irradiation.* Journal of Catalysis, **2006**, 237(2): 393.

(65)Sun, S.; Ding, J. J.; Bao, J.; Gao, C.; Qi, Z. M.; Li, C. X., *Photocatalytic Oxidation of Gaseous Formaldehyde on TiO_2: An In Situ DRIFTS Study.* Catalysis Letters, **2010**, 137(3-4): 239.

(66)Yu, Z. Q.; Chuang, S. S. C., *In Situ IR Study of Adsorbed Species and Photogenerated Electrons during Photocatalytic Oxidation of Ethanol on TiO_2.* Journal of Catalysis, **2007**, 246(1): 118.

(67)Yu, H. G.; Yu, J. G.; Cheng, B., *Photocatalytic Activity of the Calcined H-titanate Nanowires for Photocatalytic Oxidation of Acetone in Air.* Chemosphere, **2007**, 66(11): 2050.

(68)Chen, L. C.; Pan, G. T.; Yang, T. C. K.; Chung, T. W.; Huang, C. M., *In Situ DRIFT and Kinetic Studies of Photocatalytic Degradation on Benzene Vapor with Visible-light-driven Silver Vanadates.* Journal of Hazardous Materials, **2010**, 178(1-3): 644.

(69)Highfield, J. G.; Chen, M. H.; Nguyen, P. T.; Chen, Z., *Mechanistic Investigations of Photo-driven Processes over TiO_2 by In-situ DRIFTS-MS: Part 1. Platinization and Methanol Reforming.* Energy & Environmental Science, **2009**, 2(9): 991.

(70)Guzman, F.; Chuang, S. S. C., *Tracing the Reaction Steps Involving Oxygen and IR Observable Species in Ethanol Photocatalytic Oxidation on TiO_2.* Journal of the American Chemical Society, **2010**, 132(5): 1502.

(71)Szczepankiewicz, S. H.; Colussi, A. J.; Hoffmann, M. R., *Infrared Spectra of Photoinduced Species on Hydroxylated Titania Surfaces.* Journal of Physical Chemistry B, **2000**, 104(42): 9842.

(72) Coronado, J. M.; Kataoka, S.; Tejedor-Tejedor, I.; Anderson, M. A., *Dynamic Phenomena during the Photocatalytic Oxidation of Ethanol and Acetone over Nanocrystalline TiO_2: Simultaneous FTIR Analysis of Gas and Surface Species.* Journal of Catalysis, **2003**, 219(1): 219.

(73) Takeuchi, M.; Martra, G.; Coluccia, S.; Anpo, M., *Verification of the Photoadsorption of H_2O Molecules on TiO_2 Semiconductor Surfaces by Vibrational Absorption Spectroscopy.* Journal of Physical Chemistry C, **2007**, 111(27): 9811.

(74) Hind, A. R.; Bhargava, S. K.; McKinnon, A., *At the Solid/liquid Interface: FTIR/ATR -- the Tool of Choice.* Advances in Colloid and Interface Science, **2001**, 93(1-3): 91.

(75) Connor, P. A.; Dobson, K. D.; McQuillan, A. J., *Infrared Spectroscopy of the TiO_2/aqueous Solution Interface.* Langmuir, **1999**, 15(7): 2402.

(76) Warren, D. S.; McQuillan, A. J., *Influence of Adsorbed Water on Phonon and UV-induced IR Absorptions of TiO_2 Photocatalytic Particle Films.* Journal of Physical Chemistry B, **2004**, 108(50): 19373.

(77) Warren, D. S.; Shapira, Y.; Kisch, H.; McQuillan, A. J., *Apparent Semiconductor Type Reversal in Anatase TiO_2 Nanocrystalline Films.* Journal of Physical Chemistry C, **2007**, 111(39): 14286.

(78) Savory, D. M.; Warren, D. S.; McQuillan, A. J., *Shallow Electron Trap, Interfacial Water, and Outer-Sphere Adsorbed Oxalate IR Absorptions Correlate during UV Irradiation of Photocatalytic TiO_2 Films in Aqueous Solution.* Journal of Physical Chemistry C, **2011**, 115(4): 902.

(79) Nakamura, R.; Nakato, Y., *Primary Intermediates of Oxygen Photoevolution Reaction on TiO_2 (rutile) Particles, Revealed by In Situ FTIR Absorption and Photoluminescence Measurements.* Journal of the American Chemical Society, **2004**, 126(4): 1290.

(80) Nakamura, R.; Imanishi, A.; Murakoshi, K.; Nakato, Y., *In Situ FTIR Studies of Primary Intermediates of Photocatalytic Reactions on Nanocrystalline TiO_2 Films in Contact with Aqueous Solutions.* Journal of the American Chemical Society, **2003**, 125(24): 7443.

(81) Araujo, P. Z.; Mendive, C. B.; Rodenas, L. A. G.; Morando, P. J.; Regazzoni, A. E.; Blesa, M. A.; Bahnemann, D., *FT-IR-ATR as a Tool to Probe Photocatalytic Interfaces.* Colloids and Surfaces a-Physicochemical and Engineering Aspects, **2005**, 265(1-3): 73.

(82) Mendive, C. B.; Bredow, T.; Blesa, M. A.; Bahnemann, D. W., *ATR-FTIR Measurements and Quantum Chemical Calculations Concerning the Adsorption and Photoreaction of Oxalic Acid on TiO_2.* Physical Chemistry Chemical Physics, **2006**, 8(27): 3232.

(83) Mendive, C. B.; Bahnemann, D. W.; Blesa, M. A., *Microscopic Characterization of the Photocatalytic Oxidation of Oxalic Acid Adsorbed onto TiO_2 by FTIR-ATR.* Catalysis Today, **2005**, 101(3-4): 237.

(84) Dolamic, I.; Burgi, T., *Photoassisted Decomposition of Malonic Acid on TiO_2 Studied by In Situ Attenuated Total Reflection Infrared Spectroscopy.* Journal of Physical Chemistry B, **2006**, 110(30): 14898.

(85) Dolamic, I.; Burgi, T., *Photocatalysis of Dicarboxylic Acids over TiO_2: An In Situ ATR-IR Study.* Journal of Catalysis, **2007**, 248(2): 268.

(86)Young, A. G.; McQuillan, A. J., *Adsorption/Desorption Kinetics from ATR-IR Spectroscopy. Aqueous Oxalic Acid on Anatase TiO2.* Langmuir, **2009**, 25(6): 3538.

(87)Lin, H. X.; Wang, X. X.; Dai, W. X.; Fu, X. Z., *Study of Photocatalytic Performance of TiO_2 Membrane for Oleic Acid by FTIR-ATR Technique.* Spectroscopy and Spectral Analysis, **2005**, 25(7): 1057.

(88)Arana, J.; Tello-Rendon, E.; Dona-Rodriguez, J. M.; do Campo, C. V.; Herrera-Melidan, J. A.; Gonzalez-Diaz, O.; Perez-Pena, J., *Highly Concentrated Phenolic WastewaterTreatment by Heterogeneous and Homogeneous Photocatalysis: Mechanism Study by FTIR-ATR.* Water Science and Technology, **2001**, 44(5): 229.

(89)Arana, J.; Rendon, E. T.; Rodriguez, J. M. D.; Melian, J. A. H.; Diaz, O. G.; Pena, J. P., *Highly Concentrated Phenolic Wastewater Treatment by the Photo-Fenton Reaction, Mechanism Study by FTIR-ATR.* Chemosphere, **2001**, 44(5): 1017.

(90)Almeida, A. R.; Moulijn, J. A.; Mul, G., *In Situ ATR-FTIR Study on the Selective Photo-oxidation of Cyclohexane over Anatase TiO_2.* Journal of Physical Chemistry C, **2008**, 112(5): 1552.

(91)Mul, G.; Wasylenko, W.; Hamdy, M. S.; Frei, H., *Cyclohexene Photo-oxidation over Vanadia Catalyst Analyzed by Time Resolved ATR-FT-IR Spectroscopy.* Physical Chemistry Chemical Physics, **2008**, 10(21): 3131.

(92)Dolamic, I.; Gautier, C.; Boudon, J.; Shalkevich, N.; Burgi, T., *Adsorption of Thiol-protected Gold Nanoparticles on TiO_2 and Their Behavior under UV Light Irradiation.* Journal of Physical Chemistry C, **2008**, 112(15): 5816.

(93)Hug, S. J.; Bahnemann, D., *Infrared Spectra of Oxalate, Malonate and Succinate Adsorbed on the Aqueous Surface of Rutile, Anatase and Lepidocrocite Measured with In Situ ATR-FTIR.* Journal of Electron Spectroscopy and Related Phenomena, **2006**, 150(2-3): 208.

(94)Mendive, C. B.; Bredow, T.; Feldhoff, A.; Blesa, M.; Bahnemann, D., *Adsorption of Oxalate on Rutile Particles in Aqueous Solutions: a Spectroscopic, Electron-microscopic and Theoretical Study.* Physical Chemistry Chemical Physics, **2008**, 10(14): 1960.

(95)Dolamic, I.; Burgi, T., *In Situ ATR-IR Study on the Photocatalytic Decomposition of Amino Acids over Au/TiO_2 and TiO_2.* Journal of Physical Chemistry C, **2011**, 115(5): 2228.

(96)Sun, X. M.; Li, Y. D., *Synthesis and Characterization of Ion-exchangeable Titanate Nanotubes.* Chemistry-a European Journal, **2003**, 9(10): 2229.

(97)Wang, R.; Hashimoto, K.; Fujishima, A.; Chikuni, M.; Kojima, E.; Kitamura, A.; Shimohigoshi, M.; Watanabe, T., *Light-induced Amphiphilic Surfaces.* Nature, **1997**, 388(6641): 431.

(98)Wang, R.; Hashimoto, K.; Fujishima, A.; Chikuni, M.; Kojima, E.; Kitamura, A.; Shimohigoshi, M.; Watanabe, T., *Photogeneration of Highly Amphiphilic TiO_2 Surfaces.* Advanced Materials, **1998**, 10(2): 135.

(99)Fujishima, A.; Zhang, X., *Titanium Dioxide Photocatalysis: Present Situation and Future Approaches.* Comptes Rendus Chimie, **2006**, 9(5-6): 750.

(100) Livingston, H. K., *Cross-sectional areas of molecules adsorbed on solid surfaces.* Journal of the American Chemical Society, **1944**, 66: 569.

(101) Kataoka; S., *Thin-film Transmission IR Spectroscopy as An In Situ Probe of the Gas–solid Interface in Photocatalytic Processes.* Journal of Photochemistry and Photobiology A: Chemistry, **2004**, 163(3): 323.

(102)Gao, H. W.; Xu, W. Q.; He, H.; Shi, X. Y.; Zhang, X. L.; Tanaka, K., *DRIFTS Investigation and DFT Calculation of the Adsorption of CO on Pt/TiO_2, Pt/CeO_2 and FeO_x/Pt/CeO_2.* Spectrochimica Acta Part a-Molecular and Biomolecular Spectroscopy, **2008**, 71(4): 1193.

(103) Highfield, J. G.; Pichat, P., *Photoacoustic Study of the Influence of Platinum Loading and Bulk Doping with Chromium(III) Ions on the Reversible Photochromic Effect in Titanium-dioxide- Correlation with Photocatalytic Properties.* New Journal of Chemistry, **1989**, 13(1): 61.

(104) Ferri, D.; Baiker, A., *Advances in Infrared Spectroscopy of Catalytic Solid-Liquid Interfaces: The Case of Selective Alcohol Oxidation.* Topics in Catalysis, **2009**, 52(10): 1323.

(105) Highfield, J. G.; Chen, H. J.; Chong, C.; Chen, Z., *In-Situ Pump-Probe DRIFTS Studies of Photocatalytic Reforming of Simple Alcohols.*, in *The 17th International Conference on Photochemical Conversion & Storage of Solar Energy (IPS17)*. **2008**: Sydney, NSW, Australia. 129.

(106) Highfield, J. G.; Geiger, F.; Uenala, E.; Schucan, T. H., in *10th World Hydrogen Energy Conference*. **1994**: Cocoa Beach, Florida. 1039.

(107) Gong, D. G.; Subramaniam, V. P.; Highfield, J. G.; Tang, Y. X.; Lai, Y. K.; Kanhere, P. D.; Chung, Y. H.; Chen, Z., *In-situ ATR-FTIR Study of Photocatalytical Reactions at the Liquid/Solid Interface*, in *The 15th International Conference on TiO_2 Photocatalysis: Fundamentals and Applications*. **2010**: Town & Country Resort, San Diego, California. 71.

(108) Wu, W. C.; Chuang, C. C.; Lin, J. L., *Bonding geometry and reactivity of methoxy and ethoxy groups adsorbed on powdered TiO2.* Journal of Physical Chemistry B, **2000**, 104(36): 8719.

(109) Bates, S. P.; Gillan, M. J.; Kresse, G., *Adsorption of Methanol on TiO_2(110): A First-principles Investigation.* Journal of Physical Chemistry B, **1998**, 102(11): 2017.

(110) Lusvardi, V. S.; Barteau, M. A.; Farneth, W. E., *The Effects of Bulk Titania Crystal-Structure on the Adsoprtion and Reaction of Aliphatic-alcohols.* Journal of Catalysis, **1995**, 153(1): 41.

(111) Vorontsov, A. V.; Dubovitskaya, V. P., *Selectivity of photocatalytic oxidation of gaseous ethanol over pure and modified TiO2.* Journal of Catalysis, **2004**, 221(1): 102.

(112) Arana, J.; Dona-Rodriguez, J. M.; Cabo, C. G. I.; Gonzalez-Diaz, O.; Herrera-Melian, J. A.; Perez-Pena, J., *FTIR Study of Gas-phase Alcohols Photocatalytic Degradation with TiO_2 and AC-TiO_2.* Applied Catalysis B-Environmental, **2004**, 53(4): 221.

(113) Pichat, P., *Partial or Complete Heterogeneous Photocatalytic Oxidation of Organic-compouds in Liquid Organic or Aquesou Phases* Catalysis Today, **1994**, 19(2): 313.

(114) Pichat, P.; Mozzanega, M. N.; Disdier, J.; Herrmann, J. M., *Pt Content and Temperature Effects on the Photocatalytic H_2 Production from Aliphatic-alcohols over Pt TiO_2.* Nouveau Journal De Chimie-New Journal of Chemistry, **1982**, 6(11): 559.

(115) Jacobs, G.; Patterson, P. M.; Graham, U. M.; Crawford, A. C.; Dozier, A.; Davis, B. H., *Catalytic Links among the Water-gas Shift, Water-assisted Formic Acid Decomposition, and Methanol Steam Reforming Reactions over Pt-promoted Thoria.* Journal of Catalysis, **2005**, 235(1): 79.

(116) Iwasita, T.; Nart, F. C.; Lopez, B.; Vielstich, W., *On the Study of Adsorbed Species at Platinum from Methanol, Formic-acid and Reduced Carbon-dioxide via In Situ FT-IR Spectroscopy.* Electrochimica Acta, **1992**, 37(12): 2361.

(117) Hollins, P., *The Influence of Surface-defects o the Infrared-spectra of Adsorbed Species.* Surface Science Reports, **1992**, 16(2): 51.

(118) Ebbesen, S. D.; Mojet, B. L.; Lefferts, L., *In Situ ATR-IR Study of CO Adsorption and Oxidation over Pt/Al_2O_3 in Gas and Aqueous Phase: Promotion Effects by Water and pH.* Journal of Catalysis, **2007**, 246(1): 66.

(119) Ebbesen, S. D.; Mojet, B. L.; Lefferts, L., *CO Adsorption and Oxidation at the Catalyst-water Interface: An Investigation by Attenuated Total Reflection Infrared Spectroscopy.* Langmuir, **2006**, 22(3): 1079.

(120) Ortiz-Hernandez, I.; Williams, C. T., *In Situ Investigation of Solid-liquid Catalytic Interfaces by Attenuated Total Reflection Infrared Spectroscopy.* Langmuir, **2003**, 19(7): 2956.

(121) Alcala, R.; Shabaker, J. W.; Huber, G. W.; Sanchez-Castillo, M. A.; Dumesic, J. A., *Experimental and DFT Studies of the Conversion of Ethanol and Acetic Acid on PtSn-based Catalysts.* Journal of Physical Chemistry B, **2005**, 109(6): 2074.

(122) Alcala, R.; Mavrikakis, M.; Dumesic, J. A., *DFT Studies for Cleavage of C-C and C-O Bonds in Surface Species Derived from Ethanol on Pt(111).* Journal of Catalysis, **2003**, 218(1): 178.

(123) Park, H.; Kim, K. Y.; Choi, W., *Photoelectrochemical Approach for Metal Corrosion Prevention Using a Semiconductor Photoanode.* Journal of Physical Chemistry B, **2002**, 106(18): 4775.

(124) Howe, R. F.; Gratzel, M., *Electron-paramagnetic-res Observation of Trapped Electrons in Colloidal TiO_2.* Journal of Physical Chemistry, **1985**, 89(21): 4495.

(125) Yoneyama, H.; Takao, Y.; Tamura, H.; Bard, A. J., *Factors Influencing Product Distribution in Photocatalytic Decomposition of Aqueous Acetic-acid on Platinized TiO_2.* Journal of Physical Chemistry, **1983**, 87(8): 1417.

(126) Baltrusaitis, J.; Schuttlefield, J.; Zeitler, E.; Grassian, V. H., *Carbon Dioxide Adsorption on Oxide Nanoparticle Surfaces.* Chemical Engineering Journal, **2011**, 170(2-3): 471.

(127) Barattini, L.; Ramis, G.; Resini, C.; Busca, G.; Sisani, M.; Costantino, U., *Reaction Path of Ethanol and Acetic Acid Steam Reforming over Ni-Zn-Al Catalysts. Flow Reactor Studies.* Chemical Engineering Journal, **2009**, 153(1-3): 43.

(128) Medrano, J. A.; Oliva, M.; Ruiz, J.; Garcia, L.; Arauzo, J., *Catalytic Steam Reforming of Acetic Acid in a Fluidized Bed Reactor with Oxygen Addition.* International Journal of Hydrogen Energy, **2008**, 33(16): 4387.

(129) Basagiannis, A. C.; Verykios, X. E., *Reforming Reactions of Acetic Acid on Nickel Catalysts over A Wide Temperature Range.* Applied Catalysis a-General, **2006**, 308: 182.

(130) Ford, D. C.; Nilekar, A. U.; Xu, Y.; Mavrikakis, M., *Partial and complete reduction of O2 by hydrogen on transition metal surfaces.* Surface Science, **2010**, 604(19-20): 1565.

(131) Tripkovic, V.; Skulason, E.; Siahrostami, S.; Norskov, J. K.; Rossmeisl, J., *The Oxygen Reduction Reaction Mechanism on Pt(111) from Density Functional Theory Calculations.* Electrochimica Acta, **2010**, 55(27): 7975.

(132) Zhdanov, V. P.; KaSerno, B., *Kinetics of Electrochemical O_2 Reduction on Pt.* Electrochemistry Communications, **2006**, 8(7): 1132.

(133) Lin, H. X., *The Study of Oxygen Spillover and Back Spillover on Pt/TiO_2 by a Potential Dynamic Sweep Method.* Journal of Molecular Catalysis a-Chemical, **1999**, 144(1): 189.

(134) Abe, R.; Takami, H.; Murakami, N.; Ohtani, B., *Pristine Simple Oxides as Visible Light Driven Photocatalysts: Highly Efficient Decomposition of Organic Compounds over Platinum-loaded Tungsten Oxide.* Journal of the American Chemical Society, **2008**, 130(25): 7780.

(135) Liu, Q. S.; Bauer, J. C.; Schaak, R. E.; Lunsford, J. H., *Direct Synthesis of H_2O_2 from H_2 and O_2 over Pd-Pt/SiO_2 Bimetallic Catalysts in a H_2SO_4/ethanol System.* Applied Catalysis a-General, **2008**, 339(2): 130.

(136)Caer, S. L.; Pin, S.; Esnouf, S.; Raffy, Q.; Renault, J. P.; Brubach, J.-B.; Creff, G.; Roy, P., *A Trapped Water Network in Nanoporous Material: the Role of Interfaces.* Phys. Chem. Chem. Phys., **2011**, 13(39): 17658.

(137) Gong, D. G.; Subramaniam, V. P.; Highfield, J. G.; Tang, Y. X.; Lai, Y. K.; Chen, Z., *In Situ Mechanistic Investigation at the Liquid/Solid Interface by Attenuated Total Reflectance FTIR: Ethanol Photo-Oxidation over Pristine and Platinized TiO_2 (P25).* Acs Catalysis, **2011**, 1(8): 864.

(138)Uudsemaa, M.; Tamm, T., *Calculations of Hydrated Titanium Ion Complexes: Structure and Influence of the First Two Coordination Spheres.* Chemical Physics Letters, **2001**, 342(5-6): 667.

(139) Takeuchi, M.; Sakamoto, K.; Martra, G.; Coluccia, S.; Anpo, M., *Mechanism of photoinduced superhydrophilicity on the TiO2 photocatalyst surface.* Journal of Physical Chemistry B, **2005**, 109(32): 15422.

(140)Zubkov, T.; Stahl, D.; Thompson, T. L.; Panayotov, D.; Diwald, O.; Yates, J. T., *Ultraviolet Light-induced Hydrophilicity Effect on TiO_2(110)(1x1). Dominant Role of the Photooxidation of Adsorbed Hydrocarbons Causing Wetting by Water Droplets.* Journal of Physical Chemistry B, **2005**, 109(32): 15454.

(141) He, Y. B.; Tilocca, A.; Dulub, O.; Selloni, A.; Diebold, U., *Local ordering and electronic signatures of submonolayer water on anatase TiO2(101).* Nature Materials, **2009**, 8(7): 585.

(142) Bavykin, D. V.; Friedrich, J. M.; Walsh, F. C., *Protonated titanates and TiO2 nanostructured materials: Synthesis, properties, and applications.* Advanced Materials, **2006**, 18(21): 2807.

(143) Bavykin, D. V.; Walsh, F. C., *Elongated Titanate Nanostructures and Their Applications.* European Journal of Inorganic Chemistry, **2009**(8): 977.

(144) Ang, T. P., *Sol-gel Synthesis of a Novel Melon-SiO_2 Nanocomposite with Photocatalytic Activity.* Catalysis Communications, **2009**, 10(14): 1920.

(145) Ang, T. P.; Chan, Y. M., *Comparison of the Melon Nanocomposites in Structural Properties and Photocatalytic Activities.* Journal of Physical Chemistry C, **2011**, 115(32): 15965.

(146) Zhu, H. Y.; Gao, X. P.; Lan, Y.; Song, D. Y.; Xi, Y. X.; Zhao, J. C., *Hydrogen Titanate Nanofibers Covered with Anatase Nanocrystals: A Delicate Structure Achieved by the Wet Chemistry Reaction of the Titanate Nanofibers.* Journal of the American Chemical Society, **2004**, 126(27): 8380.

(147) Yang, H. G.; Zeng, H. C., *Synthetic Architectures of $TiO_2/H_2Ti_5O_{11}$ center dot H_2O,$ZnO/H_2Ti_5O_{11}$ center dot H_2O,$ZnO/TiO_2/H2Ti_5O_{11}$ center dot H_2O, and ZnO/TiO_2 Nanocomposites.* Journal of the American Chemical Society, **2005**, 127(1): 270.

(148) Song, Z.; Xu, H.; Li, K.; Wang, H.; Yan, H., *Hydrothermal Synthesis and Photocatalytic Properties of Titanium Acid $H_2Ti_2O_5$ center dot H_2O Nanosheets.* Journal of Molecular Catalysis A: Chemical, **2005**, 239(1-2): 87.

(149) Chong, M. N.; Jin, B.; Zhu, H. Y.; Chow, C. W. K.; Saint, C., *Application of H-titanate nanofibers for degradation of Congo Red in an annular slurry photoreactor*. Chemical Engineering Journal, **2009**, 150(1): 49.

(150) Grandcolas, M.; Louvet, A.; Keller, N.; Keller, V., *Layer-by-Layer Deposited Titanate-Based Nanotubes for Solar Photocatalytic Removal of Chemical Warfare Agents from Textiles.* Angewandte Chemie-International Edition, **2009**, 48(1): 161.

(151) Kowalska, E.; Mahaney, O. O. P.; Abe, R.; Ohtani, B., *Visible-light-induced Photocatalysis through Surface Plasmon Excitation of Gold on Titania Surfaces.* Physical Chemistry Chemical Physics, **2010**, 12(10): 2344.

(152) Tian, Y.; Notsu, H.; Tatsuma, T., *Visible-light-induced Patterning of Au- and Ag-TiO_2 Nanocomposite Film Surfaces on the Basis of Plasmon Photoelectrochemistry*. Photochemical & Photobiological Sciences, **2005**, 4(8): 598.

(153) Wang, P.; Huang, B. B.; Qin, X. Y.; Zhang, X. Y.; Dai, Y.; Wei, J. Y.; Whangbo, M. H., *Ag@AgCl: A Highly Efficient and Stable Photocatalyst Active under Visible Light.* Angewandte Chemie-International Edition, **2008**, 47(41): 7931.

(154) Bi, Y. P.; Ye, J. H., *In situ Oxidation Synthesis of Ag/AgCl Core-shell Nanowires and Their Photocatalytic Properties.* Chemical Communications, **2009**(43): 6551.

(155) Wang, P.; Huang, B. B.; Qin, X. Y.; Zhang, X. Y.; Dai, Y.; Whangbo, M. H., *Ag/AgBr/WO_3 center dot H_2O: Visible-Light Photocatalyst for Bacteria Destruction.* Inorganic Chemistry, **2009**, 48(22): 10697.

(156) Wang, P.; Huang, B. B.; Zhang, X. Y.; Qin, X. Y.; Jin, H.; Dai, Y.; Wang, Z. Y.; Wei, J. Y.; Zhan, J.; Wang, S. Y.; Wang, J. P.; Whangbo, M. H., *Highly Efficient Visible-Light Plasmonic Photocatalyst Ag@AgBr*. Chemistry-a European Journal, **2009**, 15(8): 1821.

(157) Hu, C.; Peng, T. W.; Hu, X. X.; Nie, Y. L.; Zhou, X. F.; Qu, J. H.; He, H., *Plasmon-Induced Photodegradation of Toxic Pollutants with Ag-AgI/Al_2O_3 under Visible-Light Irradiation.* Journal of the American Chemical Society, **2010**, 132(2): 857.

(158) Tang, Y. X.; Jiang, Z. L.; Deng, J. Y.; Gong, D. G.; Lai, Y. K.; Tay, H. T.; Joo, I. T. K.; Lau, T. H.; Dong, Z. L.; Chen, Z., *Synthesis of Nanostructured Silver/Silver Halides on Titanate Surfaces and Their Visible-Light Photocatalytic Performance.* Acs Applied Materials & Interfaces, **2012**, 4(1): 438.

(159) Pichat, P., *A Brief Overview of Photocatalytic Mechanisms and Pathways in Water*. Water Science and Technology, **2007**, 55(12): 167.

Appendix

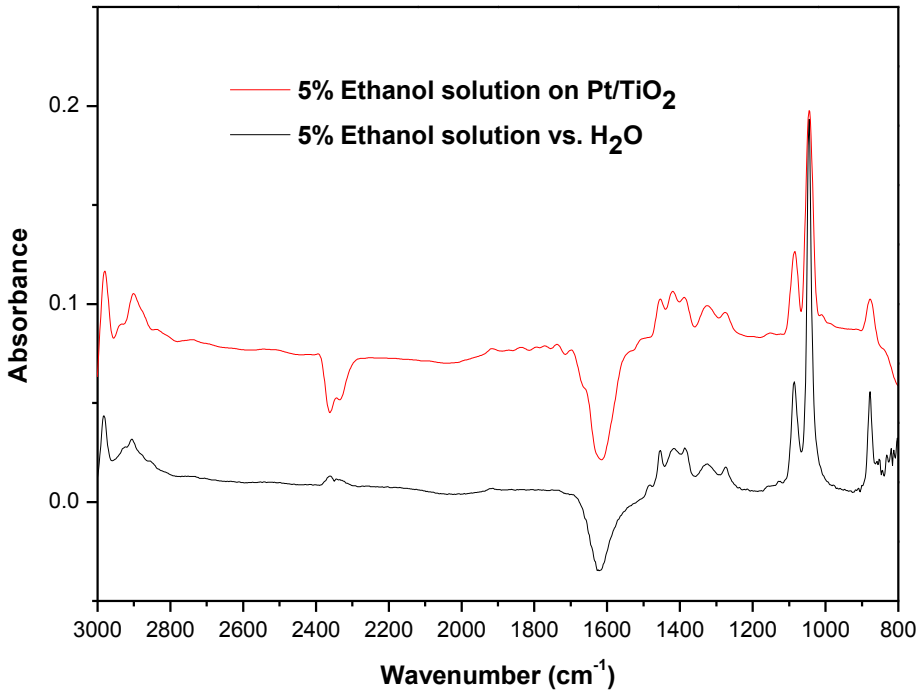

Figure S5-1 ATR-FTIR spectra of 5% EtOH solution vs. H_2O and on 0.5 wt% Pt/ P25 TiO_2

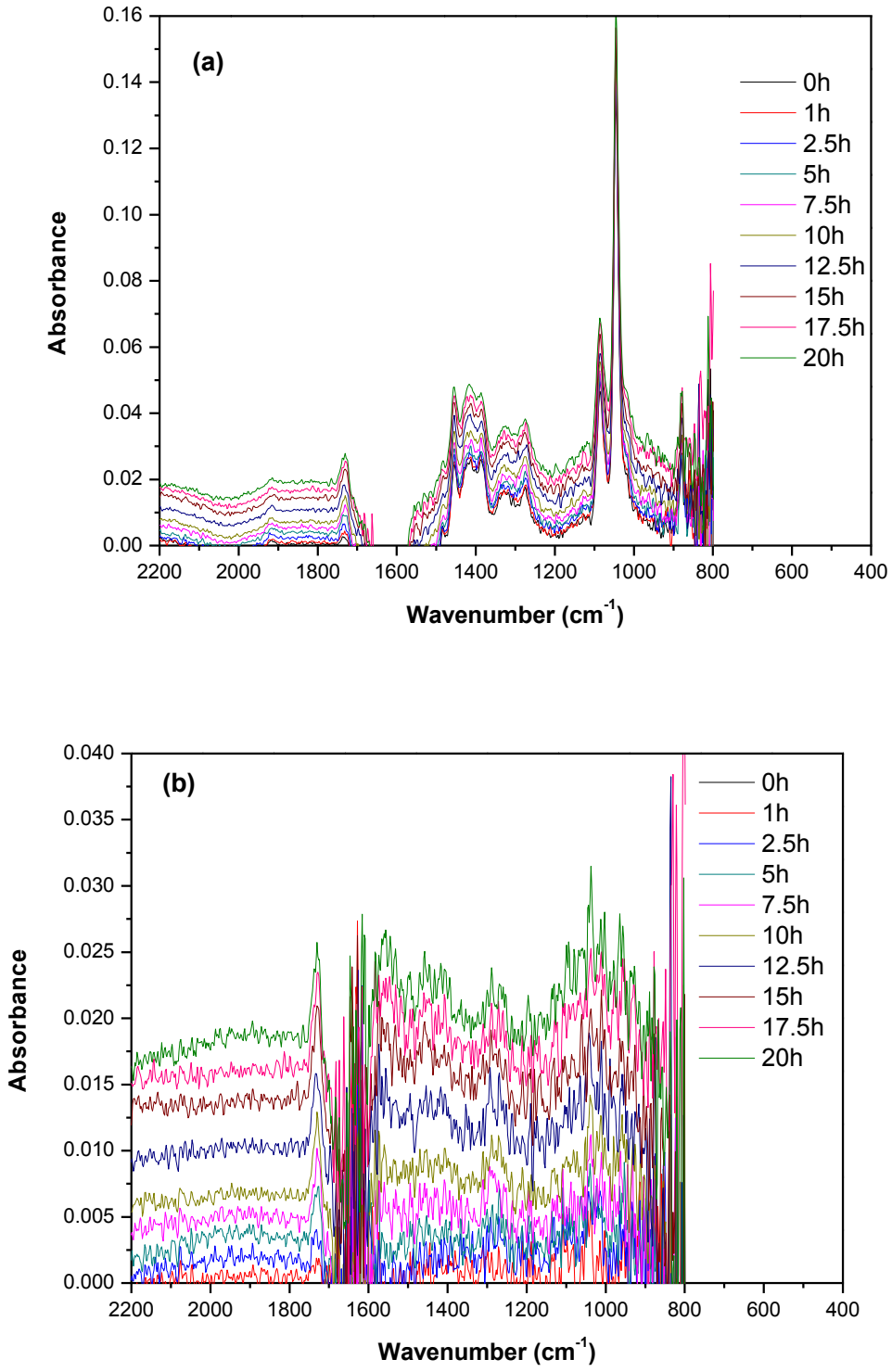

Figure S5-2 ATR-FTIR spectra recorded when 5% EtOH solution was kept dark over 0.5wt% Pt P25 TiO_2: (a) Raw spectra; (b) Difference Spectra.

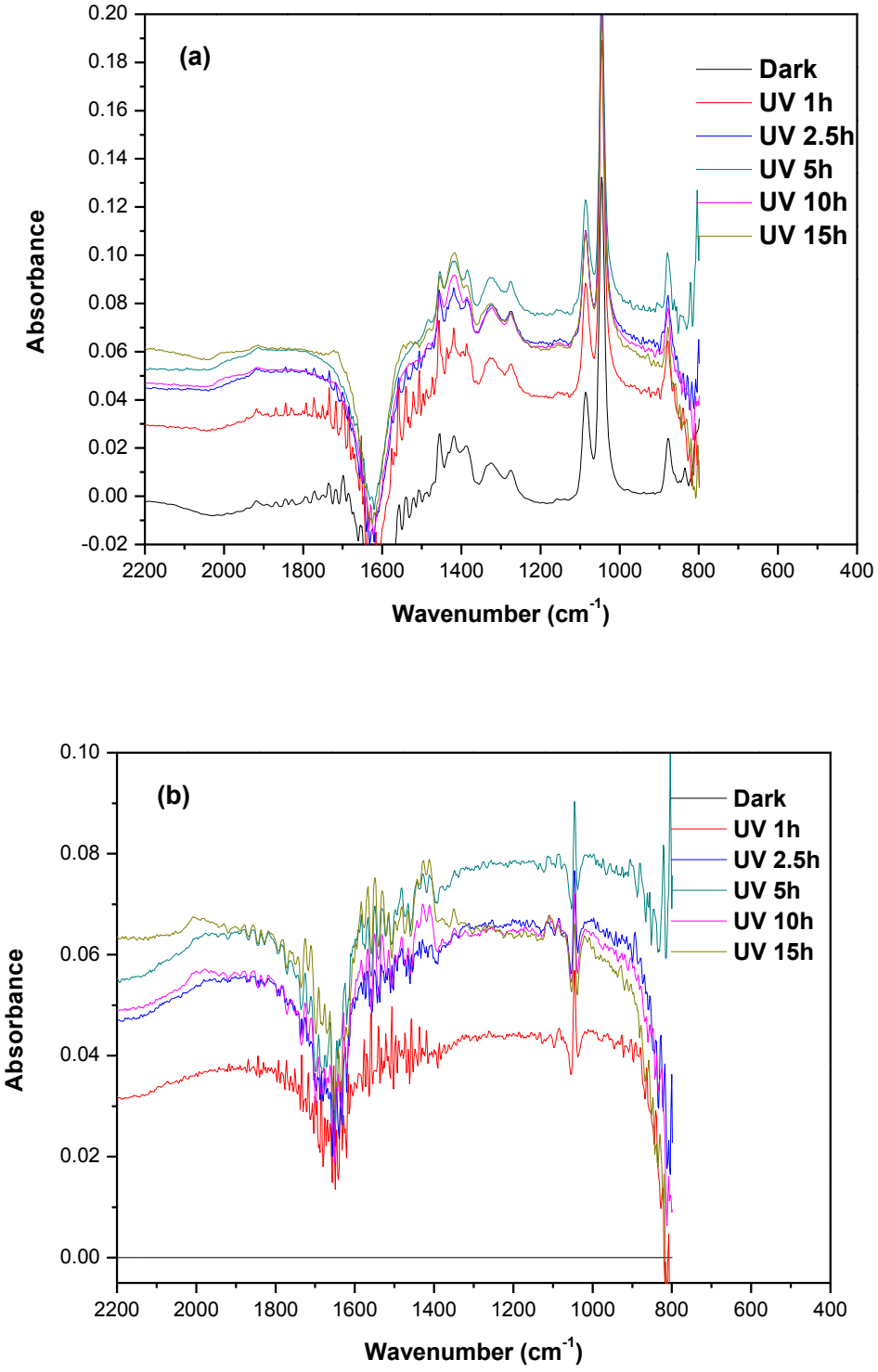

Figure S5-3 ATR-FTIR spectra recorded during 5% oxygen free EtOH solution illuminated over 0.5wt% Pt P25 TiO_2: (a) Raw spectra; (b) Difference Spectra.

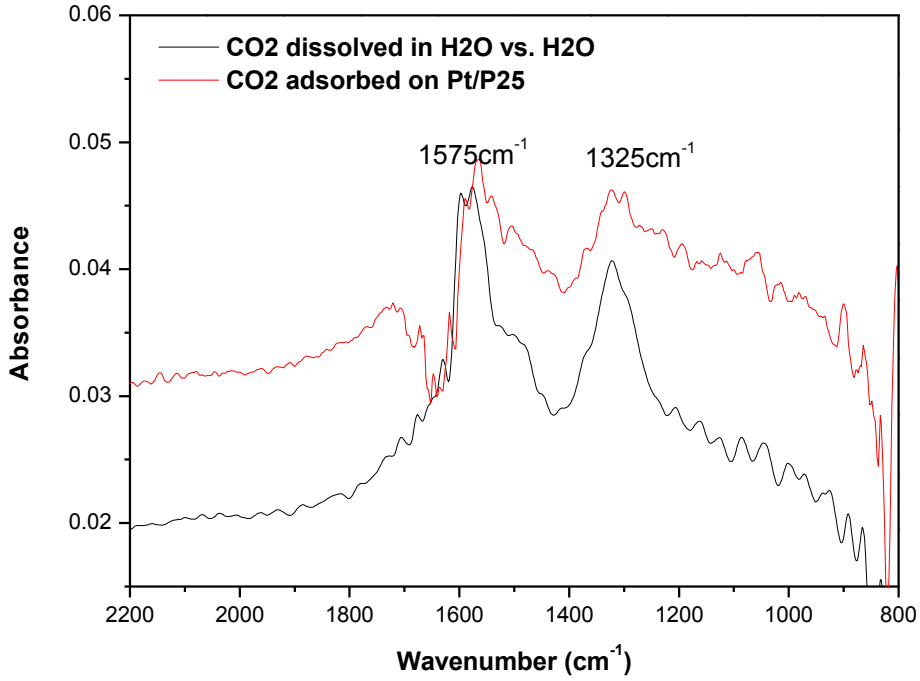

Figure S5-4 ATR-FTIR spectra of CO_2 dissolved solution vs. H_2O and on 0.5wt.% Pt/P25 TiO_2.

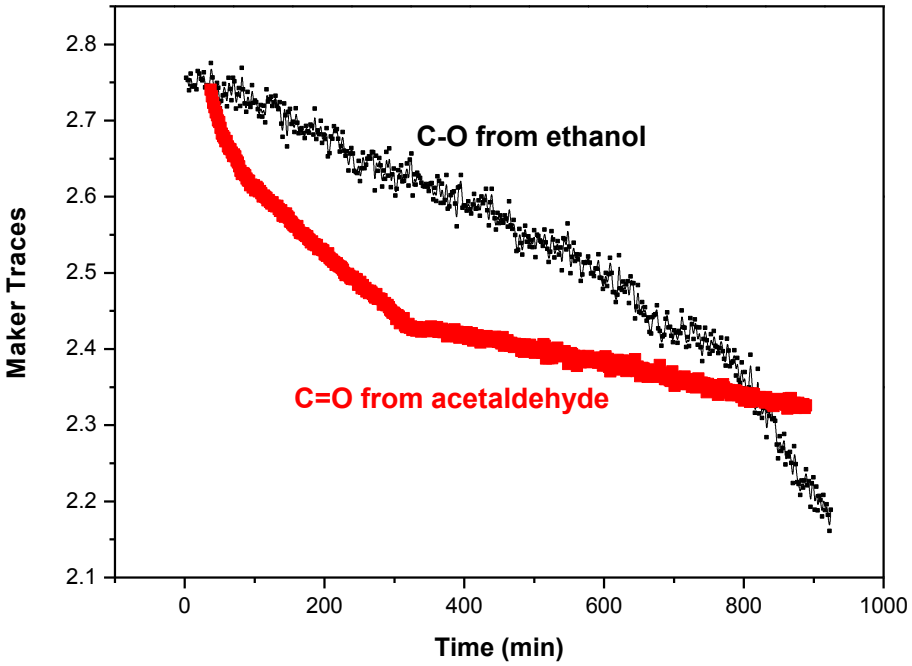

Figure S5-5 Comparison of consumption rate of ethanol and acetaldehyde during photo-oxidation by 0.5wt.% Pt/P25 TiO_2.

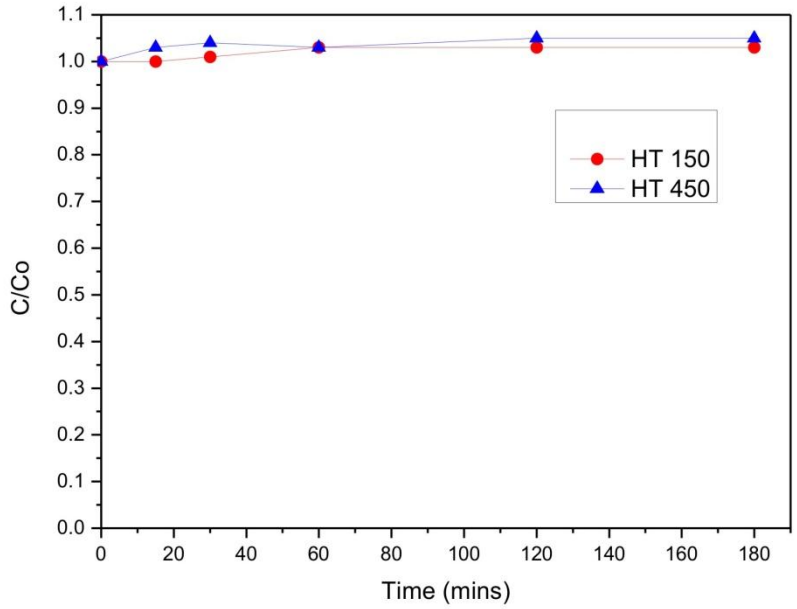

Figure S6-1 MO absorption by pristine titanate (HT 150) and anatase TiO_2 (HT 450) at the pH=6.5.